

A CONTACT LENGTH MODEL FOR GRINDING WHEEL-WORKPIECE CONTACT

HONGSHENG QI

**A thesis submitted in partial fulfilment of the
requirements of Liverpool John Moores University
for the degree of Doctor of Philosophy**

July 1995

ABSTRACT

Grinding efficiency and workpiece surface integrity are greatly affected by deflections that occur within the grinding contact zone. A new relationship for the contact between the grinding wheel and the surface of the workpiece is introduced by the equation $l_c^2 = l_f^2 + l_g^2$. The orthogonal combination of the contact length due to the deformation which would occur with zero depth of cut and the contact length due to the depth of cut is a new finding that clarifies for the first time the effects of the grinding geometry, represented by l_g , and the deflection due to the force, represented by l_f . The contacting surfaces in abrasive machining process are far from smooth. The real contact length was therefore modelled from two approaches: (i) a roughness factor approach and (ii) a contact area ratio approach. These new models more accurately describe the mechanics of grinding contact than previous models. The analysis explains why the measured contact length is much greater than the geometric contact length.

For the experimental investigation, the Applied Power Source method was used to measure contact length. The signal of the Applied Power Source method is the function of the contact area of the active grains and the number of the active grains. The measuring system also included a technique for measuring real depth of cut and a temperature measurement technique.

Experimental results were correlated with theoretical predictions for a range of grinding conditions, including depth of cut, dry and wet grinding, different workpiece materials, alumina and CBN grinding wheels. The roughness factor approach was found to give the best agreement with experiment. Values of the roughness factor, R_t , were established and the sensitivity of these values was investigated based on the effect of various grinding parameters. The application of the contact length model in adaptive control was discussed.

It is concluded that the new contact length model provides the first satisfactory explanation of experimental finding.

ACKNOWLEDGEMENTS

I would like to acknowledge the contributions of all of those who assisted towards the completion of this work. Particular gratitude is due to my supervisor, Professor W. Brian Rowe, for his invaluable guidance and encouragement throughout the theoretical and experimental investigations.

Thanks are also expressed to Professor J.L. Moruzzi, and Professor Ben Mills, for their help and advice.

The assistance from the technician staff in the School of Engineering and Technology Management is gratefully acknowledged. In particular Mr. Paul Wright, Mr. Stephen Ebbrell and Mr. Peter Moran who assisted in the experiments.

Thanks are also expressed to Mr. Sean Black, Mr. David Allanson, Mr. Mike Morgan and other members of staff in the AMT research laboratory for their practical help.

Gratitude is due to the China National Education Committee for initial funding to study at the Liverpool John Moores University, and to the Liverpool John Moores University for providing the research funding necessary for me to continue the doctoral research programme.

Finally, and not least, I would like to acknowledge the support and encouragement of friends and family especially my wife Dr. Li Yan over past years.

Hong-Sheng Qi

NOMENCLATURE

<i>Symbol</i>	<i>Meaning</i>	<i>Unit</i>
a	The contact radius of Hertz theory	mm
a	The wheel depth of cut or incremental radial infeed	mm
a_0	The contact radius for smooth surfaces given by Hertz theory	mm
a^*	The effective 'contact radius' of a rough surface defined by Greenwood & Tripp	mm
a_e	The real depth of cut	mm
A_a	Apparent contact area of grinding contact zone	mm^2
A_r	Real contact area of grinding contact zone	mm^2
A_i	Contact area of the i^{th} contact spot of active grain-workpiece	mm^2
b	Width of cut in plunge grinding	mm
c	Dynamical factor, $c = p_{\max}/H_V$	
C	Density of the number of active grains	$1/\text{mm}^2$
C'	Number of active grains per unit grinding width	$1/\text{mm}$
C_A	Contact area factor, $C_A = R_A (R_p/c)$	
C_p	A constant which is related to machine efficiency	
d_e	Equivalent diameter of the grinding wheel	mm
d_s	Diameter of the grinding wheel	mm
d_{sd}	Undeformed diameter of the grinding wheel	mm
d_w	Diameter of the workpiece	mm
d_2	Undeformed diameter of the contact curve of workpiece surface	mm
E_s	Modulus of elasticity of the grinding wheel	N/mm^2
E_w	Modulus of elasticity of the workpiece	N/mm^2

e_c	Specific energy	
f_w	Vibration break frequency for the workpiece	Hz
f_s	Vibration break frequency for the grinding wheel	Hz
F_n	Normal grinding force	N
F_{ng}	Normal force acting on an individual active grain	N
F_t	Tangential grinding force	N
F_n'	Specific normal force	N/mm
F_t'	Specific tangential force	N/mm
F_{th}'	Threshold normal grinding force per unit axial width	N/mm
H_v	Hardness of workpiece	N/mm ²
k	Yield shear stress	N/mm ²
L_s	The spacing of successive active grains	mm
l_c	Theoretical contact length	mm
l_{cr}	Theoretical contact length based on rough surfaces	mm
l_{ca}	Theoretical contact length based on real contact area	mm
l_f	Contact length between surfaces acted on by a normal force	mm
l_{fs}	Contact length for smooth surfaces with a normal force	mm
l_{fr}	Contact length for rough surfaces with a normal force	mm
l_g	Geometric contact length	mm
l_e	Measured contact length	mm
l_{ef}	Effective contact length for thermal modelling	mm
l_k	Kinematic contact length	mm
l_{kumar}	Contact length based on Kumar's theory	mm
l_{maris}	Contact length based on Maris' empirical equation	mm
l_{max}	Maximum measured contact length	mm
l_{av}	Average measured contact length	mm
l_i	Contact size of the i^{th} contact spot of active grain-workpiece	mm
l_{cut}	The cutting zone where cutting action dominates	mm
l_{c-pl}	The cutting and ploughing zone where plastic	

	deformation dominates	mm
l_1	The length of the first part of the signal which is high in magnitude	mm
l_2	The length of the signal which includes the high and intermediate levels of magnitude	mm
l_3	The length between the first spike and the last spike of the signal	mm
N	The number of experimental observations	
n	Number of asperities in contact	
P	Normal contact force	N
P	Normal contact force per unit axial width in the contact of two cylindrical bodies	N/mm
P'	Specific grinding power	W/mm
p	Contact pressure	N/mm ²
p_m	Mean Hertz contact pressure	N/mm ²
p_0	Maximum Hertz contact pressure	N/mm ²
p_{max}	Maximum contact pressure of the real contact	N/mm ²
$p_{average}$	Average contact pressure for apparent area, F_N/A_a	N/mm ²
p_{mav}	Mean contact pressure for the real contact area, F_N/A_r	N/mm ²
$p_{n,cut}$	The pressure on the workpiece at a cutting point	N/mm ²
R	Radius of relative curvature of Hertzian contact	mm
R	Energy partition ratio	
q	Speed ratio of wheel and workpiece	
R_a	Average surface roughness	mm
R_r	The roughness factor, $R_r = l_{fr} / l_{fs}$, a^*/a_0	
R_{r2}	The roughness factor for the thermal modelling	
R_l	Contact length ratio, $R_l = l_e / l_g$	
R_A	Contact area ratio, $R_A = A_a / A_r$	
R_p	Ratio of p_{max}/p_{av}	
S	The feed per cutting point	mm
t_c	Contact time	second

$w(x,y)$	Surface displacement	mm
h	The separation between the two surfaces of a Hertzian contact	mm
v_f	The infeed rate	mm/s
v_s	Peripheral wheel speed	m/s
v_w	Peripheral workpiece speed	m/s
α	Roughness parameter, $\alpha = \sigma_s/\delta_0$	
α	Thermal diffusivity = $\frac{k}{\rho c}$	m^2/s
β	Radius of the tip of asperities on a rough surface	mm
δ, δ_0	The bulk compression extent given by Hertzian theory	mm
δ_2	The bulk compression extent of grinding wheel	mm
δ_e	The extent of the elastic recovery of the workpiece	mm
μ	The grinding friction coefficient	
σ_Y	Uniaxial tensile yield stress	N/mm^2
σ_{th}	Threshold normal stress	N/mm^2
σ_l	Deviation of the real contact length	mm
σ_s	'Root-mean-square' or standard deviation of the heights of the surface from the centre-line	mm
τ	Shear stress	N/mm^2
ν_s	Poisson ratio of the grinding wheel	
ν_w	Poisson ratio of the workpiece	
WRP	Work Removal Parameter, Z'/F_n'	$\text{mm}^3/\text{N}\cdot\text{min}$

<i>Abstract</i>	<i>i</i>
<i>Acknowledgements</i>	<i>ii</i>
<i>Nomenclature</i>	<i>iii</i>
<i>Contents</i>	<i>vii</i>
<i>List of Figures</i>	<i>xi</i>

Chapter 1 INTRODUCTION

1.1 The Importance of the Contact Length in Grinding	1
1.2 Aims	2
1.3 Scope of the Investigation	2

Chapter 2 REVIEW OF PREVIOUS WORK

2.1 The Grinding Contact Zone	4
2.1.1 Definitions of contact length	4
2.1.2 Definition of contact area	11
2.2 Effects of Contact Length on the Grinding Process	12
2.2.1 The temperature distribution	12
2.2.2 Stress and residual stress distribution	12
2.2.3 Wheel wear based on the thermal stress hypothesis	13
2.2.4 Grinding stability performance	14
2.2.5 Models for the quantitative prediction and optimisation	14
2.3 The Factors Influencing Contact Length in Grinding	15
2.3.1 Deflection	17
2.3.2 Surface roughness	23
2.4 Contact Length Measurements	24
2.4.1 Static loading tests	24
2.4.2 Sudden disengagement methods	24
2.4.3 Thermocouple methods	26
2.5 Comparison of Experimental Methods	27
2.5.1 The two-half-slot grinding technique	27
2.5.2 The cluster overcut fly grinding method	28
2.5.3 The thermocouple technique	29
2.5.4 The applied power source technique	30
2.6 Conclusions	31

Chapter 3 SURFACES IN CONTACT

3.1	The Contact of Smooth Surfaces	33
3.1.1	Spheres in contact	35
3.1.2	Cylinders in contact	37
3.2	The Contact of Rough Surfaces	41
3.2.1	Surface topography	41
3.2.2	Contact between rough curved surfaces	44
3.3	Plastic Theory	49
3.3.1	Hardness	49
3.3.2	The maximum shear stress and yield stress	50
3.4	The Temperature Field in Grinding	51
3.4.1	Jaeger analysis with a uniform band heat source	52
3.4.2	Rowe & Black's model	54

Chapter 4 MODELS OF GRINDING CONTACT

4.1	Introduction	56
4.2	A Contact Model for Smooth Surfaces	57
4.2.1	Contact geometry	57
4.2.2	Contact due to normal force and depth of cut	61
4.2.3	Discussion	64
4.3	A Contact Model from a Rough Surfaces Approach	65
4.3.1	The character of the contact surfaces in grinding	65
4.3.2	Effect of surface roughness on contact length	66
4.3.3	The roughness factor R_f	66
4.4	A Contact Model from a Contact Area Approach	70
4.4.1	Pressure in the grinding contact zone	70
4.4.2	Effect of real contact area on contact length	71
4.5	Discussion	73
4.5.1	Discussion of the contact model from a rough surfaces approach	73
4.5.2	Discussion of the contact model from a contact area approach	74

Chapter 5 EXPERIMENTAL SYSTEM

5.1	The Contact Length Workpiece System	76
5.1.1	The workpiece assembly	76
5.1.2	The contact length thermocouple	76

5.1.3	The temperature thermocouple	77
5.2	The Measuring System	78
5.2.1	The main pieces of apparatus employed	78
5.2.2	Workpiece materials and grinding wheels employed	79
5.3	Measurement of the Depth of Cut	80
5.4	Calibration of the Force Table	83
5.5	Data Logging Program	83
5.6	Wheel Stabilisation	83
5.7	Preliminary Trial	83
5.8	The Experimental Procedure	84
5.8.1	Experimental conditions	84
5.8.2	The experiments	85

Chapter 6 INTERPRETATION OF THE CONTACT PHENOMENA

6.1	Signal Interpretation	87
6.1.1	Principle of the applied power source method	87
6.1.2	Characteristics of the active grain and workpiece contact	90
6.2	The Size of Contact Zone	91
6.2.1	Effects which increase the signal contact period	92
6.2.2	Effects which reduce the contact signal period	92
6.2.3	A definition of contact length	93

Chapter 7 EXPERIMENTAL RESULTS

7.1	Grinding Force	95
7.2	Grinding Temperature	95
7.3	Contact Length	96
7.3.1	Aluminium oxide abrasive and En9 workpiece material	96
7.3.2	Aluminium oxide abrasive and cast iron workpiece material	97
7.3.3	Superabrasive CBN and En9 workpiece material	98
7.3.4	Superabrasive CBN and M2 workpiece material	99

Chapter 8 MODEL EVALUATION

8.1	Evaluation Method	100
8.2	Results	101
8.3	Refined Contact Area Approach	102
8.4	Recommended Value of R_f	103

8.4.1	A value of R_f for the average contact length	103
8.4.2	A value of R_f for thermal modelling	105
8.5	Discussion and Conclusion	105

Chapter 9 MODEL APPLICATION

9.1	Introduction	107
9.2	Model Modification for Application in Adaptive Control	107
9.2.1	Use of the grinding power	107
9.2.2	An empirical force model	109
9.3	Model Application	110
9.3.1	A criterion for $l_e = R_f l_{fr}$	112
9.3.2	A criterion for $l_e = l_g$	113
9.4	Speed Ratio	114
9.5	Surface Roughness	115

Chapter 10	CONCLUSIONS	117
------------	-------------	-----

Chapter 11	FUTURE WORK	120
------------	-------------	-----

REFERENCES	121
------------	-----

APPENDICES

Appendix 1	Computer Programs	132
A1.1	Source code for data logging	132
A1.2	Mathematica program for experimental design	135
A1.3	Mathematica program for model evaluation	137
A1.4	Mathematica program for model application	139

Appendix 2	List of the Author's Relevant Published Papers	140
------------	--	-----

FIGURES	142
---------	-----

LIST OF FIGURES		Page
Figure 2.1	Illustration of straight surface grinding geometry	142
Figure 2.2	Model of the wheel-workpiece contact by Lindsay	142
Figure 2.3	The contact length model of Brown, Saito, Shaw	143
Figure 2.4	The contact length model of Hideo Tsuwa	144
Figure 2.5	The workpiece-wheel contact length model of Kumar	144
Figure 2.6	The Workpiece-wheel contact length model of Aerens	145
Figure 2.7	The geometrical influence of surface roughness on the contact length	145
Figure 2.8	An illustration of the two-half-slot grinding technique	146
Figure 2.9	The principle of the cluster fly grinding method used in measuring the contact length	147
Figure 2.10	An illustration of the thermocouple technique	148
Figure 2.11	The applied power supply method	149
Figure 3.1	Contact of non-conforming elastic bodies	150
Figure 3.2	An illustration of contact size and pressure distribution under different condition of surface roughness	151
Figure 3.3	Contact of a smooth elastic sphere with a rough plane surface	151
Figure 3.4	Influence of the surface roughness on the effective contact radius a^* compared with the Hertz radius a_0	152
Figure 3.5	Indentation by a sphere with distribution of shear stresses and zoneof plastic deformation	152
Figure 3.6	A band heat source with a uniform heat flux distribution in the grinding zone	153
Figure 3.7	Square law heat generation in the grinding zone	153
Figure 3.8	Jaeger heat transfer theory evaluated with a uniform and asquare law heat flux distribution from Rowe & Black	154
Figure 4.1	The grinding wheel and workpiece contact	155
Figure 4.2	Simplified representation of the contact length due to deflectionunder an applied normal force	155
Figure 4.3	The contact length due to the geometry of the grinding process	156
Figure 4.4	The combined effects of normal force and grinding geometry on contact length	156

Figure 4.5	The two contact factors of the workpiece-wheel contact	157
Figure 4.6	Contact size and pressure distribution under the rough surface of a grinding wheel	157
Figure 4.7	Number of static and dynamical cutting edges	158
Figure 4.8	Static contact area diameter d_{gco} and dynamic contact area diameter d_{gc}	158
Figure 5.1	Workpiece used for measurement of contact length and contact temperature	159
Figure 5.2	The configuration of junctions on the workpiece surface	160
Figure 5.3	The single pole thermocouple arrangement used for measurement of contact length	160
Figure 5.4	The standard thermocouple arrangement used for measurement of contact length and grinding temperature	161
Figure 5.5	Standard K type foil thermocouple	161
Figure 5.6	Measurement system for the real contact length and temperature	162
Figure 5.7	Scheme for measuring the actual depth of cut	163
Figure 5.8	A comparison of the measured results by the dial indicator and by the Talymin	164
Figure 5.9(a)	Calibration set-up for the piezoelectric force table	165
Figure 5.9(b)	Calibration results of the piezoelectric force table	165
Figure 5.10	A flowchart of the data logging programme in C	166
Figure 5.11	Wheel stabilising results	167
Figure 5.12	A typical plot of contact signals in wet grinding	168
Figure 5.13	A typical plot of contact signals in dry grinding	169
Figure 5.14	Typical grinding force signals	170
Figure 6.1	A typical contact signal	171
Figure 6.2	An equivalent circuit of the applied power source transducer	171
Figure 6.3	An illustration of the three stages of contact between the grains and the workpiece	172
Figure 6.4	The distributions of the intensities of different grains acting along the contact length	172
Figure 7.1	Grinding forces and depth of cut - Alumina/En9 steel, $q = 300, \mu = 0.65$	173

Figure 7.2	Grinding forces and depth of cut - Alumina/En9 steel, $q = 150, \mu = 0.59$	173
Figure 7.3	Grinding forces and depth of cut - Alumina/En9 steel, $q = 100, \mu_w = 0.63, \mu_d = 0.57$	174
Figure 7.4	Grinding forces and depth of cut - CBN/En9 steel, $\mu_w = 0.5, \mu_d = 0.6$	174
Figure 7.5	Grinding forces and depth of cut - Alumina/Cast iron, $\mu = 0.37$	175
Figure 7.6	Grinding forces and depth of cut - CBN/M2, $\mu_{-0.1} = 0.28, \mu_{-0.17} = 0.37, \mu_{-0.25} = 0.33$	176
Figure 7.7	Normal forces and speed ratio - Alumina/En9 steel	177
Figure 7.8	Tangential forces and speed ratio - Alumina/En9 steel	177
Figure 7.9	Grinding temperature and workpiece speed - Alumina/En9 steel	178
Figure 7.10	Grinding temperature in dry and wet grinding - Alumina/En9 steel	178
Figure 7.11	Grinding temperature in dry and wet grinding - CBN/En9 steel	179
Figure 7.12	Grinding contact length and depth of cut - Alumina/En9 steel	179
Figure 7.13	Grinding contact length and depth of cut - Alumina/En9 steel	180
Figure 7.14	Grinding contact length and depth of cut - Alumina/En9 steel	180
Figure 7.15	Grinding contact length and depth of cut - Alumina/En9 steel	181
Figure 7.16	Contact length ratio and depth of cut - Alumina/En9 steel	181
Figure 7.17	Grinding contact length and depth of cut - Alumina/En9 steel with coolant	182
Figure 7.18	Contact length ratio and depth of cut - Alumina/En9 steel with coolant	183
Figure 7.19	Grinding contact length and depth of cut - Alumina/cast iron with coolant	184
Figure 7.20	Contact length ratio and depth of cut - Alumina/cast iron	185
Figure 7.21	Grinding contact length and depth of cut - CBN/En9 steel without coolant	185
Figure 7.22	Grinding contact length and depth of cut - CBN/En9 steel with coolant	186
Figure 7.23	Contact length ratio and depth of cut - CBN/En9 steel	186

Figure 7.24	Grinding contact length and depth of cut - CBN/M2 tool steel	187
Figure 7.25	Contact length ratio and depth of cut - CBN/M2 tool steel	187
Figure 8.1	Evaluation of contact length models - Alumina/Cast iron, $v_w = 0.1 \text{ m/s}$, wet	188
Figure 8.2	Evaluation of contact length models - Alumina/Cast iron, $v_w = 0.3 \text{ m/s}$, wet	189
Figure 8.3	Evaluation of contact length models - Alumina/En9 steel, $v_w = 0.1 \text{ m/s}$, dry	190
Figure 8.4	Evaluation of contact length models - Alumina/En9 steel, $v_w = 0.3 \text{ m/s}$, dry	191
Figure 8.5	Evaluation of contact length models - Alumina/En9 steel, $v_w = 0.1 \text{ m/s}$, wet	192
Figure 8.6	Evaluation of contact length models - Alumina/En9 steel, $v_w = 0.1 \text{ m/s}$, wet	193
Figure 8.7	Evaluation of contact length models - Alumina/En9 steel, $v_w = 0.3 \text{ m/s}$, wet	194
Figure 8.8	Evaluation of contact length models - CBN/En9 steel, $v_w = 0.1 \text{ m/s}$, dry	195
Figure 8.9	Evaluation of contact length models - CBN/En9 steel, $v_w = 0.1 \text{ m/s}$, wet	196
Figure 8.10	Evaluation of R_t for dry grinding, $v_s = 30 \text{ m/s}$	197
Figure 8.11	Evaluation of R_t for wet grinding, $v_s = 30 \text{ m/s}$	198
Figure 8.12	Evaluation of C_A for dry grinding, $v_s = 30 \text{ m/s}$	199
Figure 8.13	The contact length l_2 and depth of cut, Alumina/En9 steel with coolant	200
Figure 8.14	The contact length l_2 and depth of cut, Alumina/En9 steel without coolant	201
Figure 8.15	The contact length l_2 and depth of cut, CBN/En9 steel	201
Figure 8.16	Evaluation of R_{t2} for dry grinding, $v_s = 30 \text{ m/s}$	202
Figure 8.17	Evaluation of R_{t2} for wet grinding, $v_s = 30 \text{ m/s}$	203
Figure 9.1	Prediction of contact length based on the contact length model	204
Figure 9.2	A boundary for the simplification, $l_e = l_{fr}$	204
Figure 9.3	A boundary for the simplification, $l_e = l_g$	204
Figure 9.4	The effect of R_t on the grinding contact length	205

Chapter 1 INTRODUCTION

Grinding is a cutting process in which material is cut off by small, extremely hard grits. Grits are bonded together to form a grinding wheel. The grinding wheel is rotated at high speed. Grinding is widely used to machine metallic and non-metallic materials. Metallic and non-metallic materials too hard to be cut by conventional single or multi-point tools can be machined by grinding, and also very close dimensional accuracy and fine surface texture of machined surfaces can readily be obtained.

Grinding is frequently the last operation of a high precision manufacturing process. For this reason it is necessary to satisfy the quality requirements of the final product. The quality of the product includes three aspects: (i) size and shape accuracy; (ii) surface texture and (iii) subsurface integrity. These three features influence mechanical and metallurgical properties of the product, for example fatigue life, stress corrosion, wear and distortion.

1.1 The Importance of the Contact Length in Grinding

The grains of a grinding wheel are irregularly distributed. The grains also possess indeterminate and variable working angles. Under the microscope, it can be seen that often the grains possess large negative rake angles. The grains develop wear flats after grinding for a few minutes. For these reasons, the material removal process in grinding is characterised by high power consumption per unit volume of material removed, and an elevated temperature of the ground surface. The temperature rise of the ground surface depends amongst other factors on the shape, size and nature of the grinding contact zone.

The indeterminacy of the shape of the grinding contact zone, where material is

removed makes it difficult to characterise the grinding process.

The large average negative rake angle, typically -70 to -80 degrees causes the workpiece surface to plastically deform to a large extent [1, 2]. The plastic deformation has a strong influence on the integrity of the ground surface.

Compared with other cutting tools a grinding wheel has a very low modulus of elasticity [1, 2]. Consequently, the real contact length of the grinding contact zone, and the real contact area are significantly different to the values based on a traditional geometric analysis. For example, Makino [3] suggests that for conventional grinding operations the real contact length may be approximately twice the geometrical contact length.

The real contact length and the real contact area significantly influence the determination of grinding temperatures, surface stresses and subsurface integrity of the workpiece. It is therefore necessary to investigate whether the size of the contact zone can be adequately determined.

1.2 Aims

The aims of the investigation were to determine the length of the contact zone in grinding and to seek to provide a theoretical basis for the prediction of contact length.

1.3 Scope of the Investigation

A thorough study of previous research was undertaken and it was found that previous studies failed to provide a satisfactory theoretical basis for the prediction of contact length in grinding. A theoretical study was therefore undertaken on the effect of the elastic deflections, plastic deflections and the grinding geometry on contact length. As

a result of the study a new grinding contact model was developed. The new model was compared with previous models.

An experimental investigation was undertaken to obtain measured values of contact length. Experiments were performed and grinding parameters such as the real depth of cut, the real table speed, the real grinding contact time, grinding force and grinding temperature were measured.

Values of contact length from the theoretical model were compared with experimental values using a statistical analysis. As a result the contact model was refined.

The last part of the work concerned the application of the contact length model to the prediction of grinding performance.

Chapter 2 REVIEW OF PREVIOUS WORK

2.1 The Grinding Contact Zone

The real size of the contact zone is difficult to measure accurately because of the small physical dimensions of the contact zone in conventional grinding. Measurement is complicated by deflection of the wheel and workpiece due to both force and heat and the instantaneous action of grains on the workpiece [4, 5]. Different methods of measurement and different assumptions concerning the nature of the contact zone have led to different definitions of contact zone parameters.

2.1.1 Definitions of contact length

ISO 3002 part 5 [6] gives the following parameters which are to be used to describe the contact length in grinding.

- (i) Geometric grinding arc: The contact geometry for straight surface grinding is illustrated in Figure 2.1. The curve formed by the intersection of the geometric grinding contact surface and a plane perpendicular to the grinding wheel axis and passing through the principal point.
- (ii) Geometric contact length l_g : The length of the geometric grinding arc is shown in Figure 2.1. Figure 2.1 illustrates a grinding wheel of diameter d_s rotates with a peripheral velocity v_s , a depth of cut a which translates past the workpiece at a velocity v_w . Neglecting deflections of the wheel and workpiece, the geometrical contact length is l_g . For surface grinding and a cylindrical grinding wheel shape, l_g can be expressed as

$$l_g = A \cdot B = \frac{d_s \theta}{2} \quad (2.1)$$

where

$$\cos\theta = 1 - \frac{2a}{d_s} \quad (2.2)$$

Since $2a \ll d_s$, the small-angle approximation applies:

$$\cos\theta = 1 - \frac{\theta^2}{2} \quad (2.3)$$

Combining with Equations 2.1 to 2.3 leads to the result:

$$l_g = (a d_s)^{0.5} \quad (2.4)$$

This expression for the arc length l_g can be shown to be identical to the chord length AB. l_g is also called the static contact length.

A similar analysis can be applied to the external and internal grinding contact geometry. As a result, the contact lengths for surface, external and internal grinding can all be combined into the single equation:

$$l_g = (a d_e)^{0.5} \quad (2.5)$$

Where d_e is the "equivalent wheel diameter" and is defined by

$$d_e = \frac{d_s d_w}{d_w \pm d_s} \quad (2.6)$$

The positive sign is for external grinding, the negative sign is for internal grinding and $d_w = \infty$ applies for straight grinding.

- (iii) The real geometric contact length, l_{gr} is defined as the length of the contact arc taking into account the effect of machine deformation on the depth of cut.

$$l_{gr} = (a_e d_e)^{0.5} \quad (2.7)$$

where the real depth of cut, a_e , is less than the incremental radial infeed, a , due to machine deformations. If depth of cut is measured directly, the need to make a distinction between a and a_e can be avoided.

- (iv) Kinematic grinding arc: The curve formed by the intersection of the kinematic grinding contact surface and a plane perpendicular to the grinding wheel axis and passing through the principal point.

- (v) Kinematic contact length l_k : The length of the kinematic grinding arc is shown in Figure 2.1.

For the convenience of analysis, the grinding wheel action is analysed in the same way as milling, the cutting points around the wheel periphery are assumed to be equally spaced apart by a distance L_s . The grinding situation is illustrated in Figure 2.1 for straight up-grinding.

A cutting point in up-grinding begins its contact with the workpiece at point E, and follows the curved path to point B₁. The cutting path EA₁DB₁ relative to the workpiece is a trochoid consisting of the superposition of the circular motion at velocity v_s and tangential motion along the workpiece at velocity v_w . The previous cutting point followed the same geometrical path shape but displaced along the workpiece surface by the distance BB₁ which is the feed per cutting point S where

$$S = L_s \frac{v_w}{v_s} \quad (2.8)$$

The undeformed chip for up-grinding is the cross-hatched area BEB₁ for each case in Figure 2.1.

Relative to an x-y coordinate system with its origin at A₁ fixed to the workpiece in Figure 2.1, it can be shown that the trochoidal path of a cutting point initially at the origin moves horizontally:

$$x = \frac{d_s}{2} \sin\theta_1 \pm \frac{d_s v_w}{2 v_s} \theta_1 \quad (2.9)$$

where the positive sign is for up-grinding and the negative sign is for down-grinding.

Vertically

$$y = \frac{d_s}{2} (1 - \cos\theta_1) \quad (2.10)$$

as the wheel rotates through the angle θ_1 . Since θ_1 is a very small angle ($\theta_1 < \theta$)

Equations 2.9 and 2.10 can be simplified to

$$x = \left(1 + \frac{v_w}{v_s}\right) \frac{d_s \theta_1}{2} \quad (2.11)$$

and

$$y = \frac{d_s \theta_1^2}{4} \quad (2.12)$$

Eliminating θ_1 leads to the relationship for the cutting path

$$y = \frac{x^2}{d_s \left(1 \pm \frac{v_w}{v_s}\right)^2} \quad (2.13)$$

which is a parabola instead of a trochoid.

An equation for the trochoidal cutting path has also been derived for external and internal cylindrical grinding. As with straight grinding, the trochoidal cutting path can be approximated by a parabola :

$$y = \frac{x^2}{D} \quad (2.14)$$

where for external grinding

$$D = \frac{d_s \left(1 \pm \frac{v_w}{v_s}\right)^2}{1 \mp \frac{v_w d_s}{v_s d_w} \left(2 \pm \frac{v_w}{v_s}\right)} \quad (2.15)$$

and for internal grinding

$$D = \frac{d_s \left(1 \pm \frac{v_w}{v_s}\right)^2}{1 \pm \frac{v_w d_s}{v_s d_w} \left(2 \pm \frac{v_w}{v_s}\right)} \quad (2.16)$$

The upper sign is for up-grinding and the lower sign for down-grinding. For surface grinding $d_w = \infty$, both of the above expressions for D reduce to the denominator of Equation 2.13.

The length of the cutting path EA₁B₁ for straight grinding as shown in Figure 2.1 can be obtained from the equation of the cutting-path motion. The length of EA₁ in each case can be taken as half the feed per cutting point. The total cutting-path length l_k can be expressed as

$$l_k = \int_0^\theta dl_k + \frac{S}{2} \quad (2.17)$$

where

$$dl_k = \left(\left(\frac{dx}{d\theta_1} \right)^2 + \left(\frac{dy}{d\theta_1} \right)^2 \right)^{\frac{1}{2}} \quad (2.18)$$

Substituting for x and y from Equations 2.11 and 2.12 and integrating leads to the result

$$l_k = \left(1 \pm \frac{v_w}{v_s} \right) \frac{d_s \theta}{2} + \frac{\theta^3}{6 \left(1 \pm \frac{v_w}{v_s} \right)} + \frac{S}{2} \quad (2.19)$$

Since θ is a small angle, the second term is negligible compared with the first one and the quantity $d_s \theta/2$ corresponding to the arc length AB can be approximated by its chord length $(a d_s)^{1/2}$.

Therefore:

$$l_k = \left(1 \pm \frac{v_w}{v_s} \right) (ad_s)^{\frac{1}{2}} + \frac{L_s v_w}{2 v_s} \quad (2.20)$$

or

$$l_k = \left(1 \pm \frac{v_w}{v_s} \right) l_g + \frac{S}{2} \quad (2.21)$$

Repeating the analysis for external and internal grinding leads to the same result as Equation 2.21 with l_g given by Equation 2.5 with d_s replaced by d_e . The cutting path is longer for up-grinding than for down-grinding.

The cutting-path length l_k as given by Equation 2.21 can be considered as a kinematic correction to the static contact length l_g .

Since the value of S in Equation 2.21 is small, the kinematic length l_k can be simplified to

$$l_k = \left(1 \pm \frac{1}{q}\right) l_g \quad (2.22)$$

where $q = v_s/v_w$ is the speed ratio.

The real kinematic contact length l_{kr} is

$$l_{kr} = \left(1 \pm \frac{1}{q}\right) l_{gr} \quad (2.23)$$

These definitions of l_g and l_k involve purely geometric and kinematic concepts.

(vi) Real contact length l_e : The length of the real grinding arc.

In comparison with the previous definitions, the definition of the real contact length between wheel and workpiece which should be evaluated while grinding takes place is rather ambiguous. Generally speaking, it is not easy to define the principal point during a grinding operation. In many publications, l_g and l_k are used as an approximation for the real contact length between the wheel and workpiece. However, it will be shown that l_g and l_k do not accurately represent the real contact length because of the increase in contact length due to:

- deformation of the grinding wheel
- the effect of surface topography of the grinding wheel on deformation
- deformation of the workpiece
- the effect of workpiece roughness on deformation of the workpiece

Makino [3] suggested that for conventional grinding operations l_e may be approximated by $2 l_g$.

Verkerk [7] stated that “The contact length is defined by the interference length between the abrasive grain in the wheel surface and the workpiece”. The tips of active grains lie at different diameters so the interference lengths for each grain will differ from each other. It is therefore possible to interpret Verkerk’s definition as the maximum contact length measured, or some measure of average contact length.

2.1.2 Definitions of contact area

(i) The geometric contact area A_g

The idealised surface of mutual contact between wheel and workpiece if deformation, wear and roughness of wheel and workpiece are neglected is defined as the geometric contact area A_g .

(ii) The kinematic contact area A_k

If the tangential table feed is considered and both the wheel and workpiece are undeformed the contact area is called the kinematic contact area A_k .

(iii) The apparent contact area A_a

The apparent contact area is the contact area which exists when considering feed motions together with deformations and surface characteristics of both wheel and workpiece. The apparent contact area includes the areas between the real points of contact.

(iv) The real contact area A_r

The real contact area is the contact area between active grains and the workpiece in the contact zone. It is subject to the same lack of clear definition as the real contact length l_e .

2.2 Effects of Contact Length on the Grinding Process

Rowe [8] stated that the length of the contact zone between the grinding wheel and the workpiece has a significant effect on almost all physical phenomena of interest in the grinding process. It has been found that contact length is particularly relevant to the maximum surface temperature of the workpiece, the grinding wheel wear rate, the generation of residual stresses and the attenuation of higher order frequencies of vibration.

2.2.1 The temperature distribution

If other factors remain unchanged, the workpiece temperature is inversely proportional to the square root of contact length as illustrated by Equation 2.24 [8]. The effect of the large real contact length compared with the geometric contact length is that the grinding zone temperature is reduced for a particular value of specific energy e_c .

$$\theta = \frac{0.754 R e_c v_w a}{(v_w l_e)^{0.5} (k \rho c)_w^{0.5}} \quad (2.24)$$

Vansevenant (1987) [9] employed an analysis which accounted for the superposition of a surface cooling effect of the coolant on the workpiece. It was proposed that the temperature decreased with two variables: a decreasing heat source velocity v_w and an increasing contact length l_e . “In practice this means that longer contact lengths lead to more effective cooling. The coolant was in contact with the workpiece during a longer time.” [9]

2.2.2 Stress and residual stress distribution

Residual stresses in grinding arise due to thermal stresses, phase transformation stresses after heating and due to the mechanical deformation of the workpiece surface.

To analyse residual stresses the histories of the stress distribution and the temperature distribution in the workpiece during the grinding process need to be known. First, the contact length must be identified [9].

2.2.3 Wheel wear based on the thermal stress hypothesis

Hahn (1962) [1] measured the rate of wheel wear for various force intensities for several wheels of different hardness. As expected, a J grade wheel wears more rapidly than an N grade wheel. This was explained on the basis of the thermal stress hypothesis by considering the length of the interference zone. The modulus of elasticity for the J grade wheel was approximately 41×10^3 MN/m² while that for the N grade wheel was about 61×10^3 MN/m² and that for steel is about 207×10^3 MN/m². Consequently, the grinding wheel acted as a soft elastic body relative to steel, and under an applied force flattened out in the zone of contact, thus creating a finite length of contact. For the N grade wheel this length was less than for the J grade wheel and accordingly the heat was said to be reduced. This was found to result in a lower rate of wear for the N grade wheel.

It was also found that there was a “threshold” length below which thermal stress wear did not occur. If a wheel was operated in this region it glazed. This was explained by the mechanism of solubility wear and plastic deformation by which flat areas were developed on the grains of the wheel and persisted indefinitely. It was suggested by Hahn that an uniform and controlled rate of wheel wear was caused by thermal stresses set up in the surface layers of the grain, which causes a gradual flaking out from the grain and the development of wear flats. It was proposed that the rate of wheel wear is related to the quantity of heat injected into the grain. As a result, the rate of wheel wear for hard and soft wheels is a function of the actual length of the interference zone, and is not dependent upon the mechanical strength of the wheel until gross breakdown of the wheel surface occurs.

2.2.4 Grinding stability performance

Rowe [10] analysed the problem of work-regenerative waviness encountered in centreless grinding with respect to the dynamic characteristics of the machine and the effect of the geometrical configuration of the workpiece support system. Rowe showed that higher frequency waviness was inhibited by the finite arc of contact between the wheel and the workpiece. The attenuation depends on the amplitude. Greater amplitudes of vibration are attenuated more than smaller amplitudes. Malkin [11] summarised the relationship between contact length and vibration in the grinding process. Regenerative chatter waves can develop both on the wheel and on the workpiece. However, the vibration frequency causing regeneration on either body is limited by wheel-workpiece contact. Vibration frequencies with half wavelengths shorter than the contact length should be strongly attenuated by a mechanical filtering effect for workpiece wave filtering, and a similar effect applies to the wheel [12]. The break frequencies above which filtering should occur in this way are readily obtained as

$$f_w = \frac{v_w}{2 l_e} \quad (2.25)$$

for the workpiece and

$$f_s = \frac{v_s}{2 l_e} \quad (2.26)$$

for the wheel, where l_e is the contact length. The break frequencies for internal grinding tend to be somewhat lower than for external grinding owing to longer contact lengths.

2.2.5 Models for quantitative prediction and optimisation

Contact length is a basic parameter used in analysis, simulation and adaptive control of

the grinding process. Vansevenant (1987) [13] published an improved analysis for the prediction of residual stress in grinding. Several published contact length models refer to this analysis [13]. Rowe [14] presented an Intelligent CNC Grinding System. In this system, several grinding process models were included and the importance of a quality contact length model was mentioned. Process modelling plays an important role in optimisation of the grinding process. The quality of the process optimisation strategy depends to a large degree upon the accuracy of the grinding model used. The model may either be physically or empirically based. An accurate mathematical model is required which can be used to predict surface damage due to either thermal damage or residual stresses.

The need for more readily available and reliable quantitative machining performance information has been recognised for decades and re-emphasised in a recent CIRP survey. “In view of the wide variety of machining operations and numerous influencing variables for each operation the development of models for the quantitative prediction of machining performance characteristics represents a formidable task. Nevertheless such models should be achieved to satisfy the need for the effective and efficient use of machining as well as to establish machining on a sound scientific and quantitative basis.” [15] Therefore, modelling grinding contact length has great significance for the advancement of grinding technology.

2.3 Factors Influencing Contact Length in Grinding

Many authors published mathematical models to calculate the real contact length as a function of grinding parameters. Some of the models have an analytical base, others are empirical. Table 2.1 is a summary of typical published models. Table 2.2 is a summary of typical published experimental results.

Table 2.1 A Summary of Typical Published Models

Author	Typical values $R_l = l_c/l_g$	Equation
Brown	2.06 - 2.88	$l_c = 2 [A d_s]^{0.5} \left[\frac{F_n'}{l_c M} \right]^{\frac{1}{3}} + B [F_n']^{0.5}$
Lindsay		$l_c = \frac{[d_{eq} F_n']^{\frac{1}{3}}}{4.66 \{ 44.6 - (1.33 HL + 2.2 SL - 8) \}}$
Verkerk		$l_c = l_{gr} \left[1 + \frac{4 C_v h_{eq}}{q} (n_v - 1) \right]^{0.5}$
Sauer		$l_c = \left[\frac{8 E_{eq} F_n'}{\frac{1}{r_{sd}} - \frac{1}{r_{su}}} \right]^{0.5}$
Aerens		$l_c = \left[\frac{C_A F_n' d_s}{E_{eq}} + a_{cr} d_s \right]^{0.5}$
Brandin		$l_c = [(a + R_t) d_s]^{0.5} + [R_t d_s]^{0.5}$
Quiroga		$l_c = [2 a_z r_{sd}]^{0.5} + [2 (a_{cr} + a_z) r_{sd}]^{0.5}$
Kumar	1.125 - 1.2	$l_c = \alpha \beta l_g$
Salje	1.01 - 6	$l_c = (1 + \frac{1}{q}) l_g$
Rowe, Qi	2 - 5	$l_c = (R_r^2 l_f^2 + l_g^2)^{0.5}$
Maris		$l_c = [a d_{eq}]^{0.5} [q]^{-0.216} e^{[-0.0205 q^{0.33} \ln(a)]}$

Table 2.2 A Summary of Typical Published Experimental Results

Author	Typical values $R_l = l_e/l_g$	Method
Makino	1.5 - 2	Thermocouple
Verkerk	1.5 - 3	Thermocouple
Brown	1.5	Quick-stop device
Gu	2 - 2.5	Thermocouple
Gu	1.9 - 3.0	Two-half slot
Zhou	1.4 - 2.2	Applied Power Source

2.3.1 Deflection

Lindsay and Hahn [2] calculated the real contact length by assuming that the individual grinding wheel grains were analogous to a spring system. They believed that in production grinding at workspeed above 0.5 m/s the wheel depth of cut is usually small compared to the elastic flattening of the grinding wheel given that the Young modulus for a vitreous bonded wheel is approximately one quarter that of steel. The depth of cut was assumed to be negligible in calculating the length of the interference zone between the wheel and the workpiece. Figure 2.2 shows an internal grinding wheel of diameter d_s in a workpiece of diameter d_w . The wheel surface is composed of abrasive grains, each of diameter, d_g . Each grain is assumed to be mounted on a spring of stiffness, k_g . The length of elastic contact l_c was found to be:

$$l_c = (d_{eq} F_n')^{1/3} / \{4.66 [44.6 - (1.33 HL + 2.2 SL - 8)]\} \quad (2.27)$$

where HL is the hardness factor of the grinding wheel:

Hardness grade:	H	I	J	K	L	M
HL	0	1	2	3	4	5

SL is the structure number of the wheel

ex.: wheel 60 L 5 has : $d_g = 0.41$, $HL = 4$, $SL = 5$

In reference [2] it was shown how the Equation 2.27 was developed. The equation must be used with inch and lb units.

Lindsay and Hahn's work revealed the importance of grinding wheel hardness for determination of contact length. It may be noted that grinding wheel hardness is related to the Young modulus of the grinding wheel [16].

Lindsay's model fails to take account of the depth of cut and to recognise the importance of surface roughness. The length of the interference zone is only partly determined by the elastic properties of the wheel and the workpiece, the wheel depth of cut is also an important factor.

Brown, Saito and Shaw [17] proposed that the total mutual deflection of the grinding wheel and the workpiece was the sum of two deflections, (i) the elastic deflection of the grain-workpiece contact when the shape of the grain mounting surface was assumed circular, with no elastic deflection of the wheel itself as shown in Figure 2.3(a). (ii) Elastic deflection of the wheel-workpiece contact, assuming the individual grinding grains remain undeformed as shown in Figure 2.3(b). The extent of each deflection on the contact lengths were calculated using the Hertz contact theory and measured by experiment.

The contact length according to Brown, Saito and Shaw is given by Equation 2.28

$$l_c = l_c' + r' \\ = 2 (A d_s)^{0.5} [F_n / (l_c M)]^{1/3} + B F_n^{0.5} \quad (2.28)$$

where: $A = [9 \pi (K_g + K_w)^2 / (8 d_g)]^{1/3}$

$$B = 1.6 [\pi d_s (K_s + K_w)]^{1/2}$$

$$K_s = (1 - \nu_s^2) / (\pi E_s)$$

$$K_w = (1 - \nu_w^2) / (\pi E_w)$$

$$K_g = (1 - \nu_g^2) / (\pi E_g)$$

l_c = contact length according to the Brown, Saito and Shaw model

l_c' = contact length due to the elastic deflection of the grain-workpiece contact

r' = contact length due to the elastic deflection of the wheel-workpiece contact

d_s = wheel diameter

d_g = diameter of the average grain in the wheel

F_n' = specific normal grinding force

C = number of projecting grains per square millimetre of wheel surface
which are in contact with workpiece

ν_s = Poisson's ratio of wheel

ν_w = Poisson's ratio of workpiece material

ν_g = Poisson's ratio of grain material

E_s = modulus of elasticity of wheel

E_w = modulus of elasticity of workpiece material

This model has some disadvantages. (i) The model does not take into account the geometric effect of the true depth of cut which is the most important influence on the grinding contact length particularly at large depth of cut. (ii) The model considers elastic deformation but does not consider the influence of plastic deformation between the grain and the workpiece on the contact length. (iii) The topography of the wheel and the workpiece are not considered. It will be shown that these effects are more important than the effect of the elastic deflection.

Hideo Tsuwa (1975) [18] studied the length of the contact arc during the plunge cut grinding process. It was found that the arc length was 20% to 30% bigger than the geometric value. The length of the contact arc increased with an increase of grinding force. This phenomenon was said to be due to the fact that the wheel and the workpiece deform elastically in the grinding process as shown in Figure 2.4. By using Hertz static contact models the following relationship was obtained:

$$l_c = \{d_e(a + \delta)\}^{1/2} + (d_e \delta)^{1/2} \quad (2.29)$$

where δ = the extent of the elastic deformation

Since it is difficult to measure or to calculate the extent of the elastic deformation, δ , this formula is difficult to use.

Kumar and Shaw (1981) [19] believed that thermal effects were negligible and that local wheel - workpiece deflections most strongly affected the real contact length. The local wheel-workpiece deflections consisted of two components: (i) Elastic deformation of the wheel resulting in an increased local wheel diameter; (ii) Elastic deformation of the workpiece material resulting in a concave surface. The deflections of the wheel and the workpiece were analysed separately by approximating the contact to the situation of a work roll in metal rolling. Kumar and Shaw developed a relationship to include the elastic deflection and the depth of cut.

Kumar and Shaw's rigid workpiece model is illustrated in Figure 2.5(a). Assuming the workpiece to be rigid, the contact length caused by wheel deformation was given by Equation 2.30

$$l_{II} = \alpha l_g = \left[\left(1 + \frac{\delta_s}{a_e} \right) (a_e d_e) \right]^{0.5} \quad (2.30)$$

where l_{II} = contact length due to wheel deformation
 d_e = the original wheel diameter
 a_e = deformed wheel depth of cut
 δ_s = the maximum elastic displacement of the surface of the wheel due to
the load exerted by the work on the wheel

$$\alpha = \left(1 + \frac{\delta_s}{a_e} \right)^{0.5}$$

To determine δ_s it was assumed that a uniformly distributed pressure acts along the wheel-workpiece contact length (l_g) over the width of the wheel, b . This is similar to the loading of work rolls in metal rolling.

The solution for loading of work rolls by Chiu, Weinstein and Zorouski [19] where $2b/d_e$ approaches 0, is given by

$$\delta_s = \frac{0.19 p d_e (1 + v_s)}{E_s} \quad (2.31)$$

where p is the pressure between the wheel and the workpiece

$$p = \frac{F_n}{l_g b}$$

A rigid wheel was assumed and the contact length caused by workpiece deformation was as shown in Figure 2.5(b). The workpiece material deformed to a concave surface due to the load exerted by the wheel and d_w was the effective loaded diameter of the workpiece. Since this contact is similar to the contact in internal grinding, the contact length can be derived as follows

$$l_{III} = \beta l_g = \left[\frac{a_e d_e}{1 - \frac{\delta_w}{a_e}} \right]^{0.5} \quad (2.32)$$

where l_{III} = contact length due to workpiece deformation

δ_w = the maximum elastic displacement of the surface of the workpiece

due to the load exerted by the wheel on the workpiece

$$\beta = \left[\frac{1}{1 - \frac{\delta_w}{a_e}} \right]^{0.5}$$

Since the arc of contact between the wheel and workpiece is very small, it was assumed that this region was a straight boundary with a uniformly distributed pressure p acting on it. The maximum displacement, δ_w for the loaded condition was given by Timoshenko and Goodier [19] as

$$\delta_w = \frac{-2 p l_g}{\pi E_w} \ln\left(\frac{l_g}{2}\right) \quad (2.33)$$

The contact length by Kumar's model was given by equation 2.34

$$l_c = \alpha \beta (d_e a_e)^{0.5} \quad (2.34)$$

The results predicted by this model indicated that the real contact length was 15 % larger than the geometrical contact length. Extrapolated results were used to estimate the elastic deflections of a smooth contact situation. Furthermore, this model did not consider the plastic deformation of the grinding zone nor the real contact area nor the effect of surface roughness on the loaded contact area. It will be argued that these have a stronger influence on the contact length than the elastic deflection.

Aerens [9] also developed a contact length model based on the theory of Hertzian contact of two bodies. Figure 2.6(a) shows a deformed grinding wheel in contact with a flat workpiece. Figure 2.6(b) shows the same wheel and workpiece as though separated from each other but where the contact arc is unchanged. Two equations were obtained for the calculation of the real contact length.

- (i) The calculation of the geometric contact length with the deformed wheel radius is given by:

$$l_c = (d_{sd} a_e)^{0.5} \quad (2.35)$$

- (ii) The Hertz equation for two cylinders in contact is:

$$l_c = \left[\frac{C_{Aa} F_n d_{eqH}}{E_e} \right]^{0.5} \quad (2.36)$$

where d_{sd} = the diameter of the deformed wheel
 d_{eqH} = equivalent diameter according to Hertz
 a_e = real depth of cut
 C_{Aa} = coefficient dependent on the geometry of the bodies in contact
 E_e = equivalent modulus of elasticity

$$E_e = \frac{E_s E_w}{(E_s + E_w)} \quad (2.37)$$

The two bodies which were in contact, were not an outer cylinder with a flat workpiece, but an outer cylinder with an inner cylinder. The outer cylinder has the diameter of the undeformed grinding wheel and the inner cylinder the diameter of the deformed grinding wheel. According to Hertz the equivalent diameter is given by

$$d_{eqH} = \frac{d_s d_{sd}}{(d_s + d_{sd})} \quad (2.38)$$

where d_s = the diameter of the undeformed grinding wheel
 d_{sd} = the diameter of the deformed grinding wheel

The solution of the contact length from equations 2.35, 2.36 and 2.38 is given by

$$l_c = \left[a_e d_s + \frac{C_{Aa} F_n d_s}{E_e} \right]^{0.5} \quad (2.39)$$

The coefficient C_{Aa} is dependent on the workpiece material.

2.3.2 Surface roughness

Brandin [9] supposed that the difference between geometric contact length and the real contact length is only due to the geometrical effect of the roughness of the workpiece as illustrated in Figure 2.7.

$$l_c = [(a + R_t) d_s]^{0.5} + [R_t d_s]^{0.5} \quad (2.40)$$

where R_t = the surface roughness of the workpiece (peak to valley)

Brandin's model only considers the effects of the surface roughness of the workpiece on the maximum value of the true depth of cut but not the effect of the roughness on the force equilibrium contact condition within the contact zone. Brandin's equation takes no account of the fact that the average geometric contact length is unchanged by surface texture. Furthermore, the topography of the grinding wheel was not considered in this model.

Some papers also considered thermal expansion[20].

2.4 Contact Length Measurements

Contact length has been extensively measured using a diversity of measuring techniques. The measuring techniques can be mainly grouped into three groups.

2.4.1 Static loading tests

Using static loading of the wheel, Hahn and Lindsay [21] measured the length of the contact zone. The grinding wheel was pressed on a polished workpiece with force intensities comparable to those occurring in grinding, and then slightly oscillated relative to the workpiece. The length of the scratch pattern left on the workpiece was taken as representing the length of the wheel-workpiece interference zone in grinding.

2.4.2 Sudden disengagement methods

(i) A patch-grinding technique

Brown, Saito and Shaw [17] observed the local elastic deflections by a grinding technique using a small patch of grains that overcame the difficulty of separating wheel and workpiece deflections from the general deflections of the machine frame and the grinding wheel spindle. They found that the radii of cut at patch entry and exit were greater than that of the patch and that patches less than 45 degree arc length took a shallower cut than the complete strip-although both had the same radius. They explained the phenomena by considering the local elastic deflection of the wheel. Kumar and Shaw [22] suggested a method to obtain the deformed wheel-workpiece contact length which can be used to estimate local wheel-workpiece deflection. The method involved taking cuts on a flat workpiece by a specially-dressed patch or cluster (1/8 in x 1/8 in, about 3 mm x 3 mm) on the peripheral surface of the wheel. The workpiece could be withdrawn when the cluster was out of contact with the workpiece. Using a cluster overcut fly grinding technique [22, 23] Kumar and Shaw [19] investigated the wheel-workpiece contact length during grinding. They found that the influence of local wheel-workpiece deflection on contact length is relatively minor, about 15%, and that the predominant effect is due to wheel deflection and not workpiece deflection.

(ii) Methods using quick-stop devices

Using a quick-stop device which enabled the wheel to be suddenly disengaged from the workpiece, Sauer and Shaw [24] measured the contact length in surface grinding from which they calculated the deformed wheel radius. Sauer and Shaw deduced that the deformed wheel radius was larger than the normal wheel radius. Employing an explosive quick-stop device, Brown, Wager and Watson [25] separated the wheel and workpiece and measured the deformed wheel-workpiece contact length by taking Talysurf traces across the grooves cut as well as by the optical examination of the groove. They found the deformation wheel-workpiece contact length to be about 50% larger than the geometric contact length. Some individual grains were observed to take

deeper cuts in the exit region of the groove, which they suggested was due to the relaxation of local elastic deflection between the wheel and workpiece.

2.4.3 Thermocouple methods

Makino, Suto and Fukushima [3] measured the real contact length corresponding to particular settings of depth of cut by employing the thermocouple technique introduced by Peklenik. The real contact length was found to vary between 1.5 to 2 times the geometric contact length. The thermocouple method was also used by Verkerk [7], to measure the contact length in external cylindrical grinding. The contact length was obtained by multiplying the wheel-thermocouple contact time with the workspeed. He found that for a certain depth of cut, the real contact length was comparatively longer at small wheel-to-workspeed ratio which was attributed to larger grinding forces for greater workspeeds. Tsuwa, Yawada and Kawamura [18] found the actual value of the contact length between the wheel and workpiece in surface grinding to be 20-30% greater than the theoretical value, with this arc length increasing relative to an increase of grinding force. Tsuwa, Yawada and Kawamura considered that this phenomenon occurred due probably to the fact that the wheel and workpiece deform elastically in the grinding process. Under the assumption that the quantities of the elastic deformation near the contact arc can be found, using Hertz static contact model, they obtained a quantified relationship. Based on the thermocouple technique, Gu [26] and Zhou [27] developed the Critical-Contact State (CCS) Method and the Applied-Power-Source (APS) Method. Gu found that the contact zone measured by the CCS Method is approximately 30% longer than the results obtained by the conventional thermocouple method. The APS method by applying a voltage source produced a more intense signal. The experiment showed that, compared with the results of the CCS method, the results of the APS method were sometimes ten percent longer.

Other methods have been used to analyse the grinding contact zone. Pandit and

Sathyanarayanan [28] and Pandit [29] employed the Dynamic Data System (DDS) approach for the analysis of wheel-workpiece interaction in the surface grinding operation.

Considerable differences in results have been reported by a number of authors based on different measuring techniques. The advantages and disadvantages of the different measuring methods are discussed and, based on the conclusions reached, an experimental measuring method for this investigation will be selected and established.

2.5 Comparison of Experimental Methods

The advantages and disadvantages of the main methods are compared below.

2.5.1 The two-half-slot grinding technique

The two-half-slot grinding technique of Gu and Wager [20, 26] is illustrated in Figure 2.8 (a). The grinding wheel has two half slots axially displaced and oriented at 180 degrees to each other on the wheel periphery. When the workpiece was ground with this method to an appropriate depth, the workpiece surface consisted of a number of alternately raised sections, as shown in Figure 2.8 (b). One side of each raised section is the profile of the contact zone as shown in Figure 2.8 (c). The traces on these profiles give evidence on the contact zone similar to that of the passage of single grains. A profilometer can then be used to trace the arc of contact at one side of a raised section in the table moving direction to obtain the length of the contact zone [20, 26].

Advantages of the two-half-slot grinding method are:

- (i) The stiffness of the measurement system is almost the same as the stiffness in the normal grinding condition. Thus the magnitude of the deflection in the two conditions will be the same.

- (ii) Most of the cutting groove traces visible on the surface of the ground contact zones are those of the last active grains. The real contact length, the diameter of the surface curve and the surface topography can therefore be measured.
- (iii) The Rank Taylor Hobson Form Talysurf or a microscope can be used to make the measurements.

Disadvantages of the method are:

- (i) Measuring l_e after grinding instead of in-process, means that the shape of the contact zone or the length of contact measured might be different to the real shape or length because the force, temperature and deflections under which the contact length is measured are different.
- (ii) The quality of the edges of the slots made on the test grinding wheel is not easy to control. The quality of the edge of the slot influences the measured contact length and the contact shape since it is the grains located at the edges of the slots that are used to measure the grinding contact shape and the contact length.
- (iii) The vibrations and variations of grinding force caused by the edges of the slots, when the edges enter or exit the contact zone, will influence the shape of the grinding contact.
- (iv) The method is only suitable for straight surface grinding.
- (v) The method measures the cutting and ploughing regions but would be likely to underestimate the rubbing region.

2.5.2 The cluster overcut fly grinding method

The cluster overcut fly grinding method of Kumar and Shaw [22] is illustrated in Figure 2.9. This method employed a cluster of dressed grains formed directly on the surface of a grinding wheel by removing with a diamond all but a “length of cluster, L , times width of cluster, b ” area. When the wheel was used in a plunge surface grinding situation, a groove with a width, b , was produced. Moreover, if the table speed, v_w ,

was made very small compared to the wheel speed, v_s , and the grinding wheel was instantaneously withdrawn from the work, it would leave a fingerprint of the final arc of contact between the wheel and the work from which l_e may be measured. A profilometer can then be used to trace the arc of contact at the end of the groove in the work feed direction to obtain the actual chip length [22].

Advantages of the cluster fly grinding method is:

Individual traces made by individual active grains on the surface are clearer than those made by the two-half-slot measuring technique. By making the length of the cluster shorter than the spacing of the successive active grains on the surface of the grinding wheel, it is assured that along the grinding direction, only one grain is associated with each grinding trace.

Disadvantages of the method are:

- (i) To obtain an impression of the arc of contact between the wheel and the workpiece, the grinding wheel has to be instantaneously withdrawn from the workpiece which is difficult to achieve.
- (ii) Furthermore the work speed, v_w , has to be very small compared to the workspeed in a normal grinding operation to ensure that the undeformed chip thickness is the same as a normal grinding condition.

2.5.3 The thermocouple technique

The thermocouple technique of Makino, Suto and Fukushima [3] is illustrated in Figure 2.10. This is a way to measure the contact length by determining the distance that a fixed point (a thermojunction) on the workpiece surface travels during the table motion from the beginning to the end of contact with the grinding wheel surface. When the wheel grinds the insulated thermocouple pole in the workpiece surface, an electromotive force signal is generated within a circuit made by the thermocouple pole

and the workpiece. A stable thermojunction can be achieved if the insulation is thin enough.[3, 7, 26]

Advantages of the thermocouple method are:

- (i) It is an in-process method of measuring the time of contact, so the system stiffness, deflections, force and temperature are the same as in the real grinding condition.
- (ii) In addition to the contact length, other valuable information such as the cutting point spacing and temperature distribution along the surface of the workpiece and wheel, can be obtained.
- (iii) This method can be used in either surface grinding or cylindrical grinding.

Disadvantages:

- (i) The real contact length by this method is the product of work speed (v_w) and the time period of the thermal contact signal (t_c). The measured contact length is therefore obtained indirectly and the accuracy is dependent on the accuracy of the parameters v_w and t_c . In addition to this, the beginning and end of the thermal signal is not the same as the beginning and end of the contact between the grains and the workpiece because the elevated temperature persists outside the contact zone.
- (ii) The technique of assembling the thermocouple is important. Difference in the parameters chosen such as the grade, the size, the arrangement and the thickness of the insulation of the thermocouple can increase or reduce the measured contact length by approximately 25-35 percent [20].

2.5.4 The applied power source technique

The applied power source technique of Zhou and Lutterwelt [27] is illustrated in Figure 2.11. When the wheel grinds the insulated electrode in the workpiece surface, a circuit is made between the wire and the workpiece and a contact signal is produced [20, 27].

(In Chapter 5 and Chapter 6, this method is described in more detail.)

Advantages of the applied power source method are:

- (i) The signal obtained by the applied power source method is more intense because the signal is derived from an applied voltage source. The signal also depends on the conductivity of the grains and the chips.
- (ii) It is an in-process method of measuring the time of contact, so the stiffness, deflection, force and temperature are the same as in the real grinding condition.
- (iii) This method can be used in either surface grinding or cylindrical grinding.

Disadvantages of the applied power source method are:

- (i) The temperature distribution along the surface of the workpiece and wheel, cannot be obtained.
- (ii) The real contact length is the product of v_w and t_c . The measured contact length is therefore obtained indirectly and the accuracy is dependent on the accuracy of measurement of v_w and t_c .
- (iii) The correct choice of the insulation thickness is important.

In Chapter 5, the applied power source method and the thermocouple method which were used in the experiments are described in more detail.

2.6 Conclusions

Based on the above review, it was concluded that:

- (i) Real contact length in grinding is much larger than the geometrical contact length.
- (ii) Real contact length represents the real grinding process. Better understanding of the nature of the real contact is required.

- (iii) Previous workers have mainly considered the effects of deflection and workpiece surface roughness on real contact length. No analysis has been published on how much the wheel topography and real contact area contribute to increase the apparent contact size.
- (iv) Several contact length models have been published, but those models have limited ability to predict the real contact length.
- (v) Several methods have been reported for measuring contact length, but the results from those methods differ greatly from each other.
- (vi) Real contact length requires further definition.
- (vii) It is concluded that, the applied power source method and the thermocouple method are the most appropriate methods to measure contact length. The applied power source method and the thermocouple method were selected for an experimental investigation.

Chapter 3 SURFACES IN CONTACT

Many engineering situations involve the non-conforming contact of bodies defined by smooth curves. All solid bodies have surface asperities. If these asperities are considered as small spherically shaped protuberances, the contact of two macroscopically flat bodies is more realistically represented by an array of spherical contacts deforming at their tips. A study of surface contacts requires a detailed understanding of the elastic and plastic deformation of contacting surfaces.

3.1 The Contact of Smooth Surfaces

In 1882, Hertz [30] argued that two bodies in contact can be described by their principal radii of curvature at the point 0 where the bodies first touch. The elastic deformation of the two bodies in contact can be approximated to that of two elastic half-spaces. The contact area is known in advance to be elliptical in shape, with an eccentricity determined by the relative curvatures of the two bodies at 0. The situation is shown in Figure 3.1 [31]. Two elastic bodies touch initially at the origin 0 of coordinate axes in which Oz is the common normal to the two surfaces and x - y is the common tangent plane. Each surface is considered to be topographically smooth on both the micro and the macro scales. On the micro scale this implies the absence or disregard of small surface irregularities which would lead to discontinuous contact or highly local variations in contact pressure. On the macro scale the profiles of the surfaces are continuous up to their second derivative in the contact region. The profile of each surface in the region close to the origin may be approximated by an expression of the form

$$z_1 = A_1 x^2 + B_1 y^2 + C_1 xy + \dots \quad (3.1)$$

where higher order terms in x and y are neglected. By choosing the orientation of the x and y axes, x_1 and y_1 , so that the term in xy vanishes, Equation 3.1 may be written:

$$z_1 = \frac{1}{2R'_1} x_1^2 + \frac{1}{2R''_1} y_1^2 \quad (3.2a)$$

where R'_1 and R''_1 are the principal radii of curvature of one of the two surfaces at the origin. R'_1 and R''_1 are the maximum and minimum values of the radius of curvature of all possible cross-sections of the profile. If a cross-sectional plane of symmetry exists one principal radius lies in that plane. A similar expression may be written for the second surface:

$$z_2 = \frac{1}{2R'_2} x_2^2 + \frac{1}{2R''_2} y_2^2 \quad (3.2b)$$

The separation between the two surfaces is given by $h = z_1 - z_2$. By transposing equation (3.1) and its counterpart to a common set of axes x y , one equation is obtained

$$h = \frac{1}{2R'} x^2 + \frac{1}{2R''} y^2 \quad (3.3)$$

where R' and R'' are defined as the principal relative radii of curvature.

A normal load P presses the surfaces into contact over an area A , causing distant points in the two bodies T_1 and T_2 to approach each other by a distance $\delta = \delta_1 + \delta_2$. It has been shown [31] that the shape and size of the area of contact and the contact stresses are uniquely determined by surface displacements $w_1(x,y)$ and $w_2(x,y)$ which minimise the total potential energy, provided that there is no interpenetration of the surfaces, i.e. provided

$$w_1(x,y) + w_2(x,y) + h(x,y) - \delta \geq 0 \quad (3.4)$$

By making use of Equation 3.3, an expression for the elastic displacements is obtained:

$$w_1(x,y) + w_2(x,y) = \delta - \frac{1}{2R} x^2 - \frac{1}{2R''} y^2 \quad (3.5)$$

where x and y are the common coordinates of S_1 and S_2 projected onto the x - y plane.

If S_1 and S_2 lie outside the contact area so that they do not touch it follows that

$$w_1(x,y) + w_2(x,y) < \delta - \frac{1}{2R} x^2 - \frac{1}{2R''} y^2 \quad (3.6)$$

To solve the contact problem, it is necessary to find the distribution of pressure transmitted between the two bodies at their surface of contact, such that the resulting elastic displacements normal to that surface satisfy Equation 3.5 within the contact area and Equation 3.6 outside it.

3.1.1 Spheres in contact

In the case of solids of revolution, the contact area is circular, having a radius, a . The boundary condition for displacements within the contact expressed in Equation 3.5 can be written

$$w_1(x,y) + w_2(x,y) = \delta - \frac{1}{2R} r^2 \quad (3.7)$$

where $(1/R) = (1/R_1 + 1/R_2)$ is the relative curvature.

A solution for the distribution of pressure which is compatible with Equation 3.7 was proposed by Hertz

$$p = p_0 \left\{ 1 - \left(\frac{r}{a} \right)^2 \right\}^{0.5} \quad (3.8)$$

The normal displacement is given by

$$w_z = \frac{(1-v^2)}{E} \frac{\pi p_0}{4a} (2a^2 - r^2) \quad (3.9)$$

for $r \leq a$.

The pressure acting on the second body is equal to that on the first, so by writing

$$\frac{1}{E^*} = \frac{(1-v_1^2)}{E_1} + \frac{(1-v_2^2)}{E_2} \quad (3.10)$$

and substituting the expressions for w_1 and w_2 into Equation 3.7, it is found that

$$\frac{\pi p_0}{4aE^*} (2a^2 - r^2) = \delta - \frac{1}{2R} r^2 \quad (3.11)$$

from which the radius of the contact circle is given by

$$a = \frac{\pi p_0 R}{2E^*} \quad (3.12)$$

The distance between approaching points in the two solids is given by

$$\delta = \frac{\pi a p_0}{2E^*} \quad (3.13)$$

The total load compressing the solids is related to the pressure by

$$P = \int_0^a p(r) 2\pi r dr = \frac{2}{3} \pi a^2 p_0 \quad (3.14)$$

The mean pressure p_m is:

$$p_m = \frac{P}{\pi a^2} = \frac{2}{3} p_0 = \frac{4E^*}{3\pi R} a \quad (3.15)$$

Hence the maximum pressure is $3/2$ times the mean p_m and the mean pressure p_m is proportional to the size of contact area, a . In a practical problem, it is usually the total load, P which is specified, so that it is convenient to write

$$a = \left(\frac{3PR}{4E^*} \right)^{1/3} \quad (3.16)$$

$$\delta = \frac{a^2}{R} = \left(\frac{9P^2}{16RE^{*2}} \right)^{1/3} \quad (3.17)$$

$$p_0 = \frac{3P}{2\pi a^2} = \left(\frac{6PE^{*2}}{\pi^3 R^2} \right)^{1/3} \quad (3.18)$$

These expressions provide absolute values for the contact size, compression and maximum pressure.

3.1.2 Cylinders in contact

When two cylindrical bodies with their axes parallel to the y -axis in the coordinate system in Figure 3.1 are pressed in contact by a force P per unit length, the problem becomes a two-dimensional one. The bodies make contact over a long strip of width $2a$ parallel to the y -axis. Hertz considered this case as the limit of an elliptical contact

when b was allowed to become large compared with a . Equation 3.3 for the separation between corresponding points on the unloaded surfaces of the cylinders becomes

$$h = \frac{1}{2} \left(\frac{1}{R_1} + \frac{1}{R_2} \right) x^2 = \frac{1}{2R} x^2 \quad (3.19)$$

For points lying within the contact area after loading, Equation 3.3 becomes

$$w_1(x) + w_2(x) = \delta - \frac{1}{2R} x^2 \quad (3.20)$$

and for points outside the contact region

$$w_1(x) + w_2(x) > \delta - \frac{1}{2R} x^2 \quad (3.21)$$

By using Hertz' approximation the displacements w_1 and w_2 can be obtained by regarding each body as an elastic half-space, but a difficulty arises here which is absent in the three-dimensional cases. This difficulty was discussed in detail by Johnson [31]. "The value of the displacement of a point in an elastic half-space loaded two-dimensionally could not be expressed relative to a datum located at infinity, in view of the fact that the displacement decreases with distance r from the loaded zone as $\ln r$. Thus w_1 and w_2 can only be defined relative to an arbitrarily chosen datum." So the approach of distant points in the two cylinders, denoted by δ in Equation 3.21, can take any value up to the real value depending upon the choice of datum. This means that the approach δ cannot be found without the consideration of the stress distribution within the bulk of each body.

The difficulty is avoided by differentiating Equation 3.21 to obtain a relationship for the surface gradients. Thus

$$\frac{\partial w_1}{\partial x} + \frac{\partial w_2}{\partial x} = -\left(\frac{1}{R}\right)x \quad (3.22)$$

Based on the analysis of line loading of an elastic half-space, it can be seen that the surface gradient due to a pressure $p(x)$ acting on the strip $-a \leq x \leq a$ is given by

$$\frac{\partial w_z}{\partial x} = -\frac{2(1-n^2)}{p E} \int_{-a}^a \frac{p(s)}{x-s} ds$$

The pressure on each surface is the same, so that

$$\frac{\partial w_1}{\partial x} + \frac{\partial w_2}{\partial x} = -\frac{2}{p E^*} \int_{-a}^a \frac{p(s)}{x-s} ds \quad (3.23)$$

Substituting in Equation 3.22

$$\int_{-a}^a \frac{p(s)}{x-s} ds = \frac{\pi E^*}{2 R} x \quad (3.24)$$

The solution of this type of equation for the required distribution of pressure is obtained as [31]

$$p(x) = \frac{\pi E^*}{2R} \frac{x^2 - \frac{a^2}{2}}{\pi(a^2 - x^2)^{0.5}} + \frac{P}{\pi(a^2 - x^2)^{0.5}} \quad (3.25)$$

This expression for the pressure is not uniquely defined until the semi-contact width, a , is related to the load P . First it is noted that the pressure must be positive throughout the contact for which

$$P \geq \frac{\pi a^2 E^*}{4R} \quad (3.26)$$

If P exceeds the value given by the right-hand side of Equation 3.26 then the pressure rises to an infinite value at $x = \pm a$. The profile of an elastic half-space is loaded by a pressure distribution of the form $p_0\{1 - (x/a)^2\}^{-1/2}$. In this case, the surface gradient just outside the loaded region is infinite. Such a deformed profile is clearly inconsistent with the condition of the present problem, expressed by Equation 3.21, that contact should not occur outside the loaded area. It must be concluded therefore that

$$P = \frac{\pi a^2 E^*}{4R} \quad (3.27)$$

or

$$a^2 = \frac{4PR}{\pi E^*} \quad (3.28)$$

whereupon

$$p(x) = \frac{2P}{\pi a^2} (a^2 - x^2)^{0.5} \quad (3.29)$$

which falls to zero at the edge of the contact.

The maximum pressure

$$p_0 = \frac{2P}{\pi a} = \frac{4}{\pi} p_m = \left(\frac{P E^*}{\pi R}\right)^{0.5} \quad (3.30)$$

where p_m is the mean pressure.

$$p_m = \frac{P}{2a} = \frac{\pi E^*}{8R} a \quad (3.31)$$

The same situation applies as in the contact of a sphere on a plane, the mean pressure p_m is proportional to the size of contact area, a .

3.2 The Contact of Rough Surfaces

3.2.1 Surface topography [32]

The real surfaces of solids, irrespective of the method of formation contain irregularities or deviations from the geometrical forms prescribed. Even the smoothest surfaces, such as those obtained by cleavage of some crystals, contain irregularities the height of which exceeds the interatomic distances by several times. Any measurement of surface characteristics should take into account the ideal geometrical form by comparing it with the actual surface. The deviations of the actual surface with respect to the ideal geometrical surface can be divided into several classes dependent on the sampling length under consideration. First order deviations are shape deviations; second order deviations are waves. The surface roughness includes third order deviations.

There are several ways to describe surface roughness properties such as R_a , R_z and R_t . Stylus instruments provide an electrical signal analogous to the surface profile heights. Williamson and Hunt [33] found that the distribution of peak heights for most modes of machining is approximately Gaussian. A Gaussian distribution may therefore be used in such problems related to contact between surfaces, where the approach of the surfaces takes place above the mean line. Another important conclusion was that height of an asperity of height 0.1 μm may have a radius of 1 mm. In other words, the radius of curvature of asperities is typically very large.

The stationary and ergodic statistical character of the surface profile permits its description by parameters such as the following:

- (a) centre line average, average peak-to-valley height and the maximum height
- (b) the height distribution function
- (c) the auto-correlation function
- (d) the spectral density function

(i) The centre line average R_a

The centre line average R_a of the profile is defined as the average of the ordinates of the profile with respect to the mean line

$$R_a = \frac{1}{L} \int_0^L |y| dx \quad (3.32)$$

or approximately

$$R_a = \frac{\sum_{i=1}^{i=n} |y_i|}{L} \quad (3.33)$$

This form is generally used because the arithmetic mean deviations may be determined with a relatively simple electronic circuit.

(ii) The average peak-to-valley height R_z

The average peak-to-valley height R_z is defined as the difference between the arithmetic mean of the ordinates of the highest five peaks and the arithmetic mean of the ordinates of the deepest five troughs of the profile. These ordinates are measured between the limits of the sampling length with respect to a line parallel to the mean line situated outside the profile.

$$R_z = \frac{1}{5} \sum_{i=1}^{i=5} R_i - \frac{1}{5} \sum_{j=1}^{j=5} R_j \quad (3.34)$$

R_z is the mean value of the total depth of the surface asperities (or ten-point height). This parameter R_z correlates most clearly with estimates by visual observation or microscopical measurement of the surface. R_z is influenced by scratches and microcracks.

(iii) The maximum peak to valley height of the profile R_t

The maximum height R_t is defined as the distance between the highest peak and the deepest valley along the sampling length.

(iv) Representation of the profile

In some instances a simple mathematical representation of the profile is desirable. For this purpose various representations have been suggested. These include spherical and conical representation of the asperities. Moore [34] suggests a simple representation of the two main values when two surfaces come into contact; the number of contacts and the area of contact are given by

$$n = C_0 \delta^{mn} \quad (3.35)$$

and

$$A_r = C_1 + C_2 \delta^{nn} \quad (3.36)$$

where n = number of asperities in contact

A_r = area of real contact

δ = distance of approach with respect to a reference plane parallel to the

mean plane

C_0, C_1, C_2, mn and nn are constants dependent on the profile.

The area of real contact between metal surfaces which is often of considerable interest in engineering can be analysed based on hardness theory.

(v) The real and apparent contact areas [35]

A discrepancy between the real and apparent areas of contact occurs when rough surfaces are placed in contact. The apparent area of contact, A_a , is the total area of all the surface irregularities which are touching and which support the load. Suppose, for example, steel flats of area 2000 mm^2 are placed in contact. The apparent area of contact will be 2000 mm^2 and will be independent of the load. In fact, however, the surfaces will be supported on the irregularities and these will be compressed until the cross-sectional area of the asperities is large enough to support the load. For a steel for which the mean yield pressure, p_m is, say, 1000 N/mm^2 , the area over which the asperities flow plastically will be proportional to the load. If the surfaces are pressed together with a force of 1 KN the area of real contact, A_r , will be $1/2000$ th of the apparent area. For a load of 20 N the area of intimate contact will be $1/100,000$ th of the apparent area. The plastic flow of the asperities provides the real area of contact which supports the load. The stresses in the asperities are taken up by the elastic deformation of the underlying metal.

3.2.2 Contact between rough curved surfaces

Greenwood [36] described the contact of real surfaces. "When two surfaces are loaded together, contact occurs first at the tops of the highest 'asperities', and the true area of contact is very small indeed. When the load is increased, the asperities are crushed, the surfaces sink together, and the area of contact grows - and remains very small indeed. When applied mathematicians disguised as ball-bearing manufacturers or gear wheel

designers talk about a maximum Hertzian pressure of 0.5 GN/m^2 , we tribologists smile gently, because we know that with a ball-bearing steel hardened to $H_V = 800$ the real contact pressure is around 800 kg/mm^2 ; sorry, 8 GN/m^2 . Correspondingly the area of contact is, in this case, only one-sixteenth as large as Hertz says; and usually the fraction is much smaller than this. All the physical processes which take place in contact - microslip; fatigue; fretting; heat production; heat conduction, electrical conduction - take place over this reduced area of real contact.”

Johnson [31, 37] discussed the problem of contact deflection between two rough surfaces pressed together. Within the nominal contact area true contact occurs only at the tips of the asperities. At any point in the nominal contact area the nominal pressure increases with load. The real contact area also increases in proportion to load so that the average real contact pressure remains constant for elastically deforming asperities. Points of contact with the tips of higher asperities will be found outside the nominal contact area.

Bowden and Tabor [35] tackled the problem of friction and Holm [38] the problem of electrical contact resistance by assuming that solids are in contact only at isolated points. In both cases the real contact area was determined by assuming that the asperities were deformed plastically as illustrated in Figure 3.2. The application of plasticity theory was considered to be justified because (i) local strains are very large and (ii) the theory predicts that the real contact area is proportional to the normal load which is in agreement with experiment.

Greenwood and Tripp [39] analysed the contact of a smooth sphere with a rough nominally plane surface on the assumption that the asperities can be characterised by spherical crests of constant radius β which deform elastically according to the Hertz theory. The heights of the crests are assumed to be distributed normally (Gaussian) with a standard deviation σ_s . It is assumed there are C asperities per unit area. At light

loads the contacts are few and widely separated and the apparent pressures have little effect: the hills remain undeformed except for those actually in contact. But as load is increased, the overall deformation becomes more and more important, and the nominal surface through the base of the hills deforms to a shape approaching that in the Hertz theory. Figure 3.3 shows two contrasting distributions of apparent pressure: a low-load case where it is essentially proportional to the probability of finding a hill higher than the gap between the undeformed nominal surfaces, and a high-load case differing from the Hertz distribution only in the inevitable fringe of hills high enough to make contact outside the expected region of contact. The Hertzian pressure distribution falls sharply to zero at a particular radius, so that there is a clear meaning to the term "area of contact". With rough surfaces, on the other hand, there is a finite probability of a contact at any distance from the centre, and the statistical pressure distribution reflects this by becoming zero only at infinity. It is clear from Figure 3.3(a) and (b) that, with a rough surface, the effective pressure falls asymptotically to zero. The contact area, therefore, is not precisely defined. One possibility is to define the "contact" radius as the radius at which the effective pressure falls to some arbitrarily chosen small fraction of the maximum pressure. Greenwood & Tripp arbitrarily define an effective 'contact' radius a^* by

$$a^* = \frac{3p \sum [r p(r) dr]}{4 \sum [p(r) dr]} \quad (3.37)$$

For the low-load pressure distribution of Figure 3.6(a), 86 percent of the total load is carried within the effective radius. At the higher load of Figure 3.6(b), this proportion has risen to 97 percent, reflecting the diminishing effect of roughness at high loads. For the Hertzian distribution, of course, the proportion becomes 100 percent.

The radius a^* is influenced by the roughness parameter α , which is the ratio of the surface roughness σ_s and the bulk compression extent δ_0 . For the contact of spheres

$$\alpha = \frac{\sigma_s}{\delta_0} = \sigma_s \left(\frac{16 R E^*{}^2}{9 P^2} \right)^{\frac{1}{3}} \quad (3.38)$$

where R is related to the radii of the two surfaces by

$$\frac{1}{R} = \frac{1}{R_1} \pm \frac{1}{R_2} \quad (3.39)$$

and σ_s is related to the standard deviations of the roughness heights of the two contact surfaces by

$$\sigma_s^2 = \sigma_{s1}^2 + \sigma_{s2}^2 \quad (3.40)$$

Two different values of α are shown in Figure 3.3(a) and Figure 3.3(b). For small values of α the asperity deformation is small compared with the bulk deformation, so that the pressure distribution is close to that of Hertz. Where α is large the effect of the asperities is very significant; the contact pressure is reduced in magnitude and is spread over a wider area.

If σ_s and δ_0 are known, α can be obtained from Equation 3.37 and $R_f = a^*/a_0$ can be obtained from Figure 3.4. Figure 3.4 shows the theoretical values of $R_f = a^*/a_0$ compared with experimental values for various values of the roughness parameter α [31]. In reality the contact area has a ragged edge which makes its measurement subject to uncertainty. The rather arbitrary definition of a^* is therefore not of serious consequence.

Lo [40] used the same approach to solve the problem of contact between two parallel cylinders. Lo developed a mathematical model based on a surface covered with asperities having spherical tips. An approximate solution for the surface roughness

with a normal distribution was presented. It was assumed that the contact load distribution has a bell shape with zero at infinity. If the parameters such as σ_s , C and β are known, then R_r can be obtained by numerical integration. As an example, the contact of a pair of reeds used in a sealed contact reed switch was calculated. The surface properties of the pair of reeds were measured. The values of the contact area, the number of asperities in contact and the contact width were obtained from the mathematical analysis. For comparison, the corresponding values obtained by Hertzian theory for smooth contact surfaces were also given. Table 3.1 is the summary of the results.

Table 3.1 Summary of the results from Lo [40]

	Rough surfaces	Smooth surfaces
Contact area (A_r , 10^{-6} mm 2)	85	6480
Mean contact pressure (p_m , N/mm 2)	25	1
Contact length ($2 a^*$, 10^{-3} mm)	596.0	7.7

The surface hardness of the reeds was $H_V = 1500$ N/mm 2

It was shown that the real contact area predicted by the smooth surface model is about 76 times as large as that predicted by the rough surface model. The real contact area is about 0.2 % of the apparent contact area and the contact length is about 7 times the contact length obtained by Hertzian theory for smooth contact surfaces. The mean contact stress p_m predicted by the rough surface model is of the same order as the hardness H_V . For a very large range of applied loads $H_V/p_m \approx 2.5$.

3.3 Plastic Theory

3.3.1 Hardness [41]

In the contact between solid materials the hardness of the material plays an important part. Generally, hardness is defined as the resistance to penetration of a hard body, called an indenter, into the surface. Both the elastic and plastic deformation characteristics of the material, such as the elastic limit, elastic modulus, yield point, tensile strength, and brittleness, all play a part in the result obtained. For metal, the range of strain over which metals deform elastically is relatively small. Consequently, when metals are deformed or indented as when their hardness is to be estimated, the deformation is predominantly outside the elastic range and often involves considerable plastic or permanent deformation. For this reason, the hardness of metals is bound up primarily with plastic properties and negligibly with elastic properties. The indentation hardness of metals may in general be expressed in terms of the plastic and, to a lesser extent, the elastic properties of the metals concerned.

The definition of indentation hardness is the ratio of load applied to the surface area of the indentation. The Brinell Hardness Number is obtained by dividing the load by the projected area of the impression

$$H_B = \frac{4 P}{\pi d^2} \quad (3.41)$$

where P is the value of the load applied in kg and d is the diameter of the indentation in millimetres as shown in Figure 3.5.

For a Vickers diamond pyramid indenter the micro hardness is represented by Equation 3.42

$$H_v = \frac{2 P}{d^2} \sin \frac{\alpha}{2} = 1.854 \frac{P}{d^2} \quad (3.42)$$

where α is the angle subtended by opposite faces of the indenter in degrees of arc and d is the diagonal length of the indentation in microns.

The hardness number has the dimensions of a stress, and H_v is generally constant at loads above 10 N but deviations occur at lower loads.

Hardness is a complex quantity that cannot be deduced from the characteristics of the material obtained by tests under monoaxial stresses, although some relationships between these quantities have been established. It has been found that the hardness of steel is approximately three times the value of the yield stress in uniaxial tension.

$$H_v = c \sigma_Y \approx 3 \sigma_Y \approx 6 k \quad (3.43)$$

where σ_Y is the uniaxial tensile yield stress of the material and k is the yield shear stress of the material.

Hardness is a quantity that characterises the behaviour of a material, or more precisely of its surface, to penetration.

3.3.2 The maximum shear stress and yield stress [42]

It is known that the onset of plastic deformation is associated with the maximum shear stress in the material reaching a critical value, k , and it is wished to know the distribution of maximum shear stress for a body loaded with the pressure distribution given by Equation 3.8 acting over the contact area.

The maximum shear stress in plane strain conditions is given by

$$\tau_{\max} = \left(\frac{1}{4} (\sigma_x - \sigma_z)^2 + \tau_{xz}^2 \right)^{\frac{1}{2}} \quad (3.44)$$

Expressions for σ_x , σ_z and τ_{xz} can be found in Johnson [31]. The greatest value of τ_{\max} occurs at a distance $0.48a$ below the surface as shown in Figure 3.5. It is found that τ_{\max} attains the critical value of k when the maximum pressure, p_0 , at the centre of the contact area is $3.3 k$. Furthermore, even when sub-surface yielding has taken place, very little plastic deformation can occur, because the plastic zone is constrained by the surrounding elastic material. As the load is increased further, the plastic zone increases in size and ultimately spreads to the surface, so that plastic indentation can occur. This happens when the mean pressure is approximately $6k$, at approximately twice the pressure at which yield first occurred. The mean pressure at this point is essentially the indentation hardness value, H_V , of the material, which is why, for metal, Equation 3.43 applies.

3.4 The Temperature Field in Grinding

A precise knowledge of the temperature field in the uppermost layer of the workpiece is essential for further analysis and evaluation of the real contact length. A study of thermal models in grinding is the subject of other investigations [9, 43, 44, 45, 46, 47]. Early analysis of temperatures in grinding considered heat generation at the shear plane and determined a theoretical shear plane temperature [45]. Subsequently the grinding process was described by considering the frictional rubbing force on the clearance face and neglecting the shear plane cutting forces. This is known as the ‘grain rubbing hypothesis’ [46]. The justification of the grain rubbing hypothesis is based on the ratio of tangential to normal forces in grinding. The ratio of tangential to normal forces in grinding is typically of the order 0.3 to 0.5 which is characteristic of a

sliding friction process. In turning where heat generation takes place at the shear plane the ratio of tangential to normal forces are typically 2 or 3. Thus of the heat sources around the abrasive grain the clearance face is the heat source of importance. From the point of view of the workpiece a tremendous barrage of small intense heat sources move very rapidly over a short distance, the ‘grinding zone’. At any instant, only one or two grains may be in contact with the workpiece at a particular cross-section of the workpiece. These are however moving at very high speed relative to the workpiece and therefore many cutting edges pass over the interference zone as a point in the workpiece passes under the wheel. Thus the global effect of a large number of grain sources at high speed could be regarded as a continuous band source of heat moving over the workpiece. The term ‘wheel source’ is used to describe this slower moving band source of lower intensity moving over the workpiece. The resulting temperature is often called the grinding zone temperature or the workpiece background temperature and can be modelled using the classical moving heat transfer theory of Jaeger.

The model of Jaeger is reviewed below. This model assumes a uniform heat flux distribution in the grinding zone as shown in Figure 3.6. In reality, the heat intensity is proportional to the local forces on the grains of the grinding wheel. A more realistic heat flux distribution has been proposed by Rowe, Black & Qi [47] based on the physical consideration of the grain as it traverses through the grinding.

3.4.1 Jaeger analysis with a uniform band heat source [48]

Jaeger presented a two dimensional solution to the moving heat source problem. A perfect insulator of length l with a band heat source of uniform intensity at its lower surface q , is considered to move with constant velocity v , across a semi-infinite stationary body having thermal conductivity k , density ρ and specific heat capacity c .

The Peclet Number

$$L = \frac{v l}{2 \alpha} = \frac{v l_e}{4 \alpha} \quad (3.45)$$

where $2l$ = length of a band heat source

$$\alpha = \text{thermal diffusivity} = \frac{k}{\rho c}$$

For values of $L > 5$, the temperature varies approximately linearly along the slider and it may be shown that the mean surface temperature $\bar{\theta}$ to a good approximation, is

$$\bar{\theta} = 0.754 \frac{q l}{k L^{0.5}} \quad (3.46)$$

If the slider is also a heat conductor only a fraction, R of the heat dissipated at the interface will flow into the stationary member and the remaining fraction, $1-R$ will flow into the slider. Hence $R q$ must be substituted for q in Equation 3.46 to obtain the surface temperature.

For the surface grinding situation,

$$q = \frac{e_c v_w a}{l_e} \quad (3.47)$$

From Equations 3.46 and 3.47, the maximum temperature θ_m will be

$$\theta_m = 1.13 \frac{R e_c v_w a}{(v_w l_e (k \rho c)_w)^{0.5}} \quad (3.48)$$

where l_e = real contact length

e_c = specific energy

3.4.2 Rowe & Black's model [49]

In the Jaeger's solution the heat flux distribution in the grinding zone was constant. As previously stated, the heat intensity in the grinding zone is proportional to the local forces on the abrasive grain.

A more realistic heat flux distribution can be obtained by consideration of the action of the abrasive grains in the grinding zone. It has been convincingly argued that three distinct processes take place when a grain traverses through the grinding zone : rubbing (or sliding), ploughing and cutting [46]. In the rubbing region no material removal takes place, elastic and/or plastic deformation in the work material does occur. This leads into the ploughing region where the grain disturbs work material in its path resulting in predominantly plastic flow ahead of the grain. A small amount of material removal may take place due to the extruded material ahead of the grain being dislodged at the sides of the grains. Finally, the cutting action takes place and rapid material removal occurs. Chip formation occurs by fracture in the heavily stressed area ahead of the grain. With respect to material removal the cutting process is most important. However, from the foregoing discussion it is evident that heat generation takes place not only in the cutting process but also in the rubbing and ploughing regions. The rate of increase of the forces in the interference zone are found to increase from the sliding to the cutting regime [50] and as such a square law transition may be considered appropriate as shown in Figure 3.7. Previous estimates were based on a linear heat flux distribution. These however fail to take into account any transition between the three heat generation regimes.

For a square heat flux generation the dimensionless temperature distribution is :

$$\frac{\theta \pi k v}{2 \alpha q} = \int_{x-L}^{x+L} e^{-u} K_o (Z^2 + u^2)^{1/2} 3 \left(\frac{x}{2L} - \frac{u}{2L} + \frac{1}{2} \right)^2 du \quad (3.49)$$

where

$$X = \frac{v_x}{2a} \quad L = \frac{v_l}{2a} \quad Z = \frac{v_z}{2a}$$

For a variable heat flux distribution an analytical solution to Jaegers' integral cannot be obtained. Jaegers theory can be evaluated with a square law heat flux distribution by numerical integration of Equation 3.49. Jaegers' integral was evaluated numerically with a square law heat flux distribution for a wide range of Peclet numbers and the maximum temperature is given by :

$$\theta_m = 1.2 \frac{R e_c v_w a}{[v_w l_e (k \rho c)_w]^{0.5}} \quad (3.50)$$

A comparison between the two flux distributions is shown in Figure 3.8.

Several important observations can be made concerning the temperature obtained for the square law band source:

- (i) Most notably the position of the maximum temperature is seen to lie more centrally in the grinding zone which gives good agreement with experimental measurements of surface temperature in surface grinding.
- (ii) The magnitude of the maximum temperature is increased by 6.5 %.

Chapter 4 MODELS OF GRINDING CONTACT

4.1 Introduction

Deflections in the contact zone result from the elastic and plastic behaviour of both the grinding wheel and the workpiece. The deflections increase the contact area and the number of grains in contact. Many of the grains slide on the workpiece without removing material resulting in increased wear of the grains and a reduced wheel life. The deflections of the grains result in improved surface texture of the finished surface, at the expense of increased specific energy [51].

As summarised in Chapter 2, different mathematical models have been established by which the contact deflections may be described [17, 18, 19, 52]. The Hertz Contact Theory has been used by some researchers, as given in references [17, 18, 52].

The main problems in using the Hertz theory for the analysis of grinding contact are:

- (i) The Hertz theory is based on the assumption that the two contact surfaces are smooth. However, the contact surfaces of the grinding wheel and the workpiece are far from smooth, when considered at the scale of the grain contact points.
- (ii) The Hertz theory may only be used for the elastic contact condition. However, the deflection process between the grinding wheel and workpiece is an elastic plus plastic deflection process.
- (iii) The workpiece surface consists of three regions, the unground region, the region experiencing material removal and the ground region. The contact curve has a different geometry from the smooth and continuous curve of a Hertzian contact face.

According to Saini [53], the contact deflections in grinding can be viewed in two ways : microscopically and macroscopically. Microscopically, a wheel grain which removes chips is deflected because of the normal force exerted on it during grinding and the workpiece is plastically deformed in the grinding zone. Macroscopically, the grinding wheel may be considered as a thick circular plate pressed against a curved surface from which the material is ground. Due to elastic deformation, the wheel-workpiece contact length and the deformed grinding wheel radius are increased.

Johnson [31] discussed the problem of contact deflection between two rough curved surfaces. There are two scales of size in the problem: (i) the bulk (macro scale) contact which experiences elastic compression. At the macro scale the deflections may be calculated by the Hertz theory for the mean profiles of the two 'smooth' surfaces and (ii) the micro scale of the height and spatial distribution of the asperities. For the situation to be amenable to quantitative analysis these two scales of size should be very different.

Based on this viewpoint, the magnitude of the grinding contact zone can be represented by three main factors: (i) the geometric character of the grinding contact zone, (ii) the elastic deflection between the wheel body and the workpiece and (iii) the plastic deformation of the surface layer of the workpiece caused by the active grains or edges. The actual contact situation at the micro scale is illustrated in Figure 4.1.

4.2 A Contact Model for Smooth Surfaces

4.2.1 Contact geometry

The geometry of intersecting chords is used for the analysis of the geometric contact length. The geometry of intersecting chords can also be used in the analysis of the

contact length due to the elastic deflection.

Figure 4.2 illustrates the relationship between the idealised arc of contact AEC, the grinding wheel diameter d_s and the deformation DE under the influence of an applied force P. These are related according to

$$l_f^2 = AEC^2 = 4 d_s DE \quad (4.1)$$

where l_f is the contact length of the surfaces acted on by a normal force.

Figure 4.3 illustrates the geometric relationship in grinding between the arc AB, the diameter d_s and the depth of cut a. The geometric contact length l_g due to the depth of cut is

$$l_g^2 = AB^2 = a d_s \quad (4.2)$$

Figure 4.4 is a combination of the above two situations as occurs in a real grinding process. The undeformed diameter of the contact curve of the workpiece is d_2 and the undeformed diameter of the wheel body is d_s . Point A is the tangential point of curve ADC, that is, the undeformed contact curve of the workpiece. The real depth of cut is a. The following relationships are obtained.

From the circle with a diameter d_2 in Figure 4.4,

$$\begin{aligned} \overline{AFC}^2 &= \overline{CG}^2 + \overline{AG}^2 \\ &= \overline{CG}^2 + a^2 \end{aligned} \quad (4.3)$$

From the intersecting chords,

$$(d_2 - a) a = \overline{CG}^2$$

$$d_2 a - a^2 = \overline{CG}^2$$

So

$$d_2 a = a^2 + \overline{CG}^2 \quad (4.4)$$

From Equations 4.3 and 4.4,

$$\overline{AF}^2 = d_2 a \quad (4.5)$$

From the intersecting chords,

$$(d_2 - \overline{DF}) \overline{DF} = \overline{AF}^2$$

$$d_2 \overline{DF} - \overline{DF}^2 = \overline{AF}^2$$

$$\overline{AF}^2 = 4 \overline{DF}^2$$

$$= 4 d_2 \overline{DF} - 4 \overline{DF}^2 \quad (4.6)$$

From the intersecting chords of the circle with a diameter d_s in Figure 4.4,

$$\overline{AF}^2 = (d_s - \overline{EF}) \overline{EF}$$

$$\overline{AF}^2 = d_s \overline{EF} - \overline{EF}^2 \quad (4.7)$$

So

$$\overline{AF}^2 = 4 \overline{DF}^2$$

$$= 4 d_s \overline{EF} - 4 \overline{EF}^2 \quad (4.8)$$

From Figure 4.4,

$$EF = DE + DF \quad (4.9)$$

Since $d_2 \gg \overline{DF}$ as shown in Figure 4.4, then Equation 4.6 become

$$\overline{AFC}^2 \approx 4 d_2 \overline{DF} \quad (4.10)$$

From Equations 4.5 and 4.10,

$$a = 4 \overline{DF} \quad (4.11)$$

Bring Equation 4.9 into Equation 4.8,

$$\begin{aligned} \overline{AFC}^2 &= 4 d_s (\overline{DE} + \overline{DF}) - 4 (\overline{DE} + \overline{DF})^2 \\ &= 4 d_s \overline{DE} + 4 d_s \overline{DF} - 4 \overline{DE}^2 - 4 \overline{DF}^2 - 8 \overline{DE} \overline{DF} \end{aligned} \quad (4.12)$$

Since $d_s \gg \overline{DE}$ as shown in Figure 4.4, then Equation 4.12 become

$$\overline{AFC}^2 \approx 4 d_s \overline{DE} + 4 d_s \overline{DF} - 4 \overline{DF}^2 \quad (4.13)$$

Comparing Equations 4.13 and 4.6,

$$4 d_2 \overline{DF} = 4 d_s \overline{DE} + 4 d_s \overline{DF} \quad (4.14)$$

Bring Equation 4.11 into Equation 4.14,

$$d_2 a = 4 d_s \overline{DE} + d_s a \quad (4.15)$$

Since $d_2 \gg \overline{EF}$ as shown in Figure 4.4, and from Equation 4.5,

$$l_c^2 \approx \overline{AFC}^2 = d_2 a \quad (4.16)$$

From Equations 4.15 and 4.16,

$$l_c^2 = 4 d_s \overline{DE} + d_s a \quad (4.16')$$

The second term of Equation 4.16' is equal to l_g^2 , the square of the geometrical contact length as represented by Equation 4.2. The DE in Figure 4.4 and the DE in figure 4.2 have the same physical meaning, the deflection extent. When the value of a in Figure 4.4 approaches zero, the two values of DE become equal. So, the first term of Equations 4.16' can be approximately represented by l_f^2 , the square of the contact length on a plane surface acted on by a normal force as shown in Figure 4.2. It is therefore proposed that the real contact length l_c is approximately given by

$$l_c^2 = l_f^2 + l_g^2 \quad (4.17)$$

Equation 4.17 demonstrates the relationship between the real contact length and the independent effects of the contact length due to deformation on a plane surface and the contact length due to geometry.

In the next section, it will be demonstrated that Equation 4.17 applies exactly where l_f is the contact length for a cylinder of diameter d_s pressed into a plane surface.

4.2.2 Contact due to normal force and depth of cut

The contact length due to normal force for smooth surfaces in contact can be obtained by applying the theory of Hertz for curved bodies under load as described by Johnson [31].

According to Hertz [31], the contact length for elastic deflection between a cylinder and a curved surface acted on by a specific normal force F_n' is given by

$$l_c = [8 F_n' d (K_S + K_W)]^{0.5} \quad (4.18)$$

where

$$K_s = \frac{(1 - v_s^2)}{\pi E_s}$$

$$K_w = \frac{(1 - v_w^2)}{\pi E_w}$$

$$\frac{1}{d} = \frac{1}{d_s} \pm \frac{1}{d_2}$$

$$F_n' = \frac{F_n}{b}$$

b = width of the grinding contact

The two Hertzian contact surfaces curve in the same direction, so that the negative sign applies and

$$d = \frac{d_2 d_s}{d_2 - d_s} \quad (4.19)$$

From Figure 4.4, for $a \ll d_2$ the contact length $l_c = (a d_2)^{0.5}$, so that the undeformed workpiece contact curve is given by

$$d_2 = \frac{l_c^2}{a} \quad (4.20)$$

and hence from Equations 4.19 and 4.20

$$d = \frac{l_c^2 d_s}{l_c^2 - a d_s} \quad (4.21)$$

The contact length between the wheel body and the workpiece taking account of elastic

deflection and the geometric effect is therefore obtained from Equations 4.18 and 4.21 as

$$l_c^2 = 8 F_n' (K_s + K_w) d_s + a d_s \quad (4.22)$$

It is found that the first term of Equations 4.22 can be represented by l_f^2 , the square of the contact length due to elastic deflection for a cylinder of diameter d_s impressed on a plane surface which is given by

$$l_f^2 = 8 F_n' (K_s + K_w) d_s \quad (4.23)$$

Equation 4.23 is consistent with the conventional Hertz contact analysis.

The second term of Equation 4.22 is equal to l_g^2 , the square of the contact length due to grinding zone geometry which is confirmed as

$$l_g^2 = a d_s \quad (4.24)$$

Equation 4.24 is consistent with an analysis of grinding based purely on the geometry of the depth of cut.

From Equations 4.23 and 4.24, the Equation 4.22 can be written as

$$l_c^2 = l_f^2 + l_g^2 \quad (4.17)$$

The applicability of Equation 4.17 has thus been demonstrated by two approaches, the first based on geometry and the second based on the Hertz equations.

4.2.3 Discussion

(i) The influence of tangential grinding force on the contact length

In plunge grinding, the grinding force has two components, the normal force F_N and the tangential force F_t . Usually the friction coefficient $\mu = F_t/F_N$ is in the range 0.2-0.6. The influence of tangential force on the Hertz contact has been investigated by Johnson [31]. The effect of the tangential traction is to shift the centre of the contact region by a distance $x_0 = 0.1 l_c$ towards the trailing edge of the workpiece, the contact width increases by approximately 1% and the centre of pressure moves towards the trailing edge. However the comparison with the Hertz pressure distribution shows that the effect is small even for an extreme condition. It may be deduced that the influence of frictional traction upon the contact area and pressure distribution is negligible.

(ii) The two extreme grinding conditions

(a) When the depth of cut, a , is very small, a approaches zero and d_2 approaches infinity. In this case the contact condition tends to the Hertzian contact condition represented in Figure 4.5(a). Equations 4.17 and 4.22 reduce to

$$l_c = [8 F_N' (K_s + K_w) d_s]^{0.5} = l_f \quad (4.23')$$

This result is consistent with the workpiece - wheel contact model discussed by Brown, Saito and Shaw [17], Figure 2.2(b).

(b) Where the depth of cut is finite, but the normal force is very small, the contact condition tends to the geometric contact condition represented in Figure 4.5(b). Equations 4.17 and 4.22 under this condition reduce to

$$l_c = [a d_s]^{0.5} = l_g \quad (4.24')$$

Thus, at the two extreme conditions, Equations 4.17 and 4.22 accurately describe the relationship between the contact length and the grinding parameters. It is therefore proposed that the equations describe the real contact situation more accurately than those proposed by previous authors.

The equation $l_c^2 = l_f^2 + l_g^2$ is a new finding for the contact length in grinding. Stated as a theorem it requires that the contact length in grinding is the orthogonal combination of the contact length due to the deformation which would occur with zero depth of cut and the contact length due to the depth of cut.

4.3 A Contact Model from a Rough Surfaces Approach

In the previous analysis, it was assumed that the surfaces of the two contacting bodies were smooth. In an abrasive machining process however the contacting surfaces are far from smooth.

4.3.1 The character of the contact surfaces in grinding

As reviewed in Chapter 3, much research work has focused on the analysis of the character of the contact between rough surfaces. A high surface roughness of the grinding wheel surface and a small real contact area is required to allow material removal in grinding. It has been suggested [11] that the apparent contact area of the grinding contact zone is about 100 times the real contact area. The real contact length of the grinding contact zone according to various research publications is about 1.5 to 3 times the geometric contact length as shown in Table 2.1.

4.3.2 Effect of surface roughness on contact length

The contact length in grinding, has two parts as represented by Equation 4.8. The contact length due to the depth of cut is not directly influenced by the topography of the two contact surfaces. However the contact length due to elastic/plastic deflection is greatly influenced by the roughness of the contacting surfaces. The influence of surface roughness was described by Greenwood and Tripp and discussed in Chapter 3. According to Greenwood & Tripp, the contact length l_{fr} between rough surfaces can be expressed as

$$l_{fr} = R_r l_{fs} \quad (4.25)$$

where l_{fs} is the contact length which would apply for smooth surfaces due to elastic deflection and R_r is a factor which takes account of the increased contact length due to the roughness. According to Equations 4.17 and 4.22 the real grinding contact length can be written as

$$l_c^2 = l_{fr}^2 + l_g^2 \quad (4.26)$$

or

$$l_c = [R_r^2 8 F_n' (K_s + K_w) d_s + a d_s]^{0.5} \quad (4.27)$$

4.3.3 The roughness factor R_r

If the increased ratio of the contact sizes due to roughness is a^*/a_o and the increased ratio of contact lengths due to deflection in grinding is assumed to correspond to the rough surfaces condition, then the ratio R_r is

$$R_r = \frac{l_{fr}}{l_{fs}} = \frac{a^*}{a_o} \quad (4.28)$$

The value of this roughness factor R_r can be obtained from Greenwood & Tripp's work introduced in Section 3.2.2. If σ_s and δ_0 are known, α can be obtained from Equation 3.38 and $R_r = a^*/a_0$ can be obtained from Figure 3.4. Figure 3.4 shows the theoretical values of $R_r = a^*/a_0$ compared with experimental values for various values of the roughness parameter α [31]. In reality the contact area has a ragged edge which makes its measurement subject to uncertainty.

The value of the roughness factor R_r can also be obtained by a method introduced by Lo [40]. If the parameters such as σ_s , C , the intensity of the asperities and β , the radius of the tip of the asperities are known, then R_r can be obtained by numerical integration. As an example, the contact of a pair of reeds used in a sealed contact reed switch was calculated. It was shown that the value of the roughness factor R_r was about 6.8.

R_r for the grinding situation can be deduced from measured values of contact length.

From Equation 4.27

$$R_r = \left[\frac{l_c^2 - a d_s}{8 F_n (K_s + K_w) d_s} \right]^{0.5} \quad (4.29)$$

Table 4.1 gives values of R_r obtained by working backwards from published experimental results [7, 9, 54, 55], using Equation 4.30

$$R_r = \frac{1}{N} \sum_{i=1}^{i=N} R_{r,i} \quad (4.30)$$

where R_r is the mean of a set of values $R_{r,i}$ and N is the number of experimental observations. A value $R_{r,i}$ is obtained by bringing the 'i'th experimental observation, l_c, i , a_i and F_n, i into Equation 4.29. The variation of the $R_{r,i}$ can also be obtained

from the above results.

It can be seen that the contact length due to deflection is particularly influenced by the surface topography of the grinding wheel. Table 4.1 shows values of R_f in the range 4 to 15 based on published data, where the real contact length of the whole grinding contact zone is 0.5 to 2 times greater than the geometric contact length or $R_l = 1.5 \sim 3$ where $R_l = l_c/l_g$. These results demonstrate that contact lengths measured in grinding are consistent with an analysis based on rough surfaces.

From Table 4.1 it appears that R_f possibly depends on workpiece hardness. However, this is not conclusive since clearly the trend is weak and the experiments were performed under various conditions.

Table 4.1 Values of R_f from published experimental results

	Brandin	Gu	Qi	Aerens		Verkerk
q		88, 132, 264	100 ~ 300			20, 60, 100
R _f	15	8, 7, 9 (up grinding) 7, 6, 8 (down grinding)	11 ~ 13	4	11	3.9, 4.3, 4.4
Material	CK45N	FC Mild Steel	En9	100Cr6	CK45N	100Cr6
H _v	156	170	216	760	156	760

q = grinding wheel speed/ workpiece speed

It also appears from Table 4.1 that R_f possibly increases slightly as speed ratio increases. Again this result is inconsistent and inconclusive as with hardness. In a previous kinematic contact length analysis by Saljé [56, 57, 58], it was argued that increasing the speed ratio in up-grinding will cause decreasing contact length ratio as

shown in Equation 4.31

$$\frac{l_k}{l_g} = 1 + \frac{1}{q} \quad (4.31)$$

Using Equation 4.22, values of q in the range 20 - 264 have a maximum effect of 5% on l_k and therefore cannot explain the magnitude of the variations in Table 4.1.

The values of R_r in Table 4.1 were obtained from different experimental systems, and therefore include systematic deviations. There are several sources of systematic deviations.

- (i) Grinding wheel dressing conditions and the volume of material removed in grinding are known to influence the wheel sharpness, the real contact area and the wheel topography [59, 60]. Dressing conditions and material removed will therefore influence the magnitude of R_r . Verkerk [7] showed that basic wheel parameters such as wheel hardness and grain size have little influence on the real contact length.
- (ii) Different grinding machines have different stiffness and vibration characteristics. Stiffness and vibration are known to affect wheel wear [3]. Wheel wear influences the experimental results [61]. Different types of grinding such as cylindrical grinding, surface grinding or centreless grinding also introduce systematic deviations for the same reason that the progressive modification of the wheel topography is altered.
- (iii) Differences in measuring method, equipment and data processing techniques cause systematic deviations. Furthermore, different assemblies or configurations for the same measuring method will lead to differences between results.

The values of the roughness factor, R_r , are further discussed in later chapters.

4.4 A Contact Model from a Contact Area Approach

In the surface roughness approach, the roughness or surface topography of the two contact surfaces was analysed. The surface roughness approach explains why the real contact length is much longer than would be expected from geometry and from Hertz theory. Analysing the grinding contact, it is evident that the true contact area within the contact zone is much smaller than the apparent contact area. This makes the pressure distribution between rough surfaces totally different from the pressure distribution between smooth surfaces. Lindsay [62] found that the real area increased with grinding time while simultaneously, the metal removal rate, under constant force, decreased. Lindsay plotted the metal removal rate divided by force against force divided by real area (a “real” contact stress) and obtained a linear relationship. Thus, the removal capability of a wheel is proportional to the real stress it can exert upon the work material [62]. So analysing the true contact area and the true force distribution will be useful to better understand the grinding process and grinding wheel behaviour. It will also help to clarify the reason why real contact length is much larger than geometrical contact length.

4.4.1 Pressure in the grinding contact zone

As plastic deformation caused by active grains occurs, the pressure values at the cutting points, $p_{n,cut}$ is higher than the value of material hardness H_V as shown in Figure 4.6 [59]. However, the average contact pressure is equal to the normal force divided by the apparent contact area $p_{average} = F_n/A_a$. The value of the average pressure is very small, $p_{average} = 2 - 5 \text{ N/mm}^2$ [17, 19]. From this point of view, grinding is a low load process. “A high proportion of the contact lies outside the Hertzian area” [36]. In grinding the real contact area is very different from the apparent area. It has been claimed that the real area is about one percent of the apparent area [11]. The contact

width is constrained and equal to the grinding width, this further causes the contact length to be greatly different from the contact length of “smooth” surfaces.

In grinding the contact zone for a grain can be divided into three parts, rubbing, ploughing and cutting. In the ploughing and cutting zone, metal being ground is mostly in the plastic deformation stage, in other words, these regions are flowing plastically. At this stage

$$P_{max} \approx P_{n,cut} = c H_V \quad (4.32)$$

where c is a dynamical factor.

In the rubbing region, the stress increases from zero to P_{max} .

4.4.2 Effect of real contact area on contact length

Real contact area can be described as

$$A_r = \sum_{i=1}^{i=n} A_i \quad (4.33)$$

where n = the number of active grains in contact with the workpiece at the same time

A_i = i th contact area between an active grain and the workpiece

Equation 4.33 shows that the real contact area depends on two parameters, (i) the number of active grains and (ii) the size of each contact area between active grains and the workpiece. These two values have been analysed dynamically and statically [63] and the results were found to differ greatly from each other. Figure 4.7 shows that the dynamical number of cutting edges, C'_{dyn} , is much smaller than the static number of cutting edges, C'_{st} . Malkin analysed the wear area of grinding wheels by using a static

measuring method and found that the wear area was about 1% to 4 % of the apparent contact area [11, 64]. Figure 4.8 shows the difference between the dynamic contact size and the wear size of an active grain. Since the active grains penetrate into the workpiece, the size of individual contact areas, A_{dyn} , is proportional to d_{gc}^2 , and is larger than the size of individual wear flat areas, A_{ist} , which is proportional to d_{gco}^2 . The dynamical real contact area is of the same order of magnitude as the statical contact area. For simplicity, the dynamical contact area ratio R_{Adyn} is assumed to be the same as the statical contact area ratio $R_{Ast} = 100$ to 25.

The average stress of the real contact area $p_{av} = F_n/A_r$, is less than p_{max} as shown in Figure 4.6. If the ratio $R_p = p_{max}/p_{av}$, then

$$F_n = A_r p_{av} = \frac{A_r p_{max}}{R_p} = \frac{A_r c H_v}{R_p} \quad (4.34)$$

It is assumed that $R_{Adyn} = R_{Ast}$ and the apparent contact area of the grinding wheel based on the static analysis is equal to the apparent contact area of the grinding wheel in the dynamical grinding process. The theory of rough surfaces in contact in Chapter 3 can be used. In static analysis, the value of the real contact area and the apparent contact area are obtained for the condition $l_g = 0$. The real contact length is therefore $l_c = l_{fr}$ and the apparent contact area A_a is given by

$$A_a = l_{fr} b \quad (4.35)$$

where l_{fr} is the contact length caused by force.

With $R_A = A_a/A_r$ and Equations 4.34 and 4.35, the contact length caused by force is given by

$$l_{fr} = \frac{R_p R_A F_n}{b c H_v} \quad (4.36)$$

From Equation 4.17,

$$\begin{aligned} l_c &= [l_{fr}^2 + l_g^2]^{0.5} \\ &= \left[\left(\frac{R_p R_A F_n}{b c H_v} \right)^2 + a d_s \right]^{0.5} \\ &= \left[R_A^2 \left(\frac{R_p}{c} \right)^2 \left(\frac{F_n}{H_v} \right)^2 + a d_s \right]^{0.5} \end{aligned} \quad (4.37)$$

or

$$l_c = \left[C_A^2 \left(\frac{F_n}{H_v} \right)^2 + a d_s \right]^{0.5} \quad (4.38)$$

where $C_A^2 = R_A^2 \left(\frac{R_p}{c} \right)^2$.

For example, if $R_A = 1/(1\%) = 100$, then

$$l_c = \left[100^2 \left(\frac{R_p}{c} \right)^2 \left(\frac{F_n}{H_v} \right)^2 + a d_s \right]^{0.5}$$

4.5 Discussion

4.5.1 Discussion of the contact model from a rough surfaces approach

It is proposed that the real contact length can be written as

$$l_c = [R_r^2 8 F_n' (K_s + K_w) d_s + a d_s]^{0.5}$$

It has been argued that the variations of contact length experienced in grinding are

consistent with the effects of elastic/plastic deformation between the rough surface of the grinding wheel and the surface of the workpiece. The relationship is consistent with well established principles of contact mechanics which appear to be relevant to abrasive machining processes.

The new contact length model indicates that the main parameters influencing contact length are:

- (i) the real depth of cut
- (ii) the elastic deflection of the grinding wheel
- (iii) the surface topography of the grinding wheel

4.5.2 Discussion of the contact model from a contact area approach

Assuming the static contact area ratio $R_{A\text{st}}$ is equal to the dynamical contact area ratio $R_{A\text{dyn}}$, the contact length

$$l_c = [l_{fr}^2 + l_g^2]^{0.5}$$

$$= [R_A^2 \left(\frac{R_p}{c}\right)^2 \left(\frac{F_n}{H_v}\right)^2 + a d_s]^{0.5}$$

- (i) The advantage of this model is that a relationship between real contact length and real contact area is established. Using workpiece hardness to describe the surface contact makes the process more understandable.
- (ii) The factor (R_p/c) is a measure of the ratio between the extent of the plastic deformation and the extent of the elastic deformation in a grinding process. (R_p/c) can also be considered as reflecting the dynamic effect on the yield stress of the workpiece. It is suggested that this factor is normally a constant.

- (iii) When the material hardness H_V is large, a higher normal force will be required to achieve the same value of l_C and stock removal rate than when the material is soft.
- (iv) A blunt wheel or wheel loading will make the contact area ratio R_A smaller. This also requires a higher normal force for the same value of l_C and stock removal rate.
- (v) Increasing the true depth of cut, a , will increase the force F_N . As a result, the real contact length l_C will increase by both deflection and geometry.
- (vi) In practice the number of active grains increases with normal force. A more realistic contact area approach would take account of this effect.

Chapter 5 THE EXPERIMENTAL SYSTEM

5.1 The Contact Length Workpiece System

5.1.1 The workpiece assembly

A special workpiece was designed as illustrated in Figure 5.1 and Figure 5.2. Figure 5.1 shows the split test surface arrangement which allowed thermocouple wires to be inserted. Figure 5.2 illustrates the configuration of the thermocouple junctions on the workpiece surface and is a view of the area A of Figure 5.1. The length of the workpiece, L was 100 mm and was used to measure table speed using the relationship $v_w = L/t_w$, where t_w is the time for the grinding wheel to pass the workpiece. A reference surface was incorporated to facilitate measurement of the real depth of cut, a_e . The width of the reference surface and the test surface, b was 15 mm. The distance of the split section of the workpiece from the entrance edge, L_1 was 75 mm. Thin mica sheets (10 to 40 μm) were used for insulation. The two portions of the workpiece were completely insulated from the thermocouple wires to prevent a short circuit.

5.1.2 The contact length thermocouple

The contact length thermocouple design was based on the applied power source method described in Chapter 2. The overall thickness of the single pole thermocouple junction was 0.15 mm and the width 0.2 mm as shown in Figure 5.2. A chromel thermocouple pole was employed. The configuration of the contact junction is shown in Figure 5.3. When the grinding wheel passes over the junction of the wire and the workpiece, the electrical resistance between the electrode and workpiece is decreased and a contact signal is generated.

5.1.3 The temperature thermocouple

The “grindable” standard foil thermocouple technique was employed for the measurement of temperature. The overall thickness of the standard thermocouple junction was 0.1 mm and the width 0.2 mm as shown in Figure 5.2. Two standard foil thermocouple electrodes of the standard K type were used as shown in Figure 5.5. The thermocouple junction consisted of chromel and alumel wires. As stated by Nee [65], this technique eliminates the tedious calibration procedure. Because the assembly of this thermocouple sensor is standard as shown in Figure 5.4, standard calibration charts of characteristics from manufacturers can be used directly [65, 66]. Standard calibration charts of chromel-alumel characteristics were readily available from the manufacturers of the thermocouple and were used to obtain temperature readings.

For consideration of the accuracy of the technique applied for measuring temperature, a quick calibration of the sensor was performed. By pouring boiling water on the standard thermocouple junction continuously, an E.M.F. signal was obtained. The value of this output was recorded and compared with standard calibration charts of chromel-alumel characteristics [66]. The error of the output was within 5%.

As stated by Nee [65], a smaller hot junction allows a more accurate measurement of contact temperature.

Comparison with the configurations of Nee [65], it may be seen that the configuration employed gave a smaller size of hot junction. The area of the thermocouple ($0.1 \times 0.2 \text{ mm}^2$ compared with $0.46 \times 2 \text{ mm}^2$) is 46 times smaller and therefore the heat capacity was reduced. The thermal inertia was therefore smaller and the time constant was smaller. A sharper temperature peak caused by active grains was observed in the electro motive force. Because of the smaller size of the hot junction along the grinding direction (0.1 mm comparing with 0.46 mm), the electromotive force is more accurately

representative of the surface temperature at any particular position on the surface. The temperature measurements using the thermocouple foil technique was therefore considered to be more accurate than previously published results using similar techniques [7,65,67,68,69,70,71,72].

5.2 The Measurement System

Figure 5.6 shows the measurement system. The workpiece was housed in a jig in which an amplifier was embedded to amplify the temperature signal. A force dynamometer was used to measure the vertical and horizontal components of the grinding force. The contact resistance, the thermocouple E.M.F. and the force signals were recorded using an oscilloscope and a personal computer.

5.2.1 The main pieces of apparatus employed

The main pieces of apparatus used in the experiment are listed below.

- (i) Thermocouple: NiCr-NiAl armoured standard thermocouples for use under 1400°C were used to measure the temperature and contact time signals as shown in Figure 5.5.
- (ii) Dynamometer: The dynamometer employed piezo-electric transducers Z3393 and charge amplifiers FYLDE 128CA were used to measure the normal and tangential grinding forces.
- (iii) A Talymin 4-10 comparator with a resolution of 0.2 micron and a mechanical dial indicator with a 1 micron resolution were used to measure the depth of cut to an accuracy of approximately 1 μm .
- (iv) A Form Talysurf was used to measure the surface topography of the workpiece and the surface roughness R_t .
- (v) An oscilloscope was used to display and store the thermocouple and contact

signals.

(vi) A PC data logging system was developed to record the grinding force and contact signals.

(vii) The coolant used was Arrow synthetic coolant, 1:50 dilution in water.

(viii) An Abwood 5025 surface grinding machine was used for the experiments:

The maximum spindle speed (n_{smax}) was 3400 r/min.

The minimum table speed (v_{wmin}) was 0.025 m/s.

The maximum table speed (v_{wmax}) was 0.37 m/s.

The maximum spindle power ($P_{maximum}$) was 0.7 kw.

5.2.2 Workpiece materials and grinding wheels employed

Three workpiece materials were employed for the experiments:

(i) En9 :

Young's modulus : $E_w = 210 \text{ GPa}$

Hardness : $H_v = 216 \text{ Kg/mm}^2$

(ii) Cast iron :

Young's modulus : $E_w = 128 \text{ GPa}$

Hardness : $H_v = 210 \text{ Kg/mm}^2$

(iii) M2 :

Young's modulus : $E_w = 270 \text{ GPa}$,

Hardness : $H_v = 810 \text{ Kg/mm}^2$

Two grinding wheels, one alumina and the other CBN, were employed for the experiments.

The specification of the aluminium oxide grinding wheel was as follows:

Grade : 19A60L7V

Outside diameter : 170 mm

Inside diameter : 30 mm
Width : 20 mm
Young's modulus : $E_s = 49 \text{ GPa}$.

The specification of the cubic boron nitride grinding wheel was as follows:

Grade : B91ABN200
Outside diameter : 174 mm
Inside diameter : 30 mm
Width : 17 mm
Young's modulus : $E_s = 50 \text{ GPa}$.

5.3 Measurement of the Depth of Cut

Several methods of measuring the depth of cut were tried using eddy current transducers, using a mechanical dial indicator and using the Talymin 4-10 comparator. As a result of testing, a method was developed combining the use of the dial indicator with the Talymin 4-10 comparator. Figure 5.7 shows the scheme for measurement of depth of cut.

Procedure for measurement of depth of cut:

Step 1. The test surface, S_g , and the reference surface, S_r , of the workpiece were ground, keeping the infeed settings constant. The difference in height of these two surfaces located at Level 1 were measured using the dial indicator. The reading on the test surface, S_g , was h_{g1} and the reading on the reference surface, S_r , was h_{r1} . The difference between these two surfaces was

$$dh_1 = h_{g1} - h_{r1}$$

Step 2. The workpiece was taken to a Talymin 4-10 and the difference in height of these two surfaces was measured again. The reading on the test surface, S_g , is v_{g1} and the reading on the reference surface, S_r , was v_{r1} . The difference in height of these two surfaces was

$$dv_1 = v_{g1} - v_{r1}$$

Step 3. The workpiece was moved back to the grinding machine and the difference in height of the two surfaces located at Level 1 was measured again using the dial indicator. This measurement was compared with the measurement in step 1 to check the repeatability of the measurement on the machine.

Step 4. The nominal depth of cut, a , was set using the machine infeed dial and the test surface, S_g , was ground.

Step 5. The test surface, S_g , was measured at Level 2 and compared with the measurement of the reference surface, S_g , located at Level 1 using the dial indicator as shown in Figure 5.7. The reading on the test surface, S_g , was h_{g2} and the reading on the reference surface, S_r , was h_{r2} . The difference in height of these two surfaces was

$$dh_2 = h_{g2} - h_{r2}$$

The reading h_{r2} was not the same as h_{r1} due to small variations in deflection of the system between the first and second measurements. The depth of cut measured by the indicator was therefore,

$$\begin{aligned} a_e &= | dh_2 - dh_1 | = | (h_{g2} - h_{r2}) - (h_{g1} - h_{r1}) | \\ &= | (h_{g2} - h_{g1}) - (h_{r2} - h_{r1}) | \end{aligned}$$

Step 6. The workpiece was moved to the Talymin and the difference in height of these two surfaces was measured again. The reading on the test surface, S_g , was v_{g2} and the reading on the reference surface, S_r , was v_{r2} . The difference in height of these two surfaces was

$$dv_2 = v_{g2} - v_{r2}$$

The depth of cut measured by the Talymin was

$$\begin{aligned} a_e &= |dv_2 - dv_1| = |(v_{g2} - v_{r2}) - (v_{g1} - v_{r1})| \\ &= |(v_{g2} - v_{g1}) - (v_{r2} - v_{r1})| \end{aligned}$$

Step 7. The workpiece was moved back to the grinding machine and the difference in height of the two surfaces was measured with the dial indicator again. This measurement was compared with the measurement in step 5 to check for repeatability of the measurement on the machine table.

Step 8. The test surface, S_g , and the reference surface, S_r , of the workpiece were ground keeping the downfeed settings constant to make the two surfaces level. The difference in height of these two surfaces were measured using the dial indicator.

The workpiece was now ready for the second grinding test.

Figure 5.8 is a comparison of the results obtained using the dial indicator and the Talymin. From repeated experiments it was found that for depths of cut larger than 5 microns, measurements could be carried out within 10 % using the dial indicator. However, for depths of cut below 5 microns it was necessary to carry out measurements using the Talymin 4-10.

5.4 Calibration of the Force Table

Figure 5.9 shows the scheme for calibration of the force table and the calibration results. The calibration was carried out using dead weights for loading. The results show that the force table gave a linear response.

5.5 Data Logging Program

Figure 5.10 is a flowchart of the data logging program which was written in C.

5.6 Wheel Stabilisation

Stabilisation tests were performed for the aluminium oxide wheel and the CBN wheel grinding En9 and cast iron workpiece materials. Figure 5.11 illustrates the process of wheel stabilisation. From the test results the stabilisation procedure was decided. A newly dressed wheel was used for each experiment after which the stabilisation procedure consisted of grinding a 0.6 mm thick layer from the workpiece in a succession of passes.

5.7 Preliminary Trial

A preliminary trial was performed to evaluate the ability to measure the contact length.

The grinding conditions in the preliminary trial were

- (i) Grinding wheel: 19A60K7V, $d_s = 170$ mm.
- (ii) Workpiece: En9

The contact resistance signal and the thermocouple signal were recorded, displayed and stored using the oscilloscope. The data were transmitted to the PC using a ‘Grabber’

software and a serial communication link. Figure 5.12 is a typical plot of contact signals in wet grinding with coolant. Figure 5.13 is a typical plot of contact signals in dry grinding without coolant.

Figure 5.14 is a typical graph of the force signals generated using the Microsoft ‘Excel’ software. The table speed, v_w , was obtained from the force signal interval, t_w and the workpiece length, L, using the relationship $v_w = t_w L$. The value of force is a value of mean line through the points.

The preliminary trial showed that the measuring system was capable of providing temperature, force, time and contact length signals.

5.8 The Experimental Procedure

5.8.1 Experimental conditions

Dry and wet grinding experiments were performed.

In order to investigate the influence of the speed ratio, q, and the depth of cut, a, on the contact length, several values of speed ratio and depth of cut were selected.

- (i) Speed ratio:
 - $v_w = 0.1 \text{ m/s}, q= 300$
 - $v_w = 0.17 \text{ m/s}, q= 175$
 - $v_w = 0.2 \text{ m/s}, q= 150$
 - $v_w = 0.25 \text{ m/s}, q= 120$
 - $v_w = 0.3 \text{ m/s}, q= 100$
- (ii) Depth of cut: $a = 0.01 \text{ to } 0.07 \text{ mm}$

Other parameters were:

Wheel speed: $v_s = 30\text{m/s}$

Grinding wheels: 19A60L7V and CBN

Dressing conditions: $a_d = 0.02\text{ mm}$, $f_d = 0.2\text{ mm/r}$ and 10 passes

Dressing tool: A single diamond dresser

5.8.2 The experiments

Three to seven trials were carried out for each test point depending on the repeatability and stability of the trials. Mean values were obtained for the actual depth of cut, the grinding forces, the maximum contact length, the minimum contact length and the grinding temperature.

Normally the grinding wheel was redressed and stabilised after each change of table speed. In order to avoid the effect of wheel wear on the experimental results, the order in which the depth of cut was selected for a constant table speed was randomised.

Four sets of experiments were performed employing the parameters listed below.

Experiment 1:

1. Wheel: Aluminium oxide abrasive 19A60L7V
2. Workpiece: Cast iron
3. Grinding Condition: $q = 100, 300$; $a_e = 0.005$ to 0.05 (mm)
4. Coolant: Wet grinding with coolant

Experiment 2:

1. Wheel: Aluminium oxide abrasive 19A60L7V
2. Workpiece: En9
3. Grinding Condition: $q = 100, 200, 300$; $a_e = 0.005$ to 0.06 (mm)
4. Coolant: Wet grinding with coolant and dry grinding without coolant

Experiment 3:

1. Wheel: A superabrasive CBN B91ABN200
2. Workpiece: En9
3. Grinding Condition: $q = 300$; $a_e = 0.005$ to 0.05 (mm)
4. Coolant: Wet grinding with coolant and dry grinding without coolant

Experiment 4:

1. Wheel: CBN B91ABN200
2. Workpiece: M2
3. Grinding Condition: $q = 120, 175, 300$; $a_e = 0.005$ to 0.025 (mm)
4. Coolant: Wet grinding with coolant

Chapter 6 INTERPRETATION OF THE CONTACT PHENOMENA

6.1 Signal Interpretation

The contact length was obtained by multiplying the contact time, t_c , and the workspeed, v_w .

$$l_e = v_w t_c \quad (6.1)$$

The measurement of the contact time, t_c , required interpretation of the contact length signal and is therefore discussed in detail. Figure 6.1 shows a typical contact length signal obtained using the applied power source method.

The contact signal illustrated in Figure 6.1 represents the contact between active grains and the workpiece using the applied power source method. The signal is characterised by the magnitude and the frequency of the pulses. The extent of the real contact area is represented by the magnitude. Contact with individual grains is indicated by the large spikes which occur as grains on the wheel surface contact or cut the top of the electrode foil and the workpiece. The frequency of contacts between active grains and the workpiece is represented by the density of the pulses.

6.1.1 Principle of the applied power source method

When two large conductors contact over a small circular area, there is a contact resistance between them of $\rho/(2a)$, where ρ is the contact resistivity and a is the radius of the contact circle. Contact between nominally flat surfaces is known to occur as a number of clusters of microcontacts, the position of the clusters being determined by the

large-scale waviness of the surface, and the microcontacts by the small-scale surface roughness.

The contact resistance is partly determined by the number and size of the microcontacts and partly by their grouping into clusters. The simplest case is that of a large number of small equal spots distributed uniformly and densely over a circular area. The resistance, R, is then described by Holm's equation (1929) [38, 73]

$$R = \rho \left(\frac{1}{2 n a} + \frac{1}{2 \alpha} \right) \quad (6.2)$$

where a is the radius of a spot, and a the radius of the cluster.

Greenwood [73] provided further interpretation of Holm's equation. The Holm radius of the cluster, a, was defined by

$$\frac{1}{\alpha} = \frac{3 \pi}{16 n^2 s_{ij}} \quad (6.3)$$

where s_{ij} is the distance between the contacts.

The first part of Equation 6.2 called the self-resistance decreases when the mean contact radius, a, or the number of contact spots, n, is increased. The second part of Equation 6.2 called the interaction resistance decreases when the distance between the contacts or the number of contact spots is increased.

In grinding, the number of contacts at any time is small. The contacts do not form a well-defined cluster and the Holm radius is large. As a result, the second part of Equation 6.2 can be ignored. The resistance is therefore inversely proportional to the real contact area.

$$R = \frac{\rho}{2 n a} \quad (6.4)$$

The magnitude of the measured signal using the applied power source method can be interpreted by reference to the equivalent circuit in Figure 6.2. The relationship between the voltage output and the contact resistance is represented by Equation 6.5

$$V_{out} = \frac{E r}{R + r} \quad (6.5)$$

where E is the applied voltage. In this experiment the applied voltage was 1.2 V. R is the contact resistance of the junction between the electrode and workpiece. r is the internal resistance of the instrument for measuring the voltage output.

From Equations 6.4 and 6.5

$$V_{out} = \frac{E r}{\frac{\rho}{2 n a} + r} \quad (6.6)$$

and

$$\frac{1}{V_{out}} = \frac{\rho}{2 n a E r} + \frac{1}{E} \quad (6.7)$$

Since E, r and ρ are constant,

$$V_{out} \propto n a \quad (6.8)$$

V_{out} is therefore proportional to the average contact size, a, and the number of contacts, n.

It was assumed that the active grains penetrate the workpiece along the contact zone with a parabolic distribution. The contact size and the number of active grain-workpiece contacts are proportional to the grain penetration. As a result, the contact resistance decreases with increasing penetration of the active grains.

From Figure 6.1, the extent of contact between the wheel and the workpiece can be divided into three stages as illustrated in Figure 6.3. The signal magnitude at the first part of the signal is high which is described by l_1 and then it drops down to an intermediate level which is described by l_2 . Finally the signal drops to a low level with some pulses described by l_3 . The length between the first spike and the last spike is described by l_3 . The character of the signal profile can be interpreted using Equation 6.8.

6.1.2 Characteristics of the active grain and workpiece contact

It is known that there are three distinct processes taking place when a grain traverses through the grinding zone : rubbing (or sliding), ploughing and cutting [11]. In the rubbing process no material removal takes place, elastic and/or plastic deformation in the work material does occur. This leads into the ploughing process where the grain disturbs work material in its path resulting in predominantly plastic flow ahead of the grain. A small amount of material removal may take place due to the extruded material ahead of the grain being dislodged at the sides of the grains. Finally, cutting takes place and rapid material removal occurs by chip formation. This process is illustrated in Figure 6.4. The active grains are distributed circumferentially but also in the radial direction. So even in the cutting zone some active grains below the outer profile of the wheel are rubbing or ploughing instead of cutting. Similarly, some active grains are rubbing instead of ploughing in the ploughing zone. The rubbing, ploughing and cutting regions are illustrated by Figure 6.4.

The ratios of these three parts in grinding depend on the grinding conditions. Based on the above discussion, the whole contact zone can be defined as three zones:

(i) The cutting zone, l_{cut} . Cutting action dominates in this zone and rapid material removal occurs.

(ii) The cutting and ploughing zone, $l_{\text{c-pl}}$. Plastic deformation dominates in this zone and substantial heat is generated. Subsurface properties such as hardness and residual stress will be affected by the grinding behaviour within this zone.

(iii) Rubbing (or sliding), ploughing and cutting zone, l_e . In the tail part of the whole contact zone, l_{rub} , rubbing or sliding dominates and generates the final surface roughness of workpiece. The l_{rub} regime will gradually dominate the whole contact zone at the sparkout stage.

Comparing Figure 6.3 with Figure 6.4, the lengths l_1 , l_2 and l_3 in Figure 6.3 may approximately correspond to the cutting, ploughing and rubbing regions. However, no method was available to check this point.

The problem remains as to how to process the experimental data and how to obtain a value which represents the contact length.

6.2 The Size of Contact Zone

An indication of the size of the contact zone may be obtained by the density of pulses. The maximum size of the contact zone is between the first large spike and the last.

A further method of defining the size of the contact zone may be achieved by a statistical interpretation:

As illustrated in Figure 6.1, the contact zone can be represented by the value l_2 or l_3 depending on different ideas. It can be stated with a high degree of confidence that the

wheel and the workpiece are in contact in the zone l_2 and that the wheel and the workpiece are not in contact outside of the contact zone l_3 . The area represented by the value l_3 " means the wheel and the workpiece are in contact some of the time with a probability which depends on the statistical nature of the workpiece surface, the wheel surface and the grinding conditions.

6.2.1 Effects which increase the signal contact period

(i) Asperities on the workpiece

It is possible that there are some extra high asperities on the workpiece. It is also possible that there are some extra high asperities on the wheel. The asperities will make the measured contact length appear longer than otherwise, so that the measured contact length will be larger than the real contact length.

(ii) Thickness of the insulation

As shown in Figure 5.5, there is an insulation layer between the workpiece and the foil type electrode. In grinding, when an active grain first breaks the insulation at one side the contact signal increases. After the last active grain bridges the other side of the insulation, the contact signal drops to the zero level. As a result of the insulation, the contact length measured will be longer than it should be.

6.2.2 Effects which reduce the contact signal period

(iii) The measured width

In the grinding test, the whole width of the workpiece was 15 mm. But the width of the contact junction was 0.2 mm as shown in Figure 5.2. Only the contacts between active

grains and the workpiece within this 0.2 mm width are recorded. But the contact length for each of the active grains is not constant [7, 11, 25, 54, 74]. So the signal is a record of local contact as described by Zhou [27]. Zhou defined two kind of contact lengths: “Maximum contact length and local contact length. The maximum contact length, which is also the real contact length in grinding, is the distance from the beginning of engagement of the wheel with the workpiece to the end of the mutual contact, including all contacts between grains and workpiece. Local contact length is the interface length between the grains on the wheel peripheral surface and the workpiece at any point in the whole grinding zone.” The maximum value from this measurement, l_3 , is a local length which might be smaller than the maximum contact length for the whole grinding zone.

(iv) The active grain space

Because of the random radial distribution of the grains below the wheel surface, the measured contact length will be shorter in many cases. The maximum contact length of a series of tests approaches closest to the real contact length, but the probability of finding the largest contact length increases with the number of tests as proposed by Verkerk [7]. This may cause the measured result to be smaller than the actual maximum contact length.

6.2.3 A definition of contact length

The distribution of the contact magnitude can be described statistically. At any position outside of the zone represented by l_3 there is a very low probability that the wheel and workpiece are in contact or a very high probability that the wheel and workpiece are disconnected [75].

The generation of the contact trace in grinding is due to two profiles, the surface profile of the workpiece and the surface profile of the wheel. These two profiles have the

statistical characteristics of a normal distribution $f(x)$ and $f(y)$ respectively [31, 76, 77, 78, 79, 80]. There is a distribution of contact lengths which may be approximately a normal distribution. In a practical application, the most useful value should be the average contact length which has the greater significance for the analysis of temperature, the stress distribution, the vibration of the grinding system, the roundness and the surface roughness of the ground workpiece.

As illustrated in Figure 6.3, it can be stated with a high degree of confidence that the wheel and the workpiece are in contact in the zone l_2 and that the wheel and the workpiece are not in contact outside of the contact zone l_3 .

If the value of l_2 is selected to represent the contact length, the sliding contact represented by the value l_3 will be ignored. This may be too conservative a solution. Alternatively, if the value of l_3 is selected to represent the contact length, the sliding contact represented by the value l_2 may be over-emphasised. An average of l_2 and l_3 may have a more general meaning for the contact length of the wheel and the workpiece.

As the result, the average contact length is defined as the mean of the l_2 and l_3

$$l_{av} = \frac{l_2 + l_3}{2} \quad (6.9)$$

In this investigation, it was decided to investigate the average length of the contact zone, l_{av} . This average length of the contact zone is believed to be conservative. Other measures of size will be discussed only when it is necessary.

Chapter 7 EXPERIMENTAL RESULTS

7.1 Grinding Force

The forces in the grinding process are the detectable consequence of the inter-action of the wheel and workpiece in the contact zone. Figures 7.1 to 7.8 show the relationships between tangential force F_t and normal force F_n with depth of cut under different grinding conditions. It can be seen from the results that:

- (i) Grinding forces were almost proportional to depth of cut.
- (ii) The value of friction coefficient defined as $\mu = F_t/F_n$ were in the range from 0.5 to 0.65 for En9. The values of μ were similar for the CBN wheel and for the alumina wheel. However, μ was 0.37 for grinding cast iron with the alumina wheel as shown in Figure 7.5 and 0.28, 0.33 and 0.37 for grinding M2 tool steel with the CBN wheel as shown in Figure 7.6.
- (iii) Coolant had little effect on the forces for an alumina wheel as shown in Figure 7.1 and Figure 7.3. However, coolant had a significant effect on the forces for the CBN wheel as shown in Figure 7.4.
- (iv) Forces were larger at high workpiece speed than at low workpiece speed as shown in Figure 7.7 and Figure 7.8 for the same depth of cut.

7.2 Grinding Temperature

The higher surface temperature of a workpiece ground with an alumina wheel compared to grinding with CBN was an important observation. Figures 7.9 to 7.11 show variations of the grinding temperatures with depth of cut.

- (i) Grinding temperatures increased with depth of cut as would be expected due to

increased forces and energy required.

(ii) For the same depth of cut, grinding temperatures were higher at low speed ratio than at high speed ratio as shown in Figure 7.9. This may also be explained by the increased energy required at the higher removal rate.

(iii) Coolant had a smaller effect on the grinding temperatures for an alumina wheel as shown in Figure 7.10 than when grinding with CBN. Coolant had a large effect on the grinding temperatures using the CBN wheel as shown in Figure 7.11. Experience suggested that grinding dry with CBN leads to loading of the grinding wheel. Under these conditions the grinding forces are increased as shown by Figure 7.4. The increased forces offset the superior cooling properties of CBN observed when grinding with coolant.

7.3 Contact Length

The effect of depth of cut on the contact length is of fundamental interest. The results for contact length are therefore presented primarily as a function of depth of cut. The contact length between the wheel and workpiece was taken to be the average contact length obtained using the method described in Chapter 6. The following results were obtained under the grinding conditions listed on the diagrams.

Figures 7.12 to 7.25 show the measured contact length and the ratio of measured contact length to geometric contact length. Results are presented for a range of grinding conditions. The shaded areas in Figures 7.12, 7.13 and 7.14 show the variations of the real contact length in grinding between l_2 and l_3 as described in Chapter 6.

7.3.1 Aluminium oxide abrasive and En9 workpiece material

Figure 7.12 shows the results for measured contact length and depth of cut for the condition $v_w = 0.1$ m/s in dry grinding. It can be seen that the average measured

contact length increases with depth of cut. The measured values of contact length are approximately twice the geometric contact length throughout the range. Figure 7.13 shows results for the same grinding conditions when grinding with a fluid. It appears that in this case, the measured contact lengths were increased. The reason for the increased contact lengths in wet grinding was not explained. It can be seen that l_3 was increased more than l_2 and this affected the values of l_{av} . However, given the scatter of the results, it is not possible to reach any firm conclusions. It was considered unlikely that the coolant affected the resistance of the APS circuit. It was considered possible that coolant might change the distribution of normal pressure over the contact area due to hydrodynamic action [81].

Figure 7.14 shows the effect of increased removal rate at $v_w = 0.3$ m/s in dry grinding. The results are of larger magnitude than the results at low removal rate as shown in Figure 7.12. Figures 7.15 to 7.18 show further variations of contact length with different workpiece speeds. These results indicate that, in surface grinding, the workpiece speed affects the contact length significantly, as pointed out by Verkerk [7]. A higher speed make the contact length ratio bigger. However, it is clear that increasing speed increases the contact length as would be expected due to the increased normal force. This can be verified from the measured values of normal forces shown in Figures 7.5 and 7.7.

The contact length ratio $R_l = l_{av}/l_g$ reduced from 9 to 2 with an increase of the cutting depth from 0.004 mm to 0.04 mm when using coolant.

7.3.2 Aluminium oxide abrasive and cast iron workpiece material

In Figures 7.19 and 7.20 contact length results for grinding cast iron are presented for wet grinding with $v_w = 0.1$ m/s and 0.3 m/s. As for En9 workpiece material in Figure 7.18, a higher workpiece speed increased the contact length and the contact length ratio.

The ratio $R_l = l_{av}/l_g$ reduced from 3.5 to 2 with the increase of the cutting depth from 0.004 mm to 0.04 mm. The reduction is consistent with the explanation that the contact length will approach the geometric value as depth of cut increases according to Equation 4.27.

7.3.3 Superabrasive CBN and En9 workpiece material

Figures 7.21 and 7.22 show contact length results when grinding En9 with a CBN grinding wheel with and without coolant at a work speed $v_w = 0.1$ m/s. The results demonstrate similar trends to the results using an aluminium oxide grinding wheel. However, the scatter of the results appeared to be reduced when grinding with CBN. This is probably because CBN is much harder than aluminium oxide and less subject to wear. One of the main causes of scatter in grinding is the variability of the grinding forces due to wheel wear. The contact length ratio $R_l = l_{av}/l_g$ when grinding with CBN is insensitive to depth of cut. R_l lay in the range from 2 to 3 for cutting depths between 0.006 mm and 0.044 mm as shown in Figure 7.23. This is a smaller value than the ratio R_l using an aluminium oxide wheel and grinding the same material which was in the range from 2.5 to 4 as shown in Figure 7.16. However, the value of R_l grinding En9 with the CBN wheel was larger than the value of R_l grinding cast iron using the aluminium oxide wheel which was in the range from 1.5 to 2 as shown in Figure 7.20. The results cannot be explained by the force measurements since the grinding forces when grinding cast iron were larger than the forces when grinding En9 and the grinding forces when grinding En9 with CBN were larger than the forces when grinding En9 with aluminium oxide shown in Figures 7.1, 7.4 and 7.5. The results can be interpreted by considering the grinding performance especially with regard to the grinding wheel condition. Some of the pairs provided good grinding conditions such as using either the alumina wheel or the CBN wheel for grinding En9 with or without coolant. Under these grinding conditions the grinding wheel was always relatively sharp. However, the grinding condition using an alumina wheel to grind cast iron was

a poor condition. In this grinding condition the wheel was readily loaded. When the grinding wheel is loaded, the ratio of the apparent contact area to the real contact area decreases. As a result, the contact length ratio is reduced as shown in Equation 4.37. These results also show that different combinations of grinding wheel and workpiece affect the interface contact behaviour in the grinding process. This conclusion was further verified by the experimental results obtained grinding M2 tool steel using the CBN wheel.

7.3.4 Superabrasive CBN and M2 workpiece material

The results in Figure 7.24 show the contact lengths measured when grinding M2 tool steel with the CBN wheel with coolant for three different workspeeds. The results are different from the previous results using an aluminium oxide wheel shown in Figure 7.16, Figure 7.18 and Figure 7.20. Figure 7.25 indicates that the workpiece speed did not affect the contact length much. Furthermore, in contradiction to the results in Figure 7.16, Figure 7.18, Figure 7.20 and Figure 7.23, Figure 7.25 indicates that the contact length ratio was sensitive to the depth of cut but not to the workpiece speed. The contact length ratio $R_l = l_{av}/l_g$ reduced from 4.5 to 2 with the increase of the cutting depth from 0.006 mm to 0.025 mm. From the grinding force results shown in Figure 7.6, the friction coefficients for CBN grinding M2 tool steel were very low in the range of 0.28 to 0.37. The friction coefficients are similar to the values when grinding cast iron with an aluminium oxide abrasive wheel. This indicated that the grinding performance was relatively inefficient. Further investigation for grinding M2 steel with CBN is necessary. However, the results obtained show that the real contact length is much larger than the geometrical contact length when using a CBN wheel to grind the M2 steel.

Chapter 8 MODEL EVALUATION

8.1 Evaluation Method

In Chapter 4, two contact length models were developed. Model One was based on a surface roughness approach and Model Two was based on a contact area approach,

$$\text{Model One: } l_c = [R_r^2 8 F_n' (K_s + K_w) d_s + a d_s]^{0.5} \quad (4.27)$$

$$\text{Model Two: } l_c = [C_A^2 (F_n'/H_v)^2 + a d_s]^{0.5} \quad (4.38)$$

The data used for the evaluation such as values of l_c , F_n' and a were taken from the experimental results displayed in Chapter 7. The real contact length, l_e , was assumed to be equal to the measured average length, l_{av} .

If the parameters R_r and C_A in the two models were assumed as constants, then they can be obtained by a non-linear curve fit. The following is a description of the method employed. From equation 4.27, the i th value of l_c can be written as

$$l_{ci} = (R_r^2 F_n'i 8 (K_s + K_w) d_s + a_i d_s)^{0.5} \quad (8.1)$$

The process of curve fitting seeks to minimise the differences between measured values of l_e and the theoretical values of l_c . This may be stated as

$$\sum(l_{avi} - l_{ci})^2 \Rightarrow \text{Minimum} \quad (8.2)$$

The value of R_r was solved using a 'Mathematica' routine to satisfy Criterion 8.2 [82]. The value of C_A was obtained in a similar way.

Results for the two models were compared with the Maris model [83] and the Kumar model [19] using the same experimental data.

8.2 Results

The results of the evaluation are shown in Figures 8.1 to 8.9. It was clearly shown that:

- (i) The results predicted by the two new models agree with experimental results better than results using other models over the whole range.
- (ii) The results predicted by the Kumar-Shaw model demonstrated a very poor agreement with experimental results. The reason was that this model did not take into account the fact that the contact surfaces between the wheel and the workpiece were not smooth.
- (iii) The Maris model understates the real contact length by a large margin particularly at low workspeeds.
- (iv) The results show that Model One, the surface roughness approach agrees with the experimental results better than Model Two, the contact area approach. The reason can be understood from a consideration of the parameters R_r and C_A . Figures 8.10 and 8.11 show the values of R_r established by curve fitting and the values from individual point fits R_{ri} . It can be seen that R_{ri} is independent of depth of cut as assumed. The parameter, R_r can therefore be treated as a constant. Figure 8.12 shows the non - linear curve fit values for C_A and the values from individual point fits, C_{Ai} . C_{Ai} is, however, dependent on the depth of cut. It was found to decrease as the depth of cut was increased. This relationship can therefore be represented as a function of

the depth of cut,

$$C_A = f(a) \quad (8.3)$$

- (v) Comparing the values of R_T for different workpiece speeds as shown in Figures 8.10 and 8.11, it can not be seen that R_T correlates with speed.

8.3 Refined Contact Area Approach

For Model One, no modification of the values of R_T was required with variation of depth of cut. For Model Two, a modification was required which shows that Model Two as formulated is a poor representation of the physical behaviour. The basic assumptions employed for Model Two need to be reconsidered. It was realised, that the assumption that the real contact area is a constant proportion of the apparent contact area needs to be changed. In practice, the area ratio R_A reduces with the normal force and a variation of the area ratio with normal force should be assumed.

It can be seen that Equation 4.38 is fundamentally different from Equation 4.27 in that the contact length is proportional to F_n^2 instead of F_n . Further consideration makes it clear that $R_A = A_a/A_r$ is not a constant. The real contact area should, in fact, be proportional to F_n to agree with observed behaviour of rough surfaces in contact and the fact that the number of active grains in contact increases with normal force.

It is therefore proposed that

$$R_A = \frac{C_1}{F_n} \quad (8.4)$$

So that

$$l_{fr}^2 = C_1^2 \left(\frac{R_p}{c}\right)^2 \frac{F_n'}{H_v^2}$$

or

$$l_{fr}^2 = C_a^2 \frac{F_n'}{H_v^2} \quad (8.5)$$

where $C_a = C_1 \frac{R_p}{c}$

For example, if at a particular value of force F_{no} , $R_A = 100$, then $C_1 = 100 F_{no}$ and $C_a = 100 F_{no} R_p/c$.

In practice, values of C_a will need to be determined from experimental grinding results by similar methods to those proposed for values of R_r .

Further research work is required to clarify whether this refined contact area approach has any operational advantage over the roughness factor approach. However, this approach does offer a physical explanation for the effect of workpiece hardness.

8.4 Recommended value of R_r

8.4.1 A value of R_r for the average contact length

In this research the values of the roughness factor, R_r ranged from 8 to 30.

(i) Grinding wheel and workpiece material condition

Several pairs of grinding wheel and workpiece material combinations were employed in this investigation. The combinations included an alumina wheel and cast iron, an alumina wheel and En9 steel, a CBN wheel and En9 steel and a CBN wheel and a M2 tool steel. Some of the pairs provided good grinding conditions such as using either

the alumina wheel or the CBN wheel for grinding En9 with or without coolant. Under these grinding conditions the grinding performance was always relatively stable. However, some of the combinations represented a poor grinding condition such as using an alumina wheel to grind cast iron. In this grinding condition the wheel was readily loaded and the grinding performance was difficult to control. It is difficult to say whether using a CBN wheel to grind M2 tool steel provides a good grinding performance or not because of limited experience. From the grinding force results shown in Figure 7.6, the friction coefficients for CBN grinding M2 tool steel were very low in the range from 0.28 to 0.37. This indicated that the grinding performance was relatively inefficient. For the alumina/En9 and CBN/En9 combinations, the value of R_f was 11 to 15 for dry grinding and 20 to 27 for wet grinding.

(ii) Grinding with or without coolant

The values of R_f for wet grinding were found to be larger than for dry grinding. Comparing the signals for dry and wet grinding, it was found that the size of the tail region was larger for wet grinding. It was considered that the reason may be related to the effects of elastohydrodynamic lubrication [81]. Both the high grinding speed and the grinding pressure would be expected to increase the viscosity of the coolant. As a result, a third layer of rigid film would be expected especially in the tail the contact zone as represented by 13" in Figure 6.3 and by l_{rub} in Figure 6.4. This third layer will change the distribution of pressure in the contact zone. The tail of the contact zone will differ from dry grinding conditions. Consequently the size of the contact zone will be larger than in dry grinding.

Further research work would be required to confirm whether this hypothesis provides an explanation of the coolant phenomenon.

Summarising the above discussion, a recommended value of R_f for dry grinding is

$$R_r = 13 \quad (8.6)$$

8.4.2 A value of R_r for thermal modelling

In predicting the temperature of the workpiece, it is very important to know the effective length of the heat source over which the energy conducts into the workpiece. As discussed in chapter 6, it might be assumed that l_2 represents the cutting and ploughing zone. If it is assumed that most of the grinding heat is generated by the friction and plastic deformation actions in the cutting and ploughing zone, it is reasonable to assume that $l_{ef} = l_2$. Figures 8.13 to 8.15 are the measured results of l_2 . The roughness factor R_r can be obtained by the same method as described in Section 8.1. Assuming the value of l_e is equal to l_2 the value R_r was obtained and denoted as R_{r2} . Figures 8.16 and 8.17 are the results obtained for R_{r2} . For dry grinding as shown in Figure 8.16,

$$R_{r2} = 9 \quad (8.7)$$

This value of $R_{r2} = 9$ is therefore recommended for thermal modelling.

8.5 Discussion and Conclusion

- (i) The new model based on a roughness factor shows high correlation with experimental behaviour.
- (ii) The Maris model gave poor agreement with the experimental results.
- (iii) The use of coolant affects the contact length signal. This may be caused by the effects of elastohydrodynamic lubrication. Further investigation is required.

(iv) Workpiece speed has little effect on R_r . However, R_r is sensitive to the grinding conditions for some material combinations. For an inefficient grinding process where, it is easy to wear or load the wheel, R_r is reduced. For an efficient grinding process where the wheel used is in an open condition, R_r remains constant.

(v) For general analysis of grinding conditions where measured values of R_r are unavailable, it is suggested that the value $R_r = 13$ should be used for dry grinding. Consequently the grinding contact length model becomes

$$\begin{aligned} l_c &= [(13)^2 8 F_n' (K_s + K_w) d_s + a d_s]^{0.5} \\ &= [1352 F_n' (K_s + K_w) d_s + a d_s]^{0.5} \end{aligned} \quad (8.8)$$

(vi) If the kinematic concept as described in Equation 2.23 and the concept of equivalent wheel diameter are considered, then the grinding contact length model becomes

$$l_{ck} = (1 \pm \frac{1}{q}) (R_r^2 8 d_e (K_w + K_s) F_n' + a d_e)^{0.5} \quad (8.9)$$

(vii) For thermal modelling, it is suggested that the value $R_{r2} = 9$ should be used for dry grinding.

Chapter 9 MODEL APPLICATION

9.1 Introduction

A purely theoretical model is not normally suitable for direct use in a practical application. The reason is that it is difficult to measure all the parameters which are required as inputs to the theoretical model [84, 85, 86, 87, 88, 89, 90]. Therefore, translating a theoretical model into a practical model which is easy to use with a wide-ranging accuracy is a significant task.

9.2 Model Modification for Application in Adaptive Control

The normal force needs to be known before the contact length model in Equation 8.9 can be applied

$$l_{ck} = (1 \pm \frac{1}{q}) [R_r^2 8 d_c (K_w + K_s) F_n + a d_c]^{0.5} \quad (8.9)$$

In a practical grinding system, however, the *normal grinding force is not always available or easy to obtain*. There are two ways to overcome this problem: (i) by using the grinding power signal. (ii) By substituting the normal force by an empirical grinding force equation.

9.2.1 Use of the grinding power

One way to avoid the need to measure the normal grinding force is to use grinding power. The reason is the grinding power signal is easy to obtain in practice, for a plunge grinding operation and can be approximately related to the normal grinding force.

The specific grinding power,

$$P' \approx v_s F_t' \quad (9.1)$$

and

$$F_t' \approx \mu F_n' \quad (9.2)$$

where P' is the specific grinding power. F_t' is the specific tangential force. μ is the grinding friction coefficient and the value of μ is approximately 0.3 to 0.5. μ can be obtained from experiment.

The specific normal force

$$F_n' = F_t' / \mu = P' / (\mu v_s) \quad (9.3)$$

By introducing a constant, C_p

$$F_n' = C_p P' / (\mu v_s) \quad (9.4)$$

where C_p is normally smaller than 1 as machine efficiency, $C_p = 0.7$ to 0.9 [91]. C_p can be obtained from experiment.

By substituting F_n' in Equation 8.9 with Equation 9.4

$$l_e = (1 \pm \frac{1}{q}) \left(8 R_r^2 C_p \frac{d_e K_e P'}{\mu v_s} + a d_e \right)^{0.5} \quad (9.5)$$

Grinding power can be logged in the course of a grinding operation. The grinding power is also a measure of the efficiency of the grinding process. So by using this information the contact length model can self-tune its constants such as C_p and μ , or even R_r . As a result, the theoretical model will be more suitable for a particular application.

9.2.2 An empirical force model

An alternative way to avoid the normal grinding force is to make a substitution for the normal grinding force from an empirical equation. In general, grinding force may be expressed as [92, 93, 94]:

$$F'_n = 10^{(3 e_2)} F_0 \left(\frac{1}{q}\right)^{e_1} a^{e_2} d_e^{e_3} \quad (9.6)$$

where F_0 , e_1 , e_2 and e_3 are constants. F_0 is usually found to lie in the range 10 to 20 N/mm. A range for e_1 is 0 to 1 and a typical value is 0.55. For e_2 the range is approximately 0.5 to 1 and a typical value is 0.75. For e_3 the range is about 0 to 0.5 and a typical value is 0.25 [93]. a is the depth of cut, in millimetres, and d_e is the equivalent diameter of grinding wheel, in millimetres. There are relationships between e_1 , e_2 and e_3 [92]

$$e_1 = 2 e_2 - 1$$

and

$$e_3 = 1 - e_2 \quad (9.6')$$

The grinding force can therefore be obtained from Equation 9.6. Equation 8.9 becomes

$$l_e = (1 \pm \frac{1}{q}) \left[8 R_f^2 K_e F_0 10^{3 e_2} \left(\frac{1}{q}\right)^{e_1} a^{e_2} d_e^{(1 + e_3)} + a d_e \right]^{0.5} \quad (9.7)$$

where $q = v_s/v_w$.

For cylindrical grinding,

$$a = vf/n_w = \pi d_w vf/v_w \quad (9.8)$$

where d_w is diameter of the workpiece, mm, and v_f is the infeed rate, mm/s.

The coefficients such as F_0 , e_1 , e_2 and e_3 can be obtained from either a data base or from experiments. The parameters such as d_e , K_e , q , n_w , d_w and a or v_f , can be obtained from the actual grinding operation. As a result, the contact length can be obtained from Equation 9.7.

9.3 Model Application

Much previous work considered has ignored the effect of grinding deflection. In some cases the effect of the grinding geometry was ignored. The advantage of this kind of approach is to simplify the problem. Applying the simplifications without proper consideration will however lead to inaccuracy. For example, Kopalinsky [95] analysed workpiece temperature and grinding force in terms of geometric contact length, l_g instead of real contact length, l_e . The workpiece material was En9 steel and grinding was carried out with a WA46J wheel without coolant. The grinding conditions were as follows: wheel diameter, d_s , was 177 mm; wheel depth of cut, a , was 20 μm ; width of cut, b , was 3 mm; wheel speed, v_s , was 40 m/s; workpiece speed, v_w , was 0.5 m/s. “Neglecting elastic flattening of the wheel” [95], the contact length and the apparent area of contact were given as

$$l_e = (a d_e)^{0.5} \left(1 + \frac{1}{q}\right) = 1.91 \text{ mm}$$

and

$$A_a = l_e b = 5.72 \text{ mm}^2$$

However using the Equation 8.9 then

$$l_e = \left(1 + \frac{1}{q}\right) \left(a d_e + 1352 K_e F_n' d_e\right)^{0.5}$$

$$= (1 + 0.01) (3.54 + 9.00)^{0.5} \\ = 3.58 \text{ mm}$$

and

$$A_a = l_e b = 10.73 \text{ mm}^2$$

where $d_e = d_s$, $F_n' = 15/3 = 5 \text{ N/mm}$, $K_e = (6.16 + 1.36) 10^{-6} = 7.52 10^{-6} \text{ mm}^2/\text{N}$.

It can be seen that in this case depending on whether elastic flattening of the wheel is neglected or not varies the size of the heat source by approximately 87%. The size of the heat source was later used to calculate temperature in the grinding zone [95].

A discussion on simplifications is therefore essential. For example, Equation 9.7 was used to predict the contact length ratio. Based on the empirical force equation, criteria for simplifying the contact length model are proposed.

From Equation 9.7 ignoring the term $(1 \pm 1/q)$,

$$R_r^2 = \left(\frac{l_e}{l_g} \right)^2 \\ = 1 + \frac{l_r^2}{l_g^2} \\ = 1 + \frac{R_r^2 (8 10^{(3 e_2)} K_e F_0) \left(\frac{1}{q} \right)^{e_1} d_e^{e_3}}{a^{(1 - e_2)}} \quad (9.9)$$

K_e and F_0 are constants and given by $C_r = 8 10^{(3 e_2)} K_e F_0$.

$$R_r^2 = 1 + \frac{R_r^2 C_r \left(\frac{1}{q} \right)^{e_1} d_e^{e_3}}{a^{(1 - e_2)}} \quad (9.10)$$

When grinding mild steel or easy-to-grind materials with an appropriate grinding wheel, values such as $e_2 = 0.87$, $F_0 = 20 \text{ N/mm}$ were suggested [92]. Based on Equation 9.10

the relationship between R_l , v_w and a were simulated as shown in Figure 9.1. Based on this simulation, the limits were obtained for model simplification.

9.3.1 A criterion for $l_e = R_r l_{fr}$

It can be seen from Equation 9.10 and Figure 9.1 that the smaller the depth of cut is, the larger the ratio R_l in Figure 9.1. This means that the deflection of the grinding wheel has a stronger effect on the contact length at small depths of cut.

If the depth of cut, a , is small enough then the second term of Equation 9.10 is much larger than the first term. That is

$$\frac{R_r^2 C_r \left(\frac{1}{q}\right)^{\epsilon_1} d_e^{\epsilon_2}}{a^{(1-\epsilon_2)}} \gg 1 \quad (9.11)$$

In this case the first term can be ignored within an acceptable accuracy and Equation 9.10 can be reduced to

$$R_l = \left(\frac{R_r^2 C_r \left(\frac{1}{q}\right)^{\epsilon_1} d_e^{\epsilon_2}}{a^{(1-\epsilon_2)}} \right)^{0.5} \quad (9.12)$$

and

$$l_e = R_r l_{fs} \quad (9.13)$$

If for example, the error caused by this simplification is to be controlled within 5%, then a limit curve is obtained as shown in Figure 9.2. Any combination of depth of cut, a , and workspeed, v_w located to the right hand side of the boundary means that the simplification $l_e = l_{fr}$ will allow the contact length to be predicted with an error less than 5%. Most previous applications of this simplification, such as Lindsay [2] and Brown [17] ignored the conditions where the effect of grinding geometry were in contradiction

with this limitation.

The condition when the effect of geometry on the depth of cut can be ignored is given by Inequality 9.11 and Figure 9.2. The effect of grinding geometry on the contact length can be ignored without losing accuracy, where the depth of cut is very small, such as in the spark-out stage of a normal grinding cycle, or in a honing process or in very fine grinding.

9.3.2 A criterion for $l_e = l_g$

It can be seen from Equation 9.10 and Figure 9.1 that the larger the depth of cut is, the smaller is the ratio R_l . This means that the surface topography of the grinding wheel has a weaker effect on the contact length at large depths of cut.

If the depth of cut, a , is large enough then the first term of Equation 9.10 is much larger than the second term. That is, if

$$\frac{R_r^2 C_r \left(\frac{1}{q}\right)^{\epsilon_1} d_e^{\epsilon_2}}{a^{(1-\epsilon_2)}} \ll 1 \quad (9.14)$$

the second term can be ignored. In this case Equation 9.10 can be reduced to

$$R_l^2 = 1$$

and

$$l_e = l_g \quad (9.15)$$

If for example, the error caused by this simplification is to be controlled within 5%, then a boundary curve is obtained as shown in Figure 9.3. Any combination of depth of cut, a , and workspeed, v_w located to the left hand side of the boundary curve means that the simplification $l_e = l_g$ will allow the contact length to be predicted within 5%. Most

previous applications of this simplification, such as Kopalinsky [95] ignored the fact that the grinding force and the roughness were in contradiction to this criterion.

The condition when the effects of elastic flattening of the wheel and the topography of the wheel can be ignored is given by Inequality 9.14 and Figure 9.3. To satisfy this relationship, the true depth of cut must be large enough or the workpiece speed small enough as in creep feed grinding. In most cases, to ignore the effects of elastic flattening of the wheel and the topography of the wheel as assumed by many researchers [9, 62, 95, 96, 97, 98, 99, 100] does not satisfy this criterion. Their simplifications therefore often lead to unacceptable errors.

9.4 Speed Ratio

In some publications, it is suggested that speed ratio, q , affects contact length as a kinematic factor. If kinematics are taken into consideration as Equation 8.9, the contact length is

$$\begin{aligned} l_{ck} &= (1 \pm 1/q) l_c \\ &= (1 \pm 1/q)(l_{fr}^2 + l_g^2)^{0.5} \end{aligned}$$

If $q = 60$ for example, the error from ignoring the term $(1 \pm 1/q)$ is 1.7 %. So the term $(1 \pm 1/q)$ can be ignored in most applications. But comparing the experimental results at different speed ratio as shown in Figures 7.19, 7.21 and 7.22, it is found that the speed ratio has a stronger effect than described by the term $(1 \pm 1/q)$. There is an indirect effect of speed ratio on the contact length. The speed ratio affects the grinding forces and hence the grinding deflection. This can be interpreted by the modified model Equation 9.7 and Figure 9.1.

If the change of speed ratio is 3 times, for an example from 100 to 300, the change of

l_{fr}^2 will be 1.7 times.

9.5 Surface Roughness

In the Brandin contact length model the surface roughness, R_t , was considered as the main determinant as represented in Equation 2.40 [9],

$$l_c = [(R_t + a) d_e]^{0.5} + (R_t d_e)^{0.5} \quad (2.40)$$

The effect of R_t on the size of the contact zone is illustrated in Figure 9.4.

For ease of discussion it was assumed that the surface roughness on the surface to be ground and the surface ground were the same.

Surface roughness will influence the scatter of measured average length of contact and the measured maximum length of contact as shown in Figure 9.4. For example, for different surface roughness condition of a workpiece, R_{t1} and R_{t2} , the distributions are different. As a result, the maximum lengths of contact will be different as illustrated in Figure 9.4(b). However, the average length of contact will be the same. The reason why the average length of contact, l_{av} , is larger than the geometrical contact length, l_g , is, therefore, not due to the roughness of the surface ground and the surface to be ground, but due to the elastic/plastic deflection of the grinding wheel and the workpiece, the roughness of the wheel surface and the roughness of the workpiece surface within the contact zone during the grinding process.

The maximum length of contact measured l_{max} can be described by the following equation if the Brandin concept is assumed to be correct. The maximum contact length as shown in Figure 9.4 will be

$$\begin{aligned}
 l_{\max} &= l_a + l_b \\
 &= \left[\left(\frac{R_t}{2} + \delta_e + a \right) d_e \right]^{0.5} + \left[\left(\frac{R_t}{2} + \delta_e \right) d_e \right]^{0.5}
 \end{aligned} \tag{9.16}$$

where δ_e is the extent of the elastic recovery of the workpiece, as shown in Figure 9.4.

Comparing Equation 9.16 with Equation 2.40, it may be clearly shown that the Brandin model is not compatible with his own assumption.

Chapter 10 CONCLUSIONS

- (i) It has been shown that the real contact length is much larger than the geometrical contact length. This conclusion is supported by the review of published experimental work, the theoretical study undertaken in this thesis and experimental results obtained.
- (ii) A new finding of the contact length model in grinding is $l_c^2 = l_f^2 + l_g^2$. The orthogonal combination of the contact length due to the deformation which would occur with zero depth of cut and the contact length due to the depth of cut clarifies for the first time the effects of the grinding geometry, represented by l_g , and the deflection of Hertzian contact, represented by l_f , on the contact length. This relationship was used as a basis for further analysis.
- (iii) Considering that the contacting surfaces in abrasive machining processes are far from smooth as the Hertzian contact surfaces, the theoretical model was developed and represented as

$$l_c = [R_r^2 8 F_n' (K_s + K_w) d_s + a d_s]^{0.5}$$

This new contact length model indicates that the main parameters influencing contact length are: the real depth of cut, the elastic deflection of the grinding wheel and the surface topography of the grinding wheel.

- (iv) Considering the very small real contact area between the grinding wheel and the workpiece within the contact zone, the theoretical model was developed and represented as

$$l_c = [R_A^2 \left(\frac{R_p}{c} \right)^2 \left(\frac{F_n'}{H_v} \right)^2 + a d_s]^{0.5}$$

The advantage of this model is that using workpiece hardness to describe the surface contact makes the process more understandable.

- (v) A measuring system for the experimental investigation on a surface grinding machine was developed. It was found that the applied power source technique used was judged to give the most reliable measure of contact length. The new developed technique for measuring real depth of cut can carried out the measurements within 10 % error. The advantage of the thermocouple technique used is the small size of the sensing area which gives improved results compared to previously described systems.
- (vi) It is verified that the signal obtained from the applied power source method is the function of the size of average contact area of the active grains and the number of the active grains contacted with the workpiece. From this signal, it is found there are three distinguished contact extents in a contact zone which represent cutting, ploughing and sliding in grinding action respectively. The real contact length l_c can be defined as the average size of wheel-workpiece contact zone, l_{av} , in which the active grains are cutting, ploughing and rubbing the workpiece effectively.
- (vii) The results obtained from the experimental investigation show that the measured contact length in dry grinding was much larger than the geometrical contact length. The contact length in wet grinding is longer than the contact length in dry grinding.
- (viii) The contact length when grinding cast iron is shorter than the contact length when grinding mild steel or tool steel.
- (ix) The model based on a surface roughness factor demonstrates a high correlation with experimental behaviour. It is found that the parameter R_t in the model is generally insensitive to the grinding variables such as depth of cut, speed ratio,

material hardness and grinding wheel. But R_f is sensitive to the grinding conditions for some material combinations. For general analysis of dry grinding conditions an overall average value of $R_f = 13$ may be used. The effective length for thermal modelling l_{ef} should use the value l_2 . The value $R_{r2} = 9$ may be used for thermal modelling in dry grinding.

(x) The new model has been modified for application to an adaptive control system.

(a) For application based on the grinding power signal, the model becomes

$$l_e = (1 \pm \frac{1}{q}) \left(8 R_f^2 C_p \frac{d_e K_e P'}{\mu v_s} + a d_e \right)^{0.5}.$$

(b) For application based on an empirical grinding force equation, the model becomes

$$l_e = (1 \pm \frac{1}{q}) \left(8 R_f^2 K_e F_0 10^{3 e_2} \left(\frac{1}{q}\right)^{e_1} a^{e_2} d_e^{(1+e_3)} + a d_e \right)^{0.5}$$

(xi) The grinding contact length in a range from conventional grinding conditions to creep feed grinding conditions were predicted. From this prediction, the criteria for ignoring grinding geometry when $l_e = R_f l_{fr}$ or for ignoring the grinding force effect when $l_e = l_g$ were obtained. In most cases, to ignore either the effects of elastic flattening of the wheel and the topography of the wheel or the grinding geometry as assumed by many researchers [2, 9, 17, 62, 95, 96, 97, 98, 99, 100] does not satisfy the criteria and consequently leads to unacceptable errors.

Chapter 11 FUTURE WORK

There are several issues need to be investigated:

- (i) Further research work is necessary to clarify whether the refined contact area approach can successfully predict the effect of material hardness. Because of the difference in grinding conditions and wheel loading as discussed in the previous chapter it was not possible to confirm the effects of wheel hardness and workpiece hardness. More experimental work is required to do to clarify these effects especially for the superabrasive wheel. It was found that it is possible to develop a contact length model from first principles. The number of active grains increases with normal force. A more realistic contact area approach would take account of this effect.
- (ii) More experimental work is required to do to clarify the effect of coolant on the real contact length. It is worthwhile to confirm whether the hypothesis of the effects of hydrodynamic or elastohydrodynamic lubrication provides an explanation of the coolant phenomenon. More experimental work is required to do to verify the boundary for the model simplification especially in a creep feed grinding condition.
- (iii) The example of model application shows the potential to use the practical models in a model based decision making support system for an intelligent adaptive control grinding system. An investigation of the application of the practical contact length model into an intelligent adaptive control grinding system will be of great interest.

REFERENCES

- 1 Robert S. Hahn, 1962, On the Nature of the Grinding Process, Proceedings of the 3RD International M.T.D.R. Conference, Birmingham, September, Pergamon Press, 129-154
- 2 Richard P. Lindsay and Robert S. Hahn, 1971, The Principles of Grinding, Sme Technical Report, MRR71-01
- 3 Hideichi Makino, Tesuya Suto and Eiichi Fukushima, 1966, An Experimental Investigation of the Grinding Process, Journal of Mechanical Laboratory of Japan, 12,1, 17-21
- 4 W.B. Rowe, H.S. Qi, M.N. Morgan and H.W. Zheng, 1993, The effect of deformation on the contact area in grinding, Annals of the CIRP, 42, 1, p409
- 5 H.S. Qi, B. Mills and W.B. Rowe, 1994, An analysis of real contact length in abrasive machining processes using contact mechanics, Wear, 176, 137-141
- 6 International Standard, ISO 3002-5, 1989 (E)
- 7 J. Verkerk, 1975, The Real Contact length in Cylindrical plunge Grinding, Annals of the CIRP, 24, 1, 259-264
- 8 Rowe W.B., Morgan M.N., Allanson D.R., 1991, An Advance in the modelling of Thermal Effects in the Grinding Process, Annals of the CIRP, 40, 1, 339-342
- 9 Ir.E. Vansevenant, 1987, A Subsurface Integrity model in Grinding, PhD

- 10 W.B. Rowe and F. Koenigsberger, 1965, The ‘Work-Regenerative’ Effect in Centreless Grinding, *Int. J. Mach. Tool Des. Res.*, 4, 175-187
- 11 S. Malkin, 1989, *Grinding Technology -theory and applications of machining with abrasives*, Ellis Horwood Limited, Chichester
- 12 R. Snoeys and D. Brown, 1969, Dominating Parameters in Grinding Wheel and Workpiece Regenerative Chatter, *M.T.D.R.*, pp. 325-348
- 13 Ir.E. Vansevenant, 1987, An Improved Mathematical Model to Predict Residual Stresses in Surface Grinding, *Annals of the CIRP*, 36, 1, p.413
- 14 Rowe W.B., Allanson D.R., Pettit J.A., Moruzzi J.L. and Kelly S., 1991, Intelligent CNC for Grinding, *Proceedings of the Institution of Mechanical Engineers*, 205, 233-239
- 15 W. König, L. Cronjager, et. al, 1990, Machining of New Materials, *Annals of the CIRP*, 39, 2, 673-681
- 16 J. Peters and R. Snoeys, The E modulus, a suitable characteristic of grinding wheels, Vol. 11, No. 4, 1-11
- 17 R.H. Brown, K. Saito and M.C. Shaw, 1971, Local Elastic Deflections in Grinding, *Annals of the CIRP*, 19, 1, 105-113
- 18 Hideo Tsuwa, et al, 1975, On Change of Arc of Contact Length in Surface Grinding, *Journal of Japan Society of Precision Engineering*, 41, 358-363

- 19 K.V. Kumar and M.C. Shaw, 1981, "The Role of Wheel-Work Deflection in Grinding Operations", Transactions of the ASME, Journal of Engineering for Industry, February, 103, 73
- 20 Gu, D.Y., 1992, The contact zone in surface grinding, PhD Thesis, University of Western Australia, Australia
- 21 Robert S. Hahn and R. Lindsay, 1967, On the Effect of Real Area of Contact and Normal Stress in Grinding, Annals of the CIRP Vol. XV pp. 197-204
- 22 K.V. Kumar and M.C. Shaw, 1979, A New Method of Characterising Grinding Wheels, Annals of the CIRP, 28, 1
- 23 K.V. Kumar, M. Cozminca, Y. Tanaka and M.C. Shaw, 1980, A New Method of Studying the Performance of Grinding Wheels, Transactions of the ASME, Journal of Engineering for Industry, February, 102, P.80
- 24 Wolfgang J. Sauer, Milton C. Shaw, 1974, The Role of Elastic Deflections of the Wheel-work Interface in Surface grinding, International Conference of Production Engineering, Tokyo, pp. 645-648
- 25 R.H. Brown, J.G. Wager, and J.D. Watson, 1977, An Examination of the Wheel-Work Interface using an Explosive Device to Suddenly Interrupt the Surface Grinding Process, Annals of the CIRP, 25, 1
- 26 D.Y. Gu and J.G. Wager, 1990, Further Evidence on the Contact Zone in Surface Grinding, Annals of the CIRP, 39, 1, p.349

- 27 Z. X. Zhou, C. A. van Lutterwelt, 1992, The Real Contact Length between Grinding Wheel and Workpiece - A New Concept and a New measuring Method, Annals of the CIRP, 41, 1, PP. 387-391
- 28 S.M. Pandit, 1981, A New Approach to the Analysis of Wheel-workpiece Interaction in Surface Grinding, 9th NAMER. Mfg. Res. Conf., Proc., Mfg. Eng. Trans., SME
- 29 S.M. Pandit, 1981, Characteristic Shapes and Wavelength Decomposition of Surfaces in Machining, Annals of the CIRP, 30,1, PP. 487-492
- 30 Hertz, H., 1882a, On the contact of elastic solids, J. reine und angewandte Mathematik, 92, 156-171. (For English translation see Miscellaneous Papers by H. Hertz, Eds. Jones and Schott, London: Macmillan, 1896.)
- 31 K.L. Johnson, 1989, Contact Mechanics, Cambridge University Press
- 32 Ivan Iliuc, 1980, Tribology of Thin Layers, Elsevier Scientific Publishing Company, Amsterdam-Oxford-New York
- 33 Williamson, L.B.P., Hunt, R.T., 1968, The microtopography of solid surfaces, Burndy Research Rep., 59
- 34 Moore, D.F., 1969, A history of research on surface texture effects, Wear, 13, 381-412
- 35 F.P. Bowden and D. Tabor, 1986, The Friction and Lubrication of Solids, Clarendon Press, Oxford
- 36 J.A. Greenwood, 1982, The contact of real surfaces, Contact Mechanics and

Wear of Rail/Wheel Systems, University of Waterloo Press, Vancouver, British Columbia, July 6-9, 21-35

- 37 K.L. Johnson, 1987, Aspects of contact mechanics, IMechE, C246/87, 919-932
- 38 R. Holm, 1967, Electric Contact, Theory and Application, 4th edn. Springer-Verlag, New York
- 39 J.A. Greenwood and J.H. Tripp, 1967, The Elastic Contact of Rough Spheres, Journal of Applied Mechanics March, 153-159
- 40 C.C. Lo, 1969, Elastic Contact of Rough Cylinders, International Journal of Mechanical Sciences, Vol. 11, 105-115
- 41 B.W. Mott, 1956, Micro-Indentation Hardness Testing, Butterworths Scientific Publications, London
- 42 R.D. Arnell, P.B. Davies, J. Halling and T.L. Whomes, 1991, Tribology Principles and Design Applications, Macmillan Education Ltd
- 43 N. Des Ruisseaux, 1968, Thermal Aspects Of Grinding Processes, University of Cincinnati Dissertation
- 44 W.B. Rowe, J.A. Pettit, A. Boyle and J.L. Moruzzi, 1989, Avoidance of thermal damage in grinding and prediction of the damage threshold, Annals CIRP, Vol. 37/1, 327-330
- 45 A.S. Lavine, 1991, Thermal Aspects of Grinding: The Effect of Heat Generation at the Shear Planes, Annals of the CIRP, 40, 1343-345

- 46 A.S. Lavine, S. Malkin and T.C. Jen, 1989, Thermal Aspects of Grinding with CBN Wheels, Annals of the CIRP 38,1, PP. 557-560
- 47 W.B. Rowe, S. Black, B. Mills and H.S. Qi, 1994, Experimental Energy Partitioning in Grinding, Proc. of EuroMetalWorking Conf., Udine, Italy
- 48 Jaeger J.C., 1942, moving sources of heat and the temperature at sliding contacts, proceedings of the Royal society of new south wales, 76, 203-224
- 49 W.B. Rowe, S. Black, B. Mill, H.S. Qi, and M. Morgan, 1995, Experimental Investigation of Heat transfer in grinding, Annals of the CIRP, 44, 1, 329-332
- 50 Hahn R.S. and Lindsay P.L., 1971, Principle of Grinding - Part 1, Machinery, Vol. 77/1, p 55-62
- 51 W.B. Rowe, H.S. Qi, M.N. Morgan and H.W. Zheng, 1993, The real contact length in grinding based on depth of cut and contact deflections, Proc. of the Thirtieth International MATADOR Conference, UMIST, 187-194
- 52 Kazuo Nakayama, 1967, Elastic Deformation of Contact Zone in Grinding, Bull. Japan Soc. of Prec. Engg., 5, 4, 93
- 53 D.P. Saini, 1980, Elastic Deflections in Grinding, Annals of the CIRP, 29, 1, 189
- 54 D.Y. Gu and J.G. Wager, 1988, New Evidence on the Contact Zone in Grinding- Contact Length, Sliding and Cutting Regions, Annals of the CIRP, 37, 1, 335-338

- 55 Aerens R., 1983, CRIF-WTCM internal report nr.83V1
- 56 E. Saljé, R. Paulmann, 1988, Relations Between Abrasive Processes, Annals of the CIRP, 37, 2, 641
- 57 E. Saljé, H. Teiwes and Heidenfelder, 1983, Important Results on External Cylindrical Plunge Grinding with Unusual Workpiece Peripheral Speeds and Speed Ratios q in the Range of -0.2 to -20000, Annals of the CIRP, 32, 1, p.241
- 58 E. Saljé and H. Mohlen, 1986, Fundamental Dependencies upon Contact lengths and Results in Grinding, Annals of the CIRP, 35, 1, p.249
- 59 Kenji Sato, 1965, Progress of Researches on Grinding Mechanics in Japan, Bulletin of J. S. G. E. vol. 5, 1965
- 60 Pande, S.J., Lal, G.K., 1979, Effect of dressing on grinding wheel performance, Int.. MTDR, 19, 171-179
- 61 Koloc, J., 1959, On the wear of grinding wheels, Micro Technic, v. 8, 1, 13-15
- 62 Lindsay P. R., Hahn R., 1971, On the metal removal and wheel removal parameters, surface finish, geometry and thermal damage in precision grinding, Dissertation Worcester Poly. Institute
- 63 W. König, W. Lortz, 1975, Properties of cutting edges related to chip formation in grinding, Annals of the CIRP 24, 1, PP. 231-235
- 64 S. Malkin, 1968, The attritious and fracture wear of grinding wheels, Sc.D. thesis, MIT

- 65 A.Y.C. Nee and A.O. Tay, 1981, On the Measurement of Surface Grinding Temperature, Int. J. Mach. Tool Des. Res. vol. 21, No. 3/4 pp. 279-291
- 66 E.A. Brander and G.B. Brook, 1993, Smithells Metals Reference Book, Butterworth Heinemann, Seventh Edition
- 67 Peklenik, J., 1958, Der Mechanisms des Schleifens unt die Uberschliffzahl, Industrie-Anzeiger, Vol. 80/1, 10-17
- 68 I.P. Karaim, Influence of cooling method on grinding zone temperature, Machs Tool, XL, 42
- 69 V.G. Lebedev et al., 1973, Assessing ground-surface contact temperature using grindable thermocouples, Machs Tool, p. 45
- 70 V.V. Tatrenko et al., 1970, Universal thermocouple for measuring grinding temperature, Measmt Tech. 2, 265-266
- 71 D.E. Anel'chik et al., 1968, An investigation into the instantaneous temperature in the grinding of alloy steel, Ind. Dia. Rev. 539
- 72 S. Kohli, C. Guo, S. Malkin, 1995, Energy partition to the workpiece for Grinding with Aluminium Oxide and CBN Abrasive Wheels, Journal of Engineering for Industry, Transactions of the ASME, Vol. 117, 160-168
- 73 J.A. Greenwood, 1966, Constriction Resistance and the Real Area of Contact, Brit. J. Appl. Phys., vol. 17

- 74 J. Verkerk, 1977, Final report concerning CIRP Cooperative work on the characterization of grinding wheel topography, Annals of the CIRP, 26, 2, pp. 385-395
- 75 Hugh D. Young, 1962, Statistical treatment of Experimental Data, McGRAW-HILL Book company, INC.
- 76 Williamson, J.B.P., 1967-8, The microtopography of surfaces in Properties and metrology of surfaces, Proc. Inst. Mech. Eng. 182 Pt 3k, 21
- 77 Thomas, T.R., (Ed.) 1982, Rough Surfaces, London, Longman
- 78 Greenwood, J.A., 1984, A unified theory of surface roughness, proceedings, Royal Society, A393, 133
- 79 Whitehouse, D.J. and Phillips, M.J., 1978, Discrete properties of random surfaces, Phil. Trans. Royal Society, A290, 267
- 80 P. Koshy, V.K. Jain and G.K. Lal, 1993, *A model for the topography of diamond grinding wheels*, Wear, 169, p237-242
- 81 D. Dowson, G.R. Higginson, 1977, Elastohydrodynamic Lubrication, Pergamon Press Ltd.
- 82 'Mathematica' by Wolfram Research Inc., 1992
- 83 M. Maris, 1977, PhD thesis, Katholieke Universiteit te Leuven, Belgien
- 84 D.R. Allanson, 1995, PhD Thesis, Liverpool John Moores University, UK.

- 85 W.B. Rowe, S. Kelly and J.L. Moruzzi, 1989, Adaptive grinding control, J. of Advanced Manufacturing Engineering, vol. 1/5, 287-295
- 86 H. Kaliszer and J. Webster, 1982, Inprocess measurement and assessment of form errors during cylindrical grinding, Proc. 3rd Polytechnic Symposium on Manufacturing Engineering, Wolverhampton, 25th-26th May 179-189
- 87 W. König and G. Werner, 1974, Adaptive control optimisation of high efficiency external grinding - concept, technological basics and application, Annals CIRP, Vol. 23/1, 101-102
- 88 Rowe W.B., Morgan M.N., Allanson D.R., 1992, The Tribology of Grinding from Energy Considerations, Proceedings of the I Mech E. Presented at 6th IMechE/IoP Tribology Seminar, 10th April
- 89 H. Kaliszer, 1980, Keynote paper - Adaptive Control in Grinding Processes, Proc. 4th Int. Conf. on production Engineering, Tokyo, 579-593
- 90 H.K. Töenshoff, J.P. Wulfsberg, et al, 1988, Developments and Trends in Monitoring and Control of Machining Processes, Annals of the CIRP 37,2, 611-622
- 91 Taghi Tawakoli, 1993, High Efficiency Deep Grinding, VDI - Verlag GmbH, Mechanical Engineering Publications Limited, LONDON
- 92 P.G. Werner, 1979, Application and Technological Fundamentals of Deep and Creep Feed Grinding, SME TECHNICAL PAPER, MR79-319

- 93 Li Lichun, Fu Jizai, 1980, A Study of Grinding Force Mathematical Model, Annals of the CIRP 29, 1, PP. 245-249
- 94 H.K. Tönshoff, J. Peters, I. Inasaki, T. Paul, 1992, Modelling and Simulation of Grinding Processes, Annals of the CIRP 41, 2, 677-688
- 95 Eleonora M. Kopalinsky, 1984, A new approach to calculating the workpiece temperature distributions in grinding, Wear, 94, 295-322
- 96 B. Zhu, C. Guo, J.E. Sunderland, S. Malkin, 1995, Energy Partition to the Workpiece for Grinding Ceramics, Annals of the CIRP Vol. 44/1, 267-271
- 97 R. Snoeys, J. Peters, 1974, The Significance of Chip Thickness in Grinding, Annals of the CIRP, 32, 2, PP. 227-237
- 98 N.R. Des Ruisseaux and R.D. Zerkle, 1970, Thermal Analysis of the Grinding Process, Transactions of the ASME, Journal of Engineering for Industry, May, 428-434
- 99 B.W. Kruszinski, 1995, Model of Gear-Grinding Process, Annals of the CIRP, 44, 1, 321-324
- 100 L. Kops and L.M. Hucke, 1973, Thermal simulation of the grinding process, Proc. of the NAMRC, Vol. 3 pt. 95-115

APPENDICES

Appendix 1 Computer Programs

A1.1 Source code for data logging

```
/* HDTL9.C Written by Hong-Sheng Qi, 30.4.93
 - to log two force signals
 data stored in memory using DMA
 - read data from memory and write to file
 */

#include <stdio.h>
#include <stdlib.h>
#include <math.h>
#include <string.h>

#define DATA 30000          /* no. of DMA conversions */
/* #define LOG      10000    /* no. of arrys */

int data[10];           /* storage for logs */
int darray[DATA];        /* data array */

main()
{
    FILE *fopen(), *out_file;          /* data file */
    char file_name[10] = "ctl";        /* */
    char temp_file_name[10];           /* */
    char index[3];                   /* */

    int LOG = 1000, cc1=250, cc2=100;
    int i, j, k, error, batch_size, trigger_level, test, flag, check;
    int trial_number=0, mean_number=100; /* */

    int _far *buffer;                /* buffer pointer */
    int _far *alloc();               /* */
    float A;
    float sum_power, base_power, mean_power;

    printf("Hdtl9 : 1)Gain = 50, V = -500 - +500 mv. 2) C1-Fn, C2-Fn(6Hz), C3-Ft,
C4-Ft(6Hz).\n");

    printf("enter trial_number\n");    /* user enters */
    scanf ("%d", &trial_number);      /* batch_size */
    printf("Sample rate = %.2fkHz\n", FREQ);

/* ----- set up das20 ----- */

    data[0] = 0x300;                 /* ? base address &H300 */
    data[1] = 2;                     /* ? Interrupt level */
    data[2] = 1;                     /* DMA channel "1" */
```

```

if ( (error = das20(0, data)) != 0)
    printf(" mode 0 error = %d\n", error); /* set up das20 */

data[0] = cc1;                      /* set block scan */
data[1] = cc2;                      /* pacer clock */
if ( (error = das20(25, data)) != 0) /* to FREQ kHz */
    printf(" mode 25 error = %d\n", error); /* cc1*cc2*FRAQ kHz=5mHz */

data[0] = 0;                        /* Fn signal without filter */
data[1] = 5;                        /* X10 bipolar 0-+500 mv */
data[2] = 2;                        /* FIRst entry */
if ( (error = das20(1, data)) != 0) /* initialize the counters */
    printf(" mode 1 error = %d\n", error); /* at channel "0" */

data[0] = 1;                        /* Fn signal with filter 6 Hz */
data[1] = 5;                        /* X10 bipolar -+500mv */
data[2] = 0;                        /* normal queue entry */
if ( (error = das20(1, data)) != 0) /* initialize the counters */
    printf(" mode 1 error = %d\n", error); /* at channel "1" */

data[0] = 2;                        /* Ft signal without filter */
data[1] = 5;                        /* X10 bipolar -+500mv */
data[2] = 0;                        /* normal queue entry */
if ( (error = das20(1, data)) != 0) /* initialize the counters */
    printf(" mode 1 error = %d\n", error); /* at channel "2" */

data[0] = 3;                        /* Ft signal with filter 6 Hz */
data[1] = 5;                        /* X10 bipolar -+500mv */
data[2] = 1;                        /* LAST entry */
if ( (error = das20(1, data)) != 0) /* add EOQ flag */
    printf(" mode 1 error = %d\n", error); /* at channel "3" */

/* ----- */

if ( (buffer = alloc(32766)) == NULL)          /* ? allocate buffer */
    printf("cannot allocate buffer\n"); /* */
else
    printf("buffer at %04x %04x\n", segadr(buffer), offadr(buffer));

/* ----- Begin and Trigger ----- */

/* while(sample_number<batch_size)
{
    printf("To begin the data log, press any key \n");

    while( ! kbhit() )      /* To begin the data log, press any key */
    {

        printf("Begin the data logging\n");

/* ----- Begin data logging ----- */

        for (i=0; i<10; ++i )
            temp_file_name[i]=file_name[i];

        /* ++sample_number;           /* auto increment */

```

```

data[0] = LOG;           /* times of data log */
data[1] = segadr(buffer); /* buffer address */
data[2] = 2;             /* Internal clock/No gate */
data[3] = 1;             /* single cycle */
if ( (error = das20(27, data)) != 0) /* start DMA transfer */
    printf(" mode 27 error = %d\n", error); /* */

printf(" Waiting for completion of DMA transfer\n");

data[1] = 1;           /* wait for DMA completion */
while((data[1]) != 0) /* of DMA transfer */
{
    if ( (error = das20(12, data)) != 0) /* DMA stuatu */
        printf(" mode 12 error = %d\n", error); /* check */
    printf(" conversion ú = %u\n", data[2]);
}

if ( (error = das20(11, data)) != 0) /* disable DMA */
printf(" mode 11 error = %d\n", error); /* */

/* ----- read data ----- */

data[0] = LOG * 4;           /* number of data */
data[1] = segadr(buffer); /* buffer address */
data[2] = 0;                /* start position */
data[3] = offadr(darray); /* array address */
data[4] = 0;                /* ?? */
data[5] = 1;                /* */
data[6] = 0;                /* */
if ((error = das20(13, data)) != 0) /* read data from memory */
printf(" mode 13 error = %d\n", error);

/* ----- */

/* ----- print data to file ----- */

printf(" waiting to file\n");

strcat( temp_file_name, ".");
itoa(trial_number, index, 10 );
strcat( temp_file_name, index );

out_file = fopen( temp_file_name, "w"); /* ?? */
fprintf(out_file,"Hdtl9 : 1) Gain = 50, V = -0.5 - +0.5 v. 2) C1-Fn, C2-Fn(6Hz),
C3-Ft, C4-Ft(6Hz)\n");
fprintf(out_file,"%s\n", &temp_file_name);
fprintf(out_file,"time(ms)   Fn   Fn(6Hz)   Ft   Ft(6Hz)\n");
j=1;
for (i=0; i<(LOG*4); i=i+4)
{
fprintf(out_file,"%2f%10d%16d%16d%16d\n",j/FREQ, darray[i]/4.96*1.47,
darray[i+1]/4.96*1.47, darray[i+2]/4.96*1.314, darray[i+3]/4.96*1.314);
++j;
}
fclose( out_file );
}

```

A 1.2 Mathematica program for experimental design

(* Program for experimental design written by Hong-Sheng Qi, 30.2.93 *)

Input and Analysis:

```
Rlmin=1.5; Rlmax=3;
Vs=30; Ns=3400; q={80, 160, 240}; ae={0.005, 0.01, 0.03, 0.05};
Nsam=100; Lw=100; nc=4; m=32000;
ds=N[Vs 60 1000/(Pi Ns),6];Lwheel=N[(Pi ds),6];
Vw=N[Vs/q,3];
lg=N[(ae ds)^0.5,4]; lemin=Rlmin lg; lemax=Rlmax lg;
tcmin1=N[lemin/Vw[[1]],3];
tcmin2=N[lemin/Vw[[2]],3];
tcmin3=N[lemin/Vw[[3]],3];
lsmax1=N[lemax q[[1]],6];
lsmax2=N[lemax q[[2]],6];
lsmax3=N[lemax q[[3]],6];
StringForm[" Fixed condition:
Ns="` r/min", Ns]
StringForm[" If Vs="` m/s then ds="` mm", Vs,ds]
StringForm[" If q="` , then ", q]
StringForm[" Vw="` m/s", Vw]
StringForm[" ae="` mm", ae]
StringForm[" lg="` mm", lg]
StringForm[" lemin="` mm", lemin]
StringForm[" lemax="` mm", lemax]
StringForm[" (Vw="` ) tcmin="` ms", Vw[[1]],tcmin1]
StringForm[" (Vw="` ) tcmin="` ms", Vw[[2]],tcmin2]
StringForm[" (Vw="` ) tcmin="` ms", Vw[[3]],tcmin3]
StringForm[" (q="` ) lsmax="` mm", q[[1]],lsmax1]
StringForm[" (q="` ) lsmax="` mm", q[[2]],lsmax2]
StringForm[" (q="` ) lsmax="` mm", q[[3]],lsmax3]

StringForm[" Lwheel="` mm", (Pi ds)//N]

t=tcmin3[[4]];
Do[t=If[t>tcmin3[[i]],tcmin3[[i]],t],{i,4}];
Do[t=If[t>tcmin2[[i]],tcmin2[[i]],t],{i,4}];
Do[t=If[t>tcmin1[[i]],tcmin1[[i]],t],{i,4}];
Print["The minimum contact time: t=",t,"ms"];
x=(Lwheel/2);
Print["The half of the wheel cycle =",x,"mm"];

Do[If[x>lsmax3[[i]],Print[lsmax3[[i]],
",",q[[2]],",",ae[[i]],")"],x],{i,4}]
Do[If[x>lsmax2[[i]],Print[lsmax2[[i]],
",",q[[2]],",",ae[[i]],")"],x],{i,4}]
Do[If[x>lsmax1[[i]],Print[lsmax1[[i]],
",",q[[1]],",",ae[[i]],")"],x],{i,4}]

ratemax=N[Nsam/t,3];
Print["The max sample rate (quality): Rsmax=",ratemax,"kHz"];
ttime=N[Lw/(1000 Vw),3];
Print["The grinding time per one test: Tt=",ttime,"s"];
Nt=N[m/nc,6];
```

```
ratelimit=N[Nt/(1000 ttime),3];
Print["The limit sample rate (quantity) are: ",ratelimit,"kHz"];
```

Output:

Fixed condition: Ns=3400 r/min
If Vs=30m/s then ds=168.517mm
If q={80, 160, 240}, then
Vw={0.375, 0.188, 0.125}m/s
ae={0.005, 0.01, 0.03, 0.05}mm
lg={0.9179, 1.298, 2.248, 2.903}mm
lemin={1.37689, 1.94721, 3.37267, 4.3541}mm
lemax={2.75377, 3.89442, 6.74534, 8.70819}mm
(Vw=0.375) tcmin={3.67, 5.19, 8.99, 11.6}ms
(Vw=0.188) tcmin={7.34, 10.4, 18., 23.2}ms
(Vw=0.125) tcmin={11., 15.6, 27., 34.8}ms
(q=80) lsmax={220.302, 311.554, 539.627, 696.656}mm
(q=160) lsmax={440.604, 623.108, 1079.25, 1393.31}mm
(q=240) lsmax={660.905, 934.662, 1618.88, 2089.97}mm
Lwheel=529.412mm
The minimum contact time: t=3.67ms
The half of the wheel cycle =264.706mm
220.302(80,0.005)
The max sample rate (quality): Rsmax=27.2kHz
The grinding time per one test: Tt={0.267, 0.533, 0.8}s
The limit sample rate (quantity) are: {30., 15., 10.}kHz

A 1.3 Mathematica program for model evaluation

(* Program for model evaluation written by Hong-Sheng Qi, 20.3.94 *)

Input:

```
Cba = {0,0,0,0,0,0,0,0,0,0,0,0,0,0,0,0};  
Cbr = {0,0,0,0,0,0,0,0,0,0,0,0,0,0,0,0};  
de=170;  
Vs=30; Vw=0.3; q=Vs/Vw
```

The workpiece material: Cast iron;
 $E_w = 180 \text{ GPa}$; $p_{sw} = 0.3$; $H_v = 150 \text{ GPa}$;

The wheel: 19A60L7V;
 $E_s = 49.6 \text{ GPa}$; $p_{ss} = 0.2$; $d_s = 170 \text{ mm}$;

Variables (an example)

```
aem={ 2.2,5.4,9.5,17,19};  
Fn'={5.22,10.4,14.4,17.3,21};  
le ={ 1.3,2.2,2.7, 3, 3.7};
```

Analysis:

```
Eeq = Ew Es/(Ew+Es);  
Ks = N[(1- pss^2)/( Pi Es )]  
Kw = N[(1- psw^2)/( Pi Ew )]  
Kg = N[(1- psg^2)/( Pi Eg )]  
Vw = N[Vs/q]  
de=N[(ds dw/(ds+dw))];  
ae = aem/1000;  
Num = Length[ae];  
aemax = Max[ae];  
rangeae =N[Ceiling[aemax 100]/100];  
lemax = Max[le];  
rangele = Ceiling[lemax];  
pn = Fn'/le  
lg=(ae de)^0.5  
lcMaris1 = lg 4.95 q^(-0.216) Exp[-0.0205 q^0.33 Log[ae 1000]]  
lcMaris2 = lg 4.95 q^(-0.216) Exp[-0.0205 q^0.33 Log[ae]]  
le  
dats = 0.19 (Fn' de (1+pss)/(2 lg Es));  
datw = - 2 (Fn' Log[lg/2]/(Pi Ew));  
arlf = (1 + dats/ae)^0.5;  
balt = 1/(1 - datw/ae)^0.5;  
lckumar = lg arlf balt
```

Model of Rowe & Qi :

```
Do[Print[Cbr[[i]]=N[((le[[i]]^2-ae[[i]] de)/(8 Fn'[[i]] de (Ks+Kw)))^0.5]],{i,Num}];  
Rrmean=Sum[Cbr[[i]],{i,Num}]/Num  
lfr2=(Rrmean^2 8 Fn' de (Ks+Kw));  
lcr=(lfr2 +lg^2)^0.5
```

```
Do[Print[Cba[[i]]=(le[[i]]^2-ae[[i]] de)^0.5 Hv/(Fn'[[i]])],{i,Num}];  
Ramean=Sum[Cba[[i]],{i,Num}]/Num  
lfa=Ramean Fn'/Hv;  
lca=(lfa^2 +lg^2)^0.5
```

```

Dr = (le - lcr)/le 100
Da = (le - lca)/le 100
Dck = (le - lckumar)/le 100
DcM = (le - lcMaris1)/le 100
Rle=le/lg
Rlr=lcr/lg
Rla=lca/lg
Rlck=lckumar/lg
RlcM=lcMaris1/lg

```

Graph:

```

curve={Table[{ae[[i]],le[[i]]},{i,Num}],
Table[{ae[[i]],lcr[[i]]},{i,Num}],
Table[{ae[[i]],lca[[i]]},{i,Num}],
Table[{ae[[i]],lckumar[[i]]},{i,Num}],
Table[{ae[[i]],lcMaris1[[i]]},{i,Num}],
Table[{ae[[i]],Rle[[i]]},{i,Num}],
Table[{ae[[i]],Rlr[[i]]},{i,Num}],
Table[{ae[[i]],Rla[[i]]},{i,Num}],
Table[{ae[[i]],Rlck[[i]]},{i,Num}],
Table[{ae[[i]],RlcM[[i]]},{i,Num}],
Table[{ae[[i]],Cbr[[i]]},{i,Num}],
Table[{ae[[i]],Cba[[i]]},{i,Num}]}

grf1=ListPlot[curve[[1]],PlotJoined->True];
grf2=ListPlot[curve[[2]],PlotJoined->True];
grf3=ListPlot[curve[[3]],PlotJoined->True];
grf4=ListPlot[curve[[4]],PlotJoined->True];
grf5=ListPlot[curve[[5]],PlotJoined->True];
grf6=ListPlot[curve[[6]],PlotJoined->True];
grf7=ListPlot[curve[[7]],PlotJoined->True];
grf8=ListPlot[curve[[8]],PlotJoined->True];
grf9=ListPlot[curve[[9]],PlotJoined->True];
grf10=ListPlot[curve[[10]],PlotJoined->True];
grf11=ListPlot[curve[[11]],PlotJoined->True];
grf12=ListPlot[curve[[12]],PlotJoined->True];
Show[grf1,grf2,grf3,grf4,grf5]
Show[grf6,grf7,grf8,grf9,grf10]
Show[grf11,grf12]

```

A1.4 Mathematica program for model application

(* Program for model application written by Hong-Sheng Qi, 10.2.95 *)

```
Unprotect[In,Out]
Clear[In,Out]
ClearAll
{}
ClearAll
SetOptions[Plot3D,
           ViewPoint->{-3.841, 6.525, 0.999},
           AxesLabel -> {"a","q","Rl^2"},
           PlotRange -> {0,20}]
```

Input

Experimental data - Qi;

Cr = 0.49;

Rr = 13

e2=0.87;

e1 = 2 e2 - 1

e3 =1-e2

de=170;

Analysis

(*Band1=Rr[[1]]^2 Cr ae^(e2-1) q^(-e1) de^e3;*)

Rl1=1.10;

Rl213=1+Rr^2 Cr ae^(e2-1) q^(-e1) de^e3;

```
pl132=Plot3D[Rl213, {ae, 0.005, 0.05}, {q, 60, 300}];
pl1=Plot3D[Rl1, {ae, 0.005, 0.05}, {q, 60, 300}];
```

Show[pl1,pl132, ViewPoint->{-6.436, 4.024, 0.848}]

Rl13=Rl213^0.5;

```
SetOptions[Plot3D, ViewPoint->{-3.841, 6.525, 0.999}, AxesLabel ->
           {"a","q","Rl"}, PlotRange -> {0,6}];
```

pl13=Plot3D[Rl13, {ae, 0.005, 0.05}, {q, 60, 300}];

```
Show[pl1,pl13, ViewPoint->{-6.436, 4.024, 0.848},
      AxesLabel -> {"a","q","Rl"}, PlotRange -> {0,5}];
```

Appendix 2 List of the Author's Relevant Published Papers

- 1 W.B.Rowe, H.S.Qi, M.N. Morgan and H.W. Zheng, 1993, The Real Contact Length in Grinding Based on Depth of Cut and Contact Deflections, Proceedings of 30th International MATADOR Conference, UMIST, Manchester, United Kingdom, 31 March - 1 April, 187-193
- 2 W.B. Rowe, H.S. Qi, M.N. Morgan and H.W. Zheng, 1993, The effect of deformation on the contact area in grinding, Annals of the CIRP, 42, 1, p409
- 3 H.S. Qi, B. Mills and W.B. Rowe, 1994, An analysis of real contact length in abrasive machining processes using contact mechanics, Wear, 176, 137-141
- 4 H.S. Qi, W.B. Rowe, 1993, Contact Mechanics in Abrasive Processes, The Mission of Tribology Research, 7 December, IMECHE HQ, LONDON
- 5 S. Black, W.B. Rowe, H.S. Qi, and B. Mills, 1995, Temperature Measurement in Grinding, Proceedings of 31th International MATADOR Conference, UMIST, Manchester, United Kingdom, April, 409-413
- 6 W.B. Rowe, S. Black, B. Mills and H.S. Qi, 1994, Experimental Energy Partitioning in Grinding, Proceeding of the Conference 'EUROMETALWORKING 1994', September 28, Udine (Friuli-Venezia Giulia Region), Italy, 048
- 7 W.B. Rowe, S. Black, B. Mills, H.S. Qi, and M. Morgan, 1995, Experimental Investigation of Heat Transfer in Grinding, Annals of the CIRP, 44, 1, 329-332

- 8 W.B. Rowe, H.S.Qi, and B. Mills, 1995, Contact Length Measurement in Grinding, (Submitted to the IMechE, the Journal of Engineering Tribology)
- 9 H.S. Qi, W.B. Rowe and B. Mills, 1995, An Evaluation of Contact Length Models in Grinding, (Submitted to the IMechE, the Journal of Engineering Tribology)
- 10 H.S. Qi, W.B. Rowe and B. Mills, 1995, Experimental Investigation of the Contact Behaviour in Grinding, (Submitted to the Tribology International)
- 11 W.B. Rowe, S. Black, B. Mills and H.S. Qi, 1995, Analysis of Grinding Temperature by Energy Partitioning, (Submitted to the IMechE, Journal of Engineering Manufacture)

FIGURES

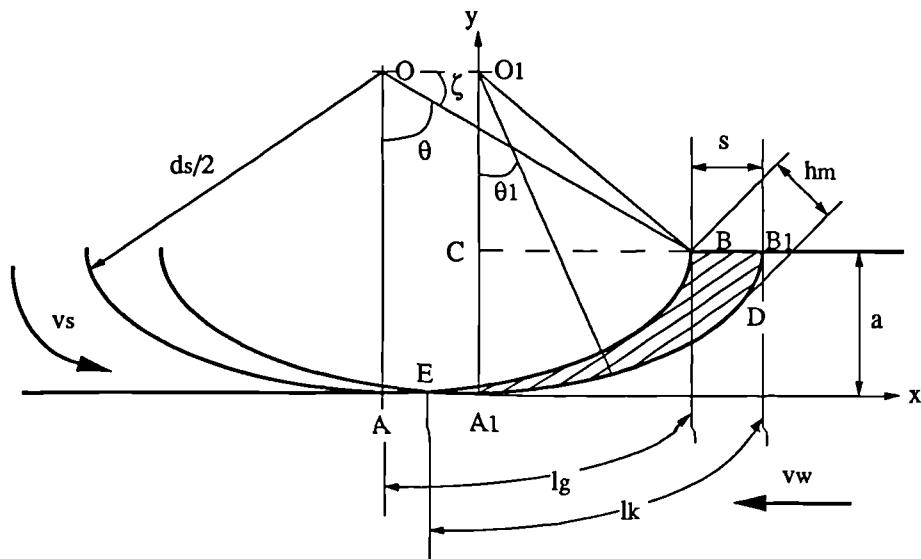


Figure 2.1 Illustration of the geometry of surface grinding

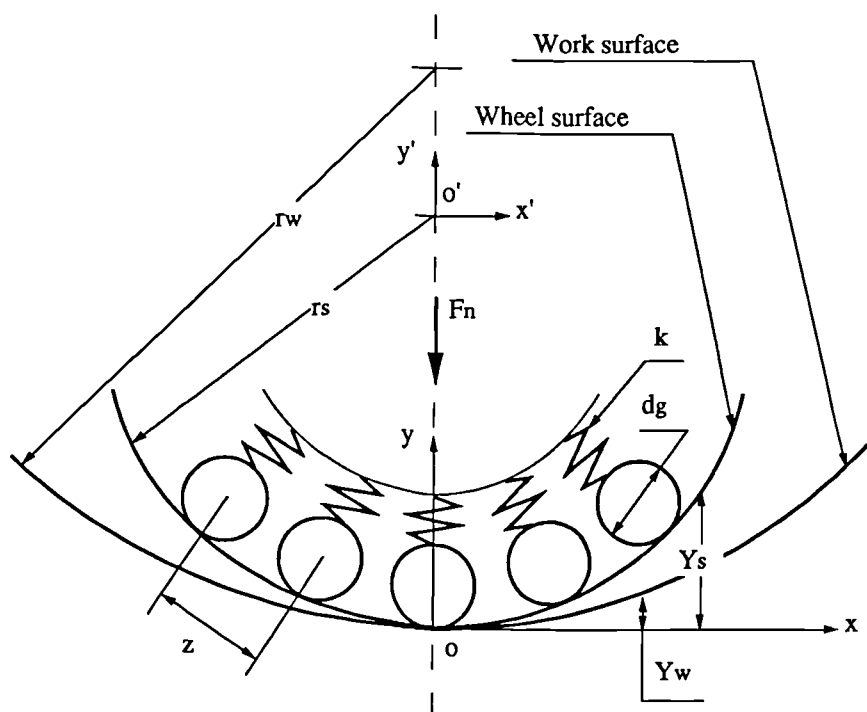
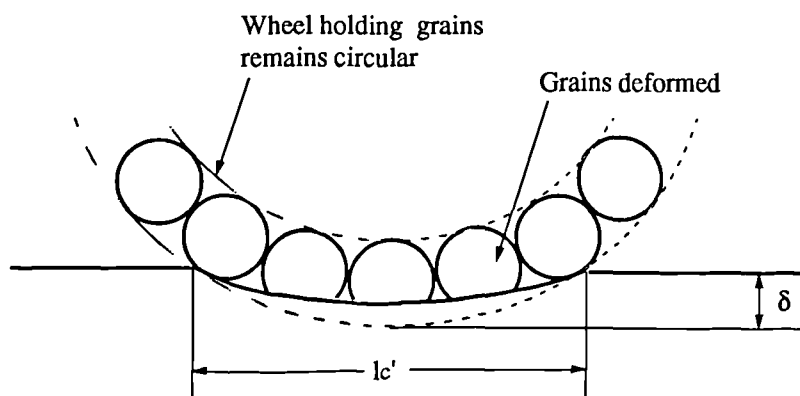
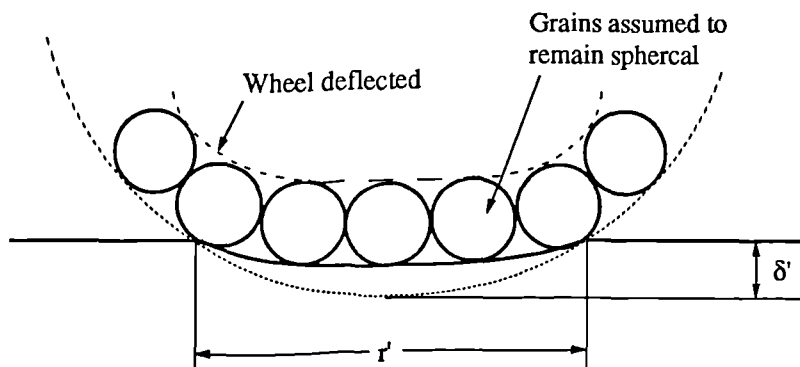


Figure 2.2 Model of the wheel-workpiece contact by Lindsay



(a) The elastic deflection of the grain-workpiece contact assuming the shape of the grain mounting surface remains circular



(b) Elastic deflection of the wheel-workpiece contact assuming the individual grinding grains are undeformed

Figure 2.3 The contact length model by Brown, Saito and Shaw

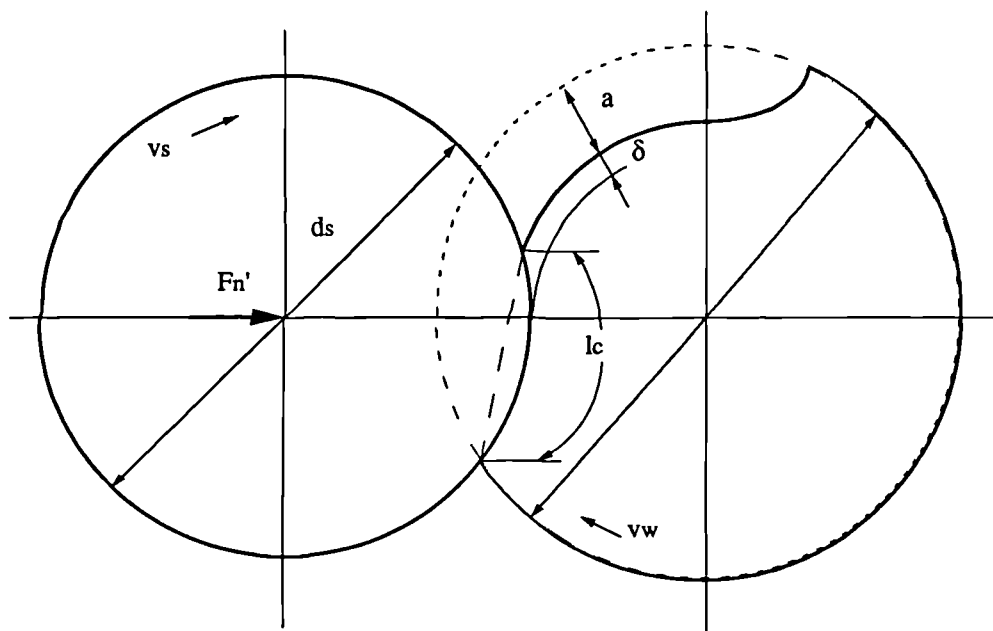
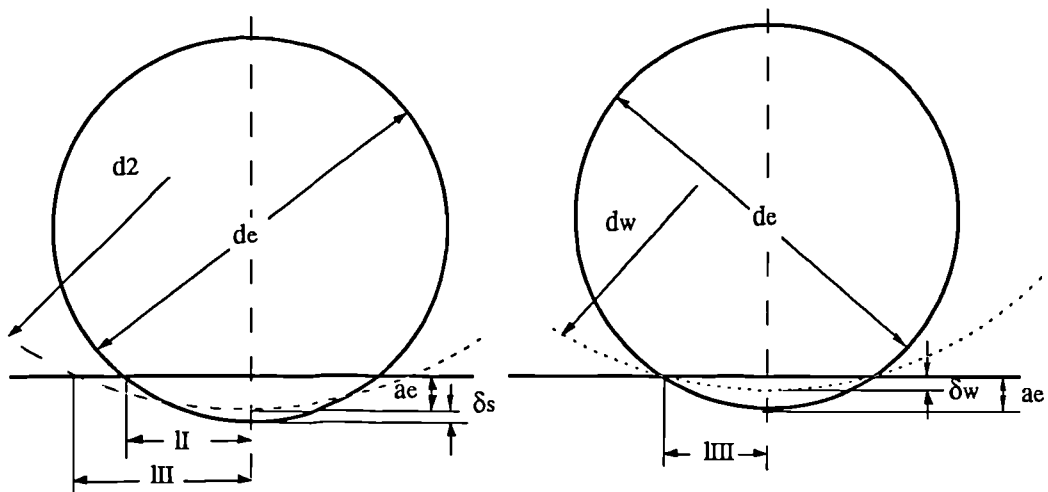


Figure 2.4 The contact length model by Hideo Tsuwa



(a) Contact length with and without wheel deformation

(b) Local deflection of the workpiece

Figure 2.5 The workpiece-wheel contact length model by Kumar & Shaw

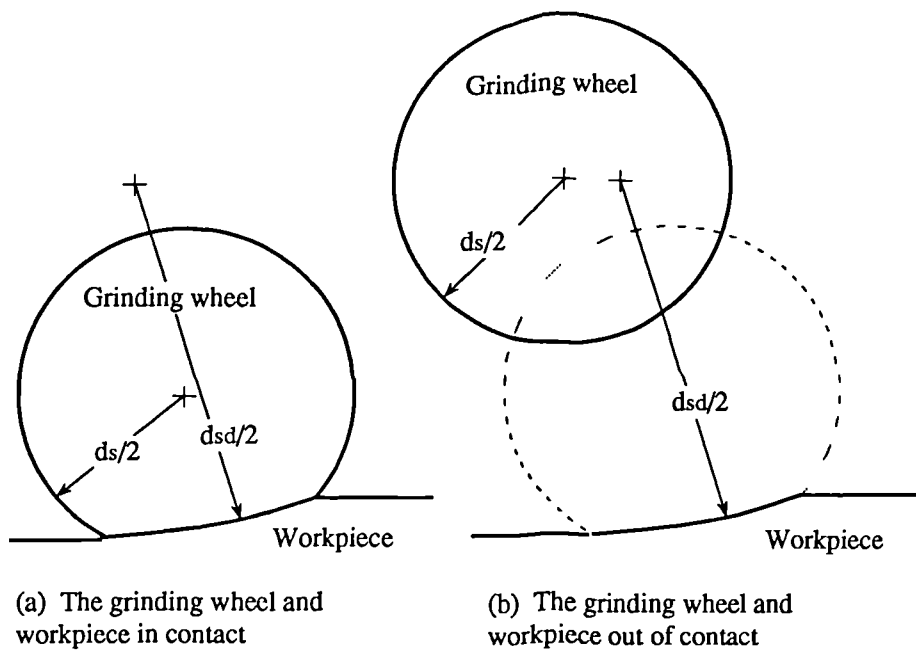


Figure 2.6 The workpiece-wheel contact length model by Aerens

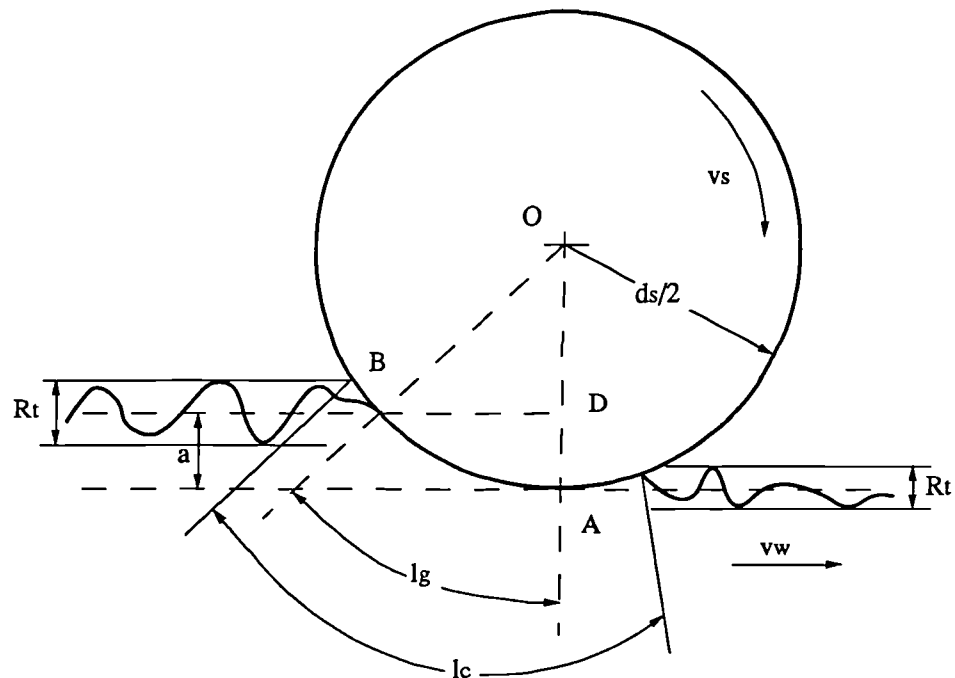


Figure 2.7 The geometrical influence of surface roughness on the contact length

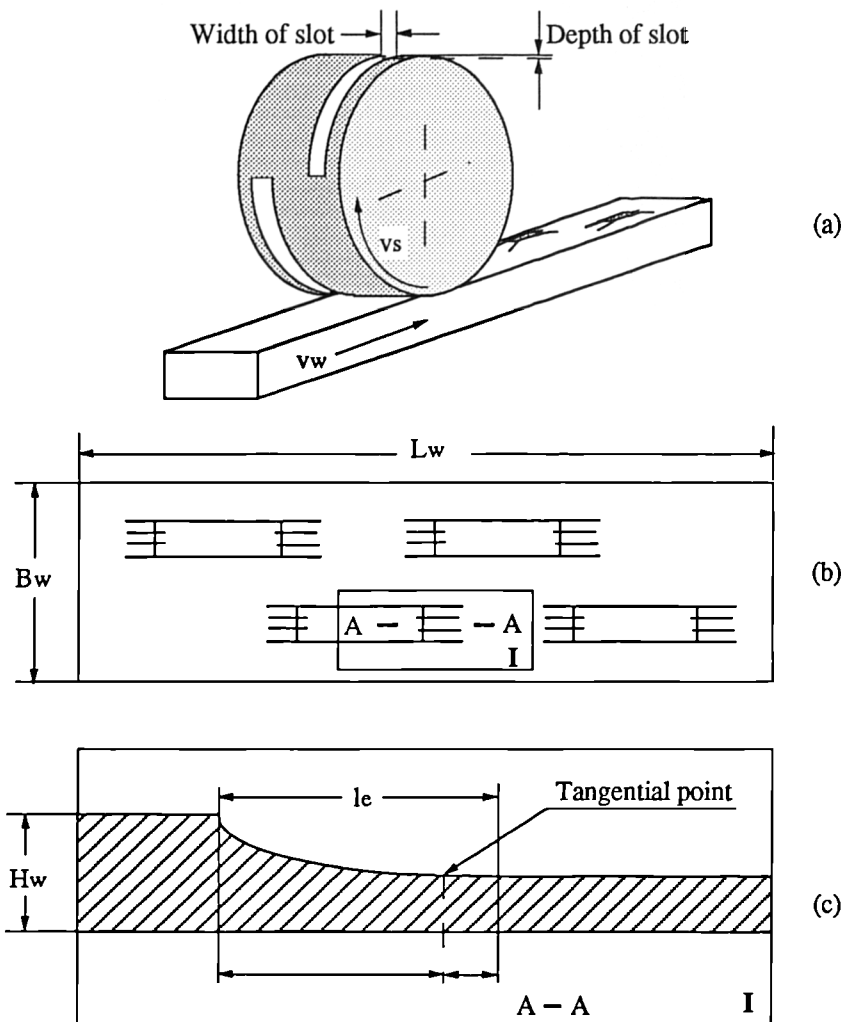


Figure 2.8 An illustration of the two-half-slot grinding technique

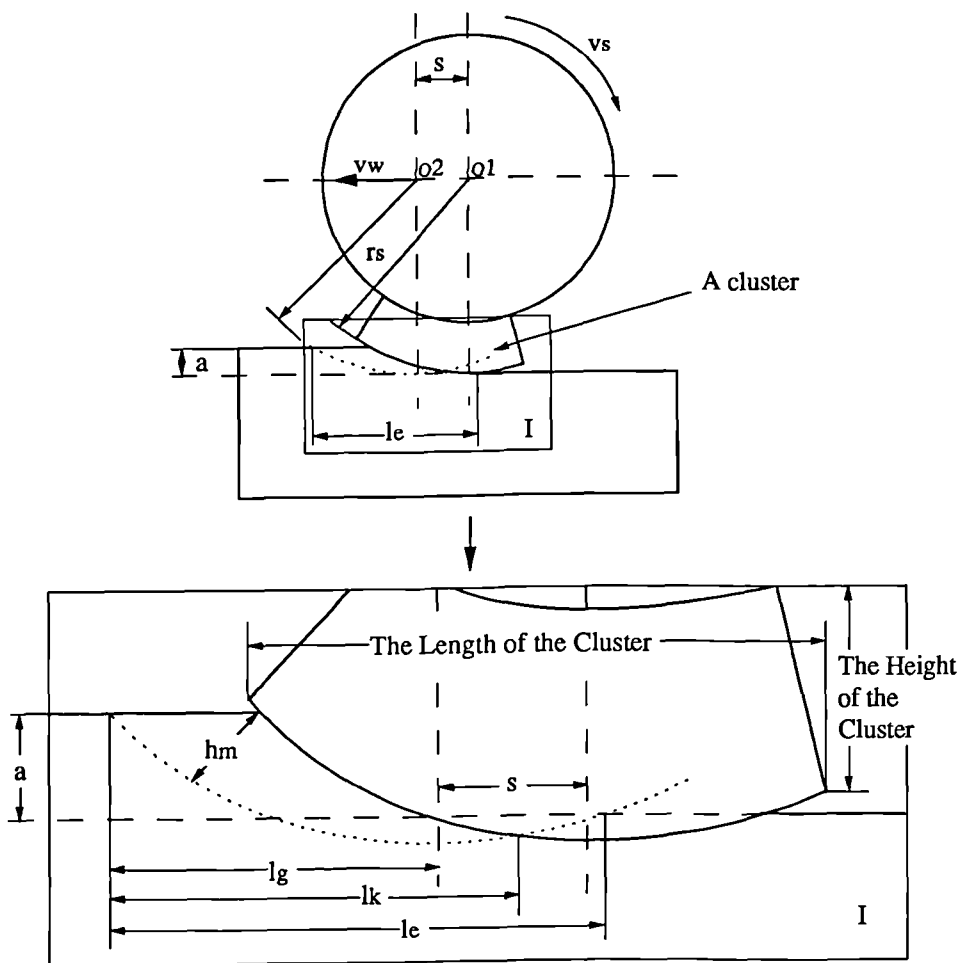


Figure 2.9 The principle of the cluster fly grinding method used in measuring the contact length

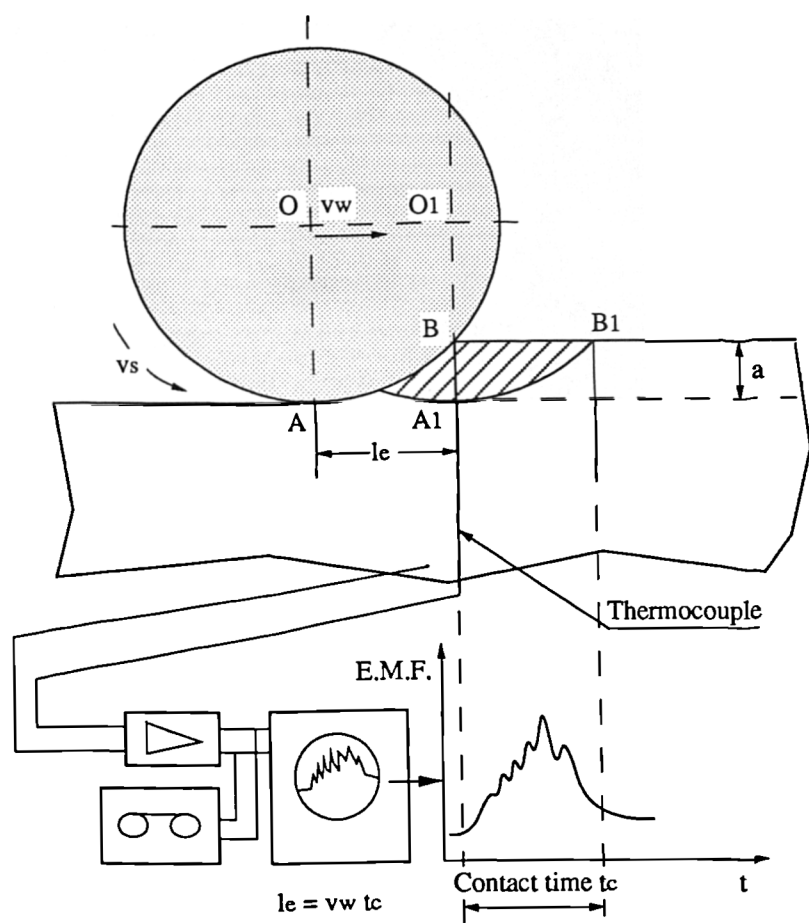


Figure 2.10 An illustration of the thermocouple technique

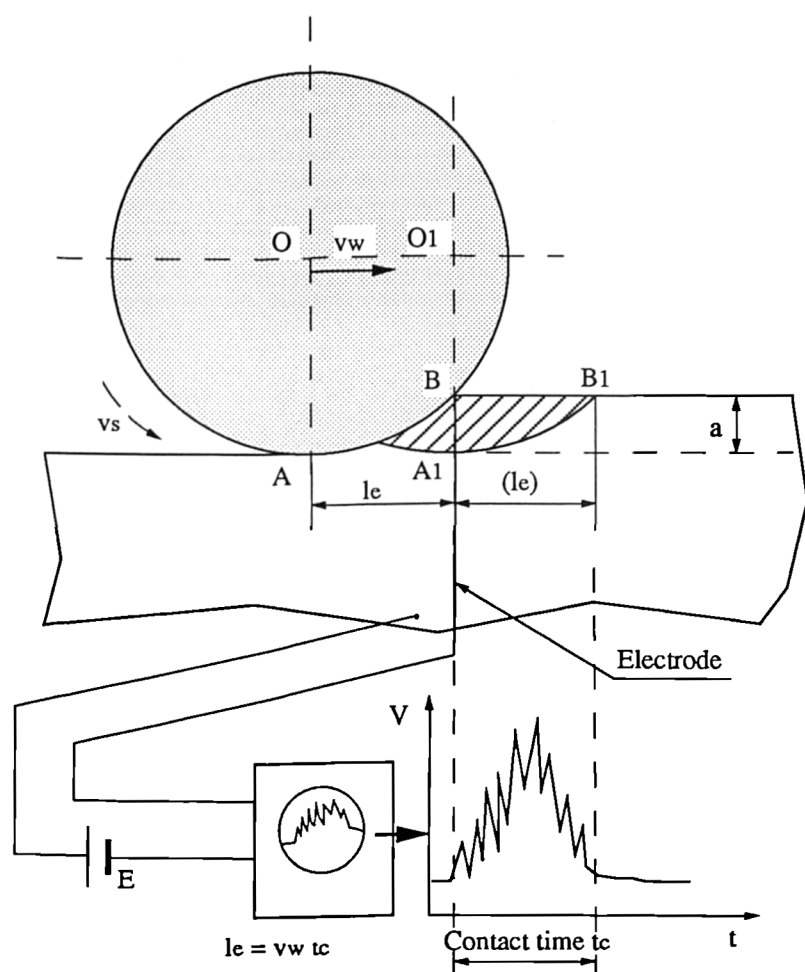


Figure 2.11 The applied power supply method

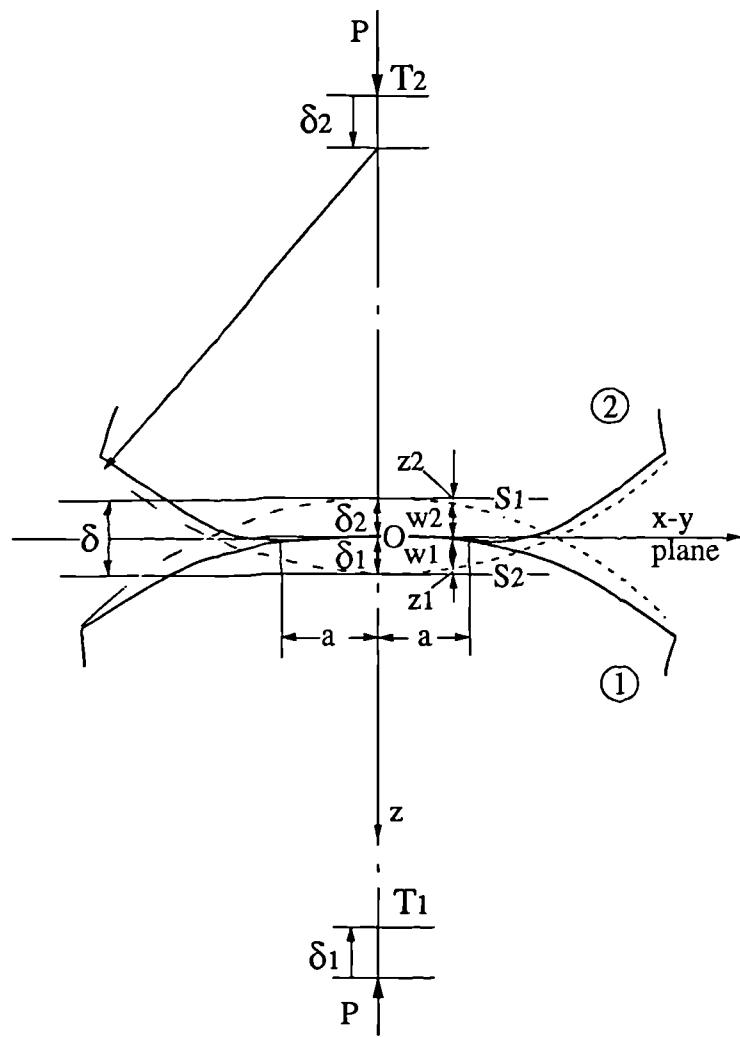


Figure 3.1 Contact of non-conforming elastic bodies

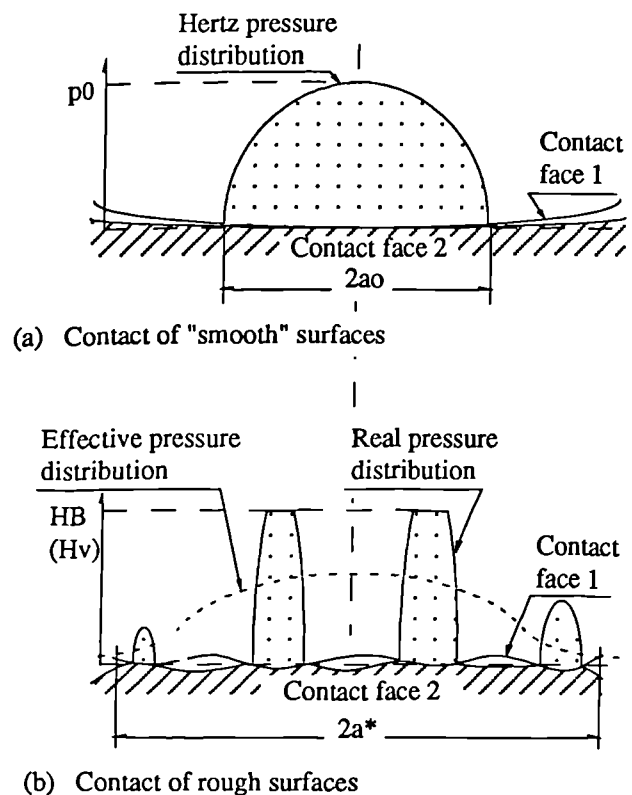


Figure 3.2 An illustration of contact size and pressure distribution under different condition of surface roughness

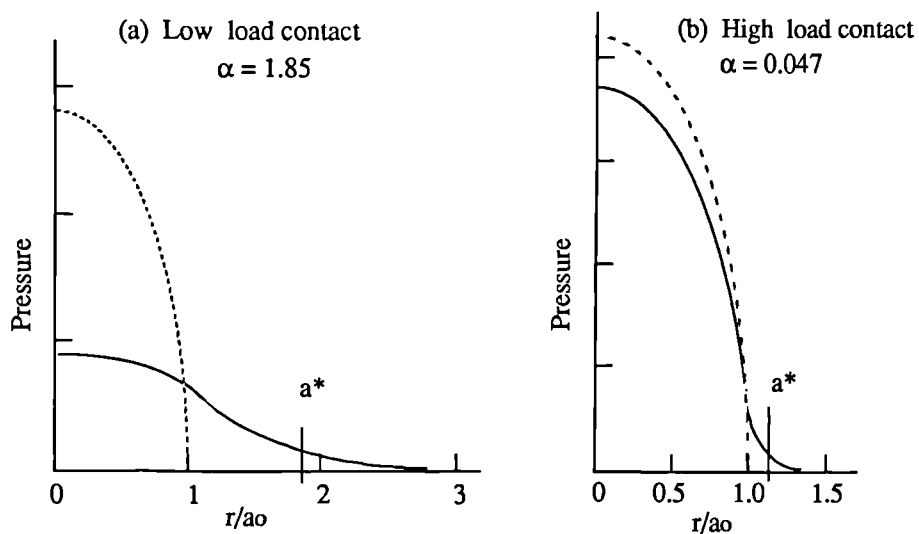


Figure 3.3 Contact of a smooth elastic sphere with a rough plane surface:
 Solid line - effective pressure distribution
 Broken line - Hertz pressure (smooth surfaces)
 Effective radius a^* defined by Equation 3.37 [36]

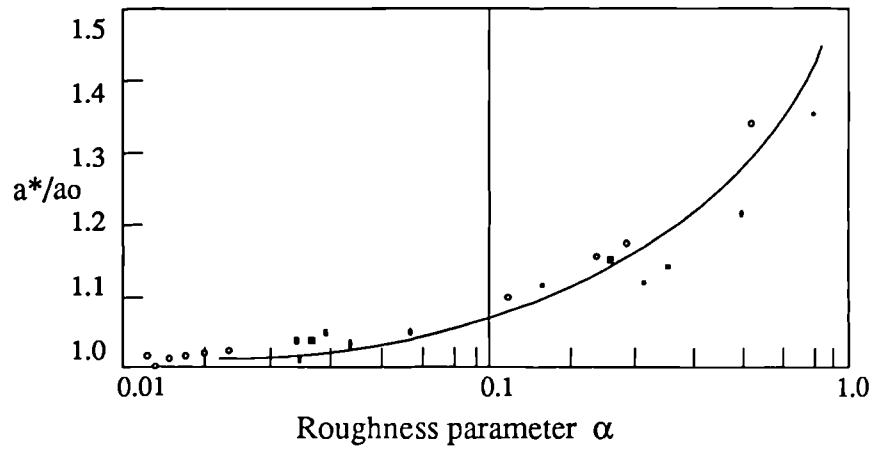


Figure 3.4 Influence of the surface roughness on the effective contact radius a^* compared with the Hertz radius a_0 [31]

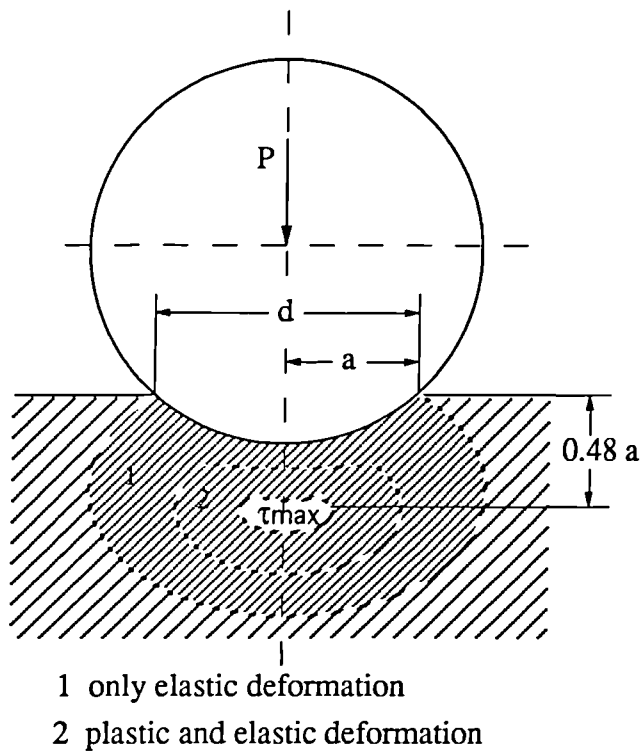


Figure 3.5 Indentation by a sphere with distribution of shear stresses and zone of plastic deformation

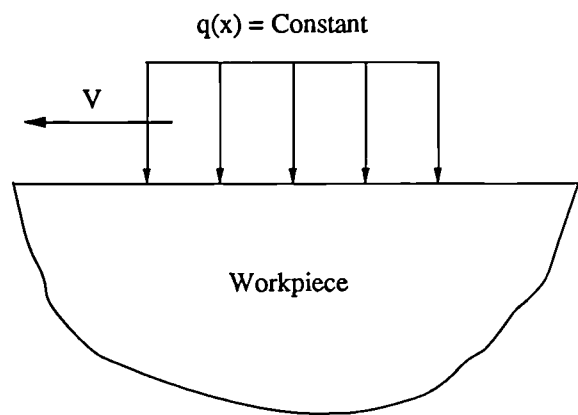


Figure 3.6 A band heat source with a uniform heat flux distribution in the grinding zone

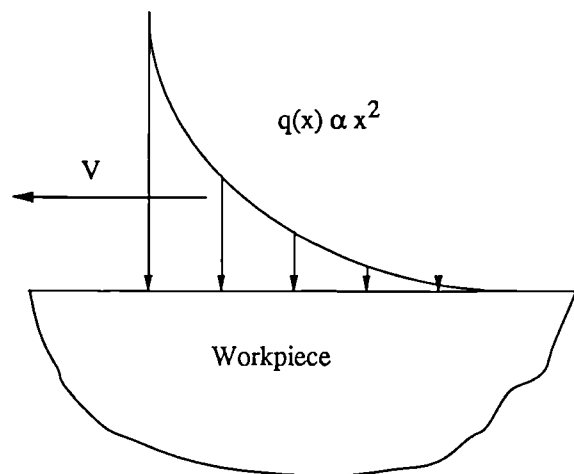


Figure 3.7 Square law heat generation in the grinding zone

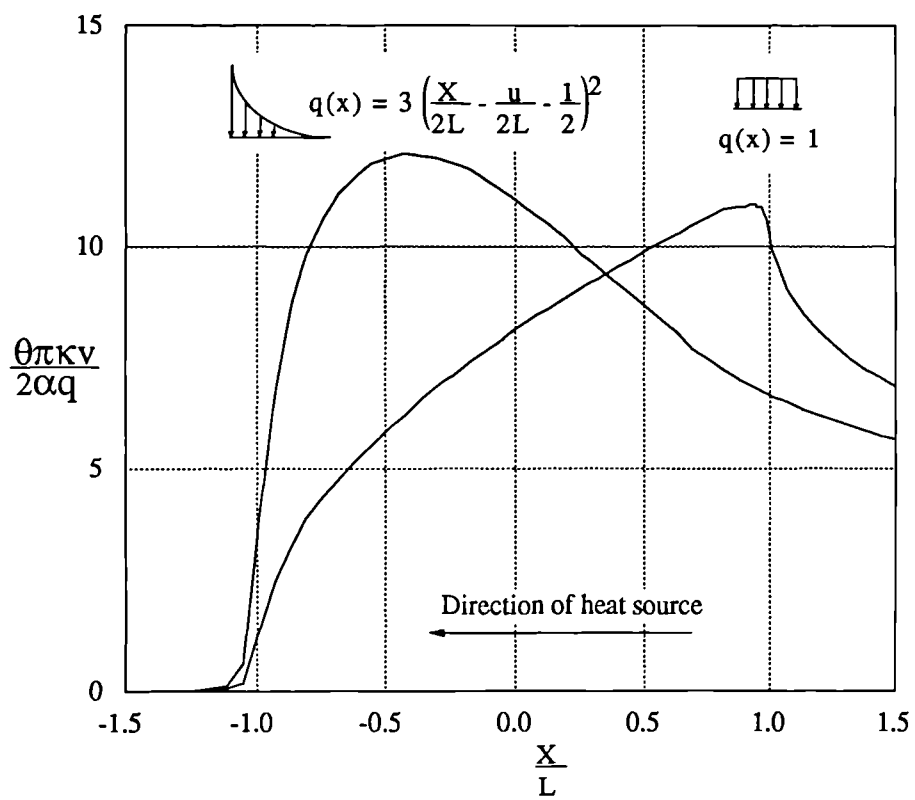


Figure 3.8 Jaegers moving heat transfer theory evaluated with a uniform and a square law heat flux distribution from Rowe & Black [49]

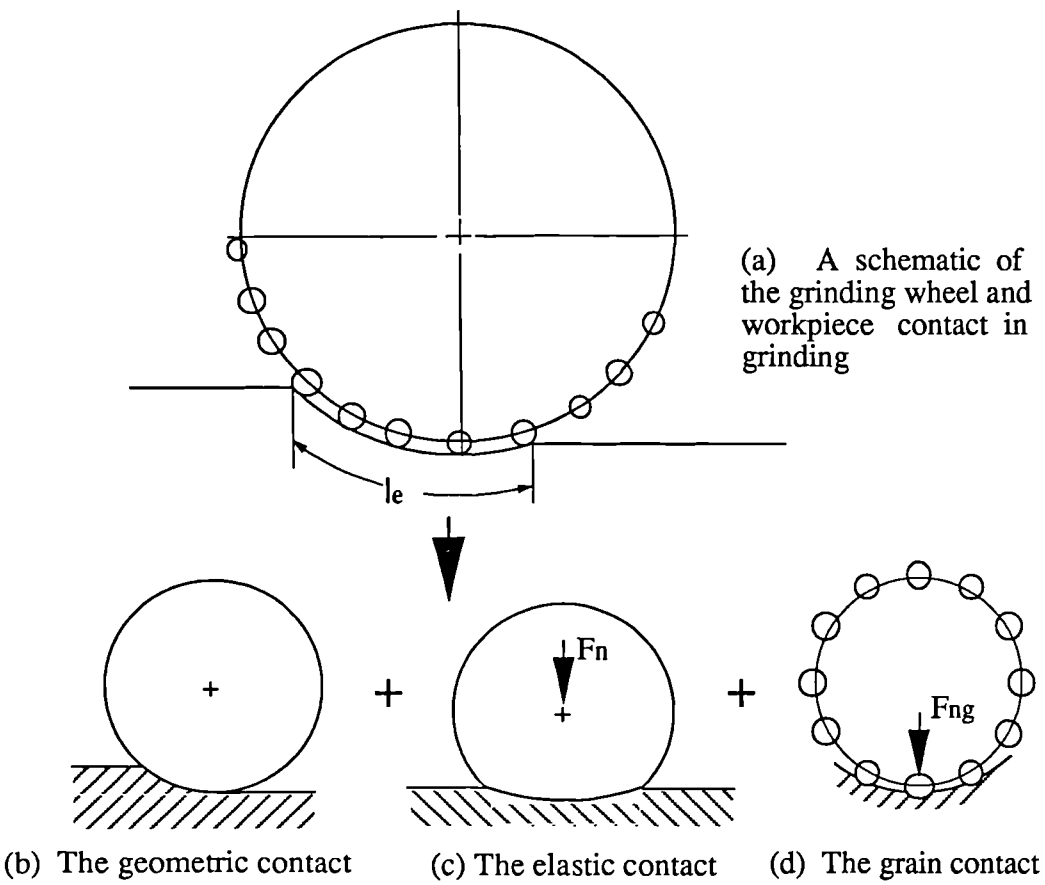


Figure 4.1 The grinding wheel and workpiece contact

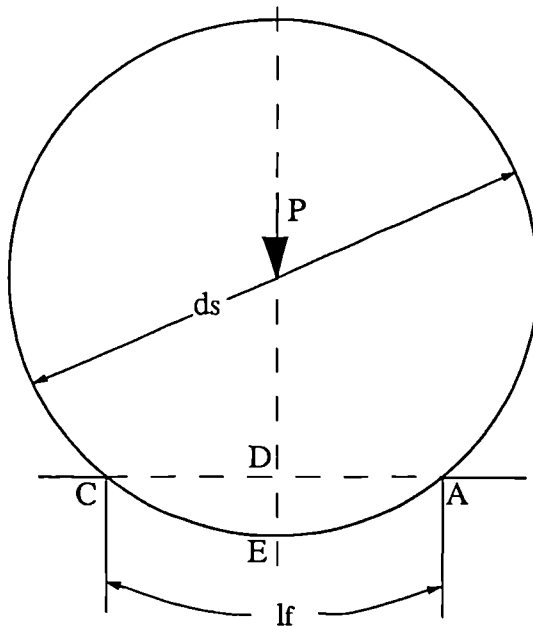


Figure 4.2 Simplified representation of the contact length due to deflection under an applied normal force

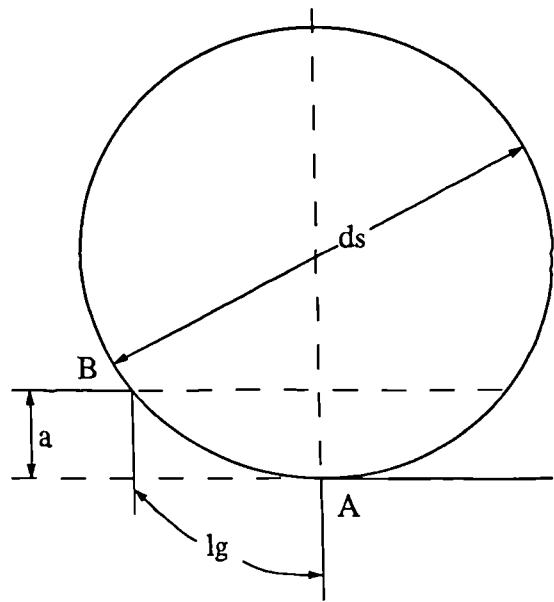


Figure 4.3 The contact length due to the geometry of the grinding process

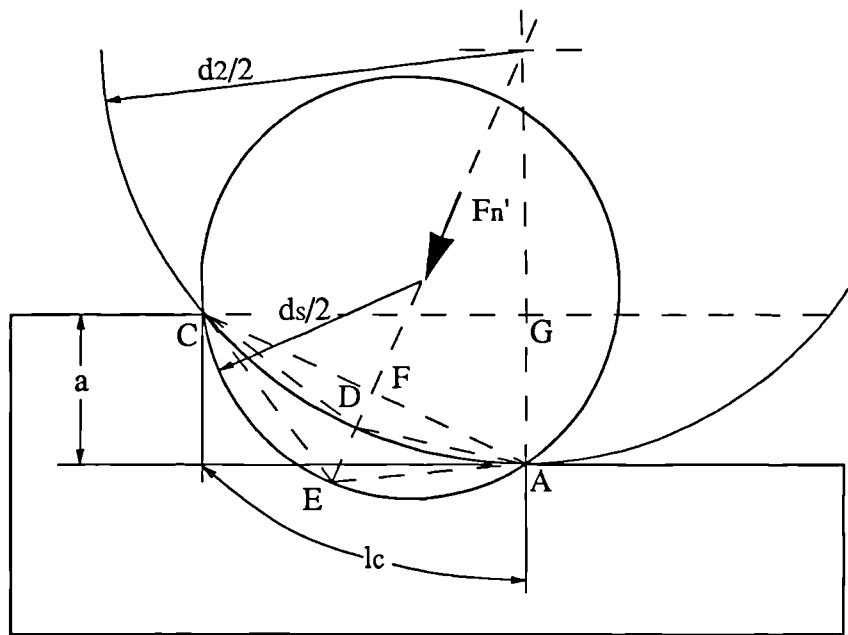


Figure 4.4 The combined effects of normal force and grinding geometry on contact length

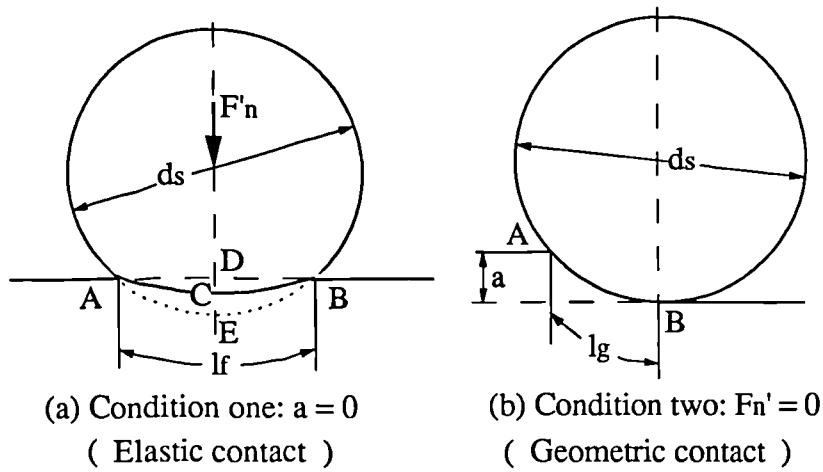


Figure 4.5 The two contact factors of the workpiece-wheel body contact

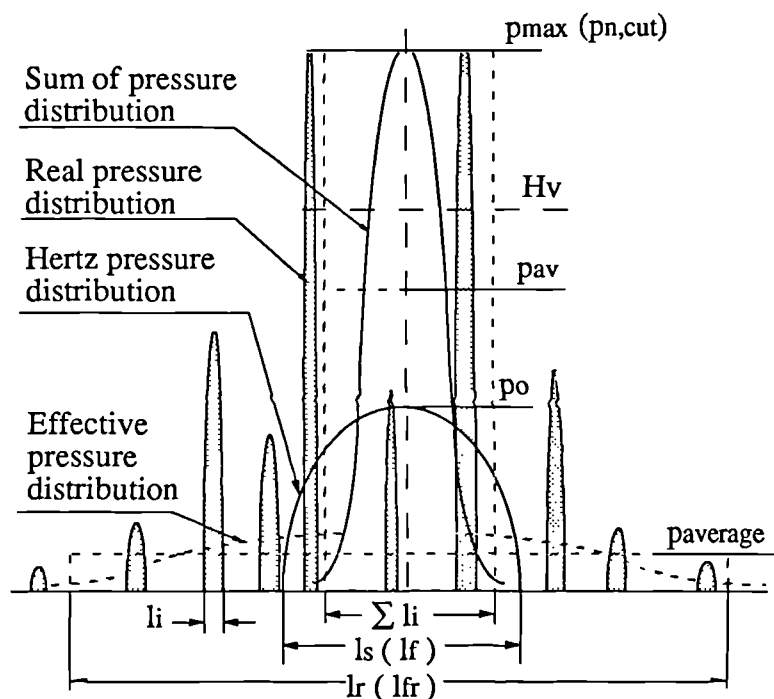


Figure 4.6 Contact size and pressure distribution under the rough surface of a grinding wheel

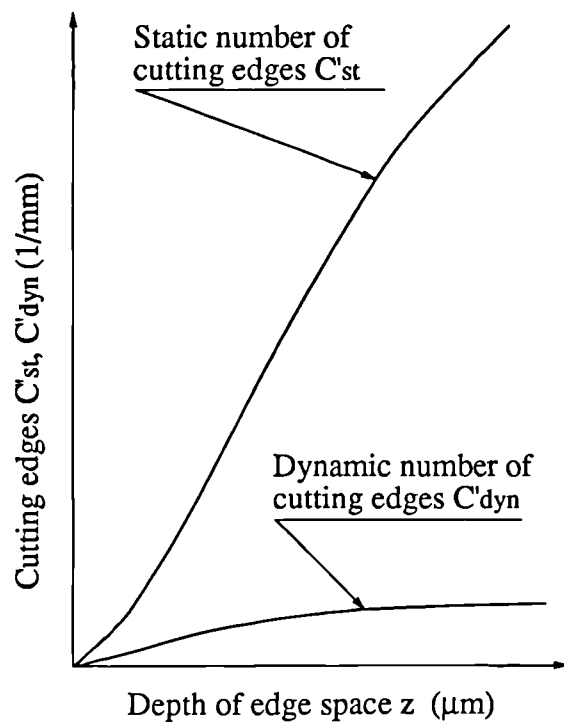


Figure 4.7 Number of static and dynamical cutting edges

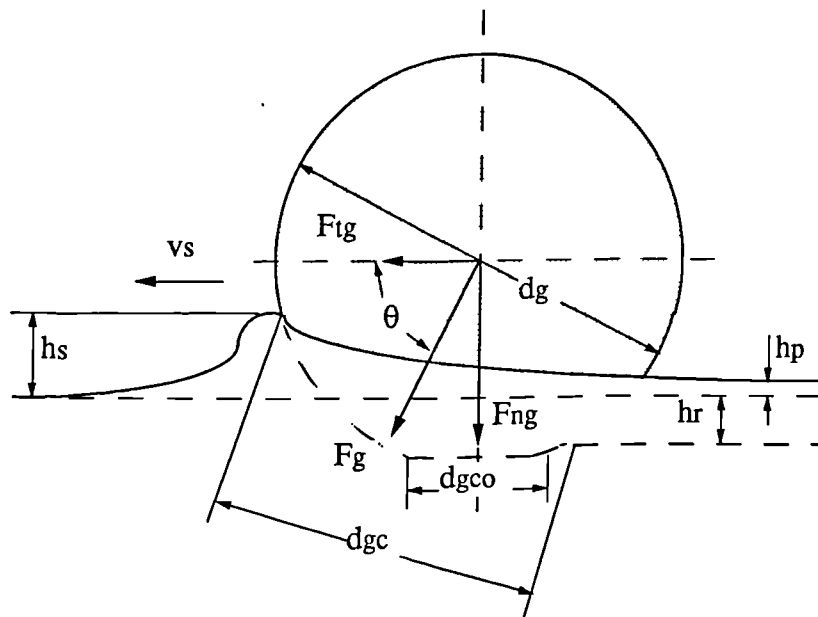


Figure 4.8 Static contact area diameter d_{gco} and dynamic contact area diameter d_{gc}

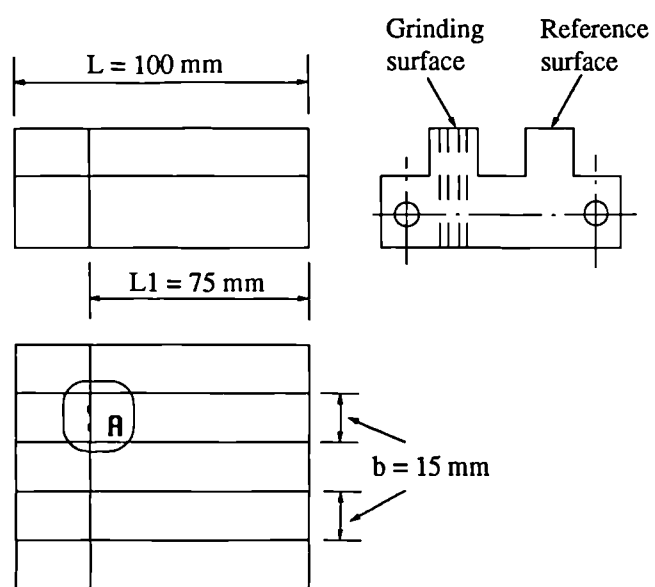
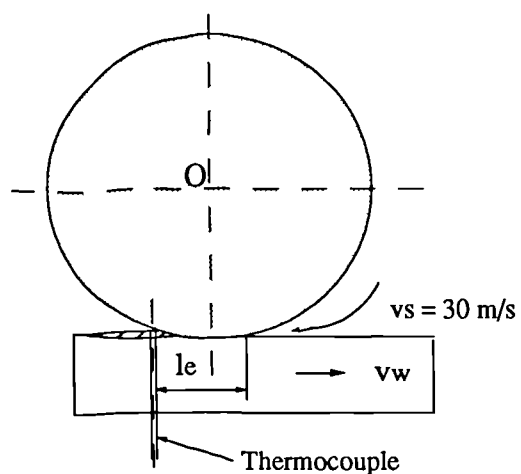


Figure 5.1 Workpiece used for measurement of contact length and contact temperature

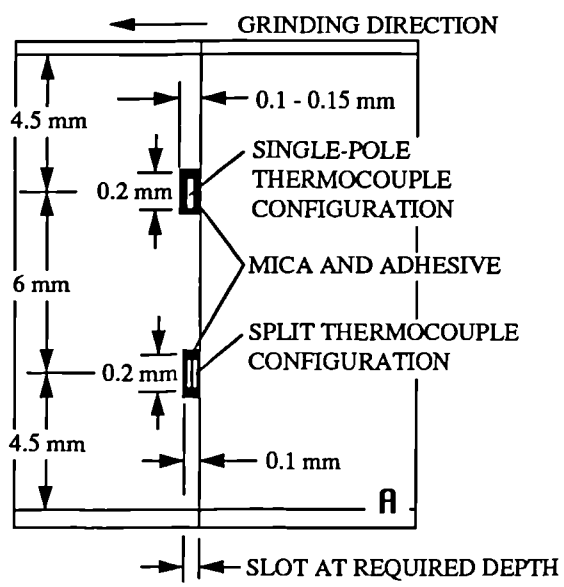


Figure 5.2 The configuration of junctions on the workpiece surface

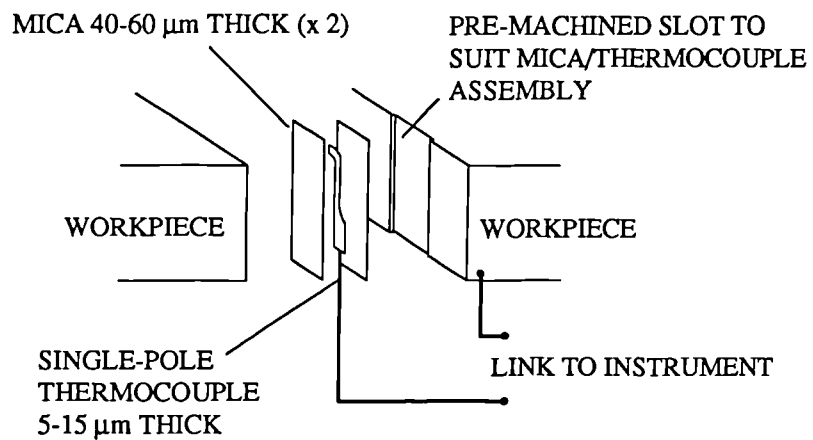


Figure 5.3 The single pole thermocouple arrangement used for measurement of contact length

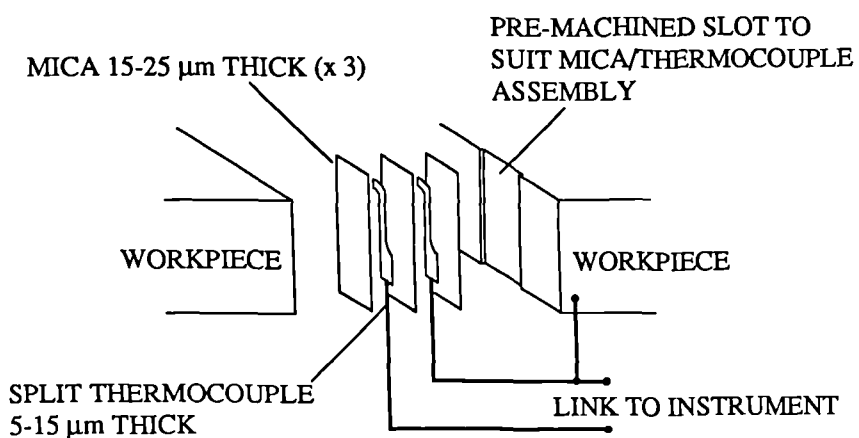


Figure 5.4 The standard thermocouple arrangement used for measurement of contact length and grinding temperature

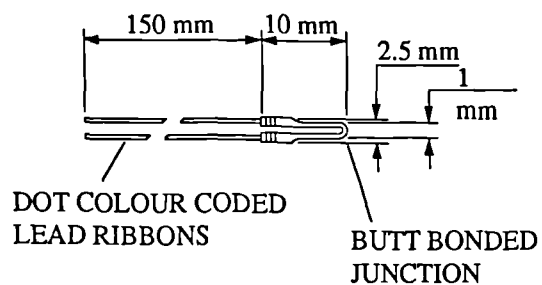


Figure 5.5 Standard K type foil thermocouple

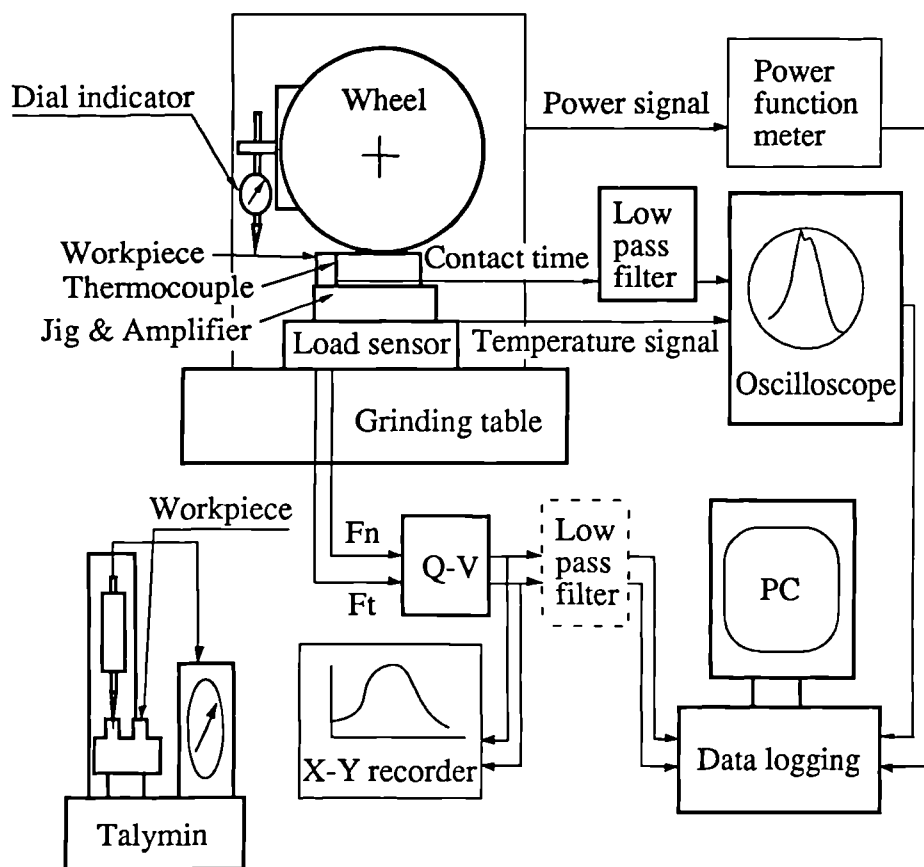
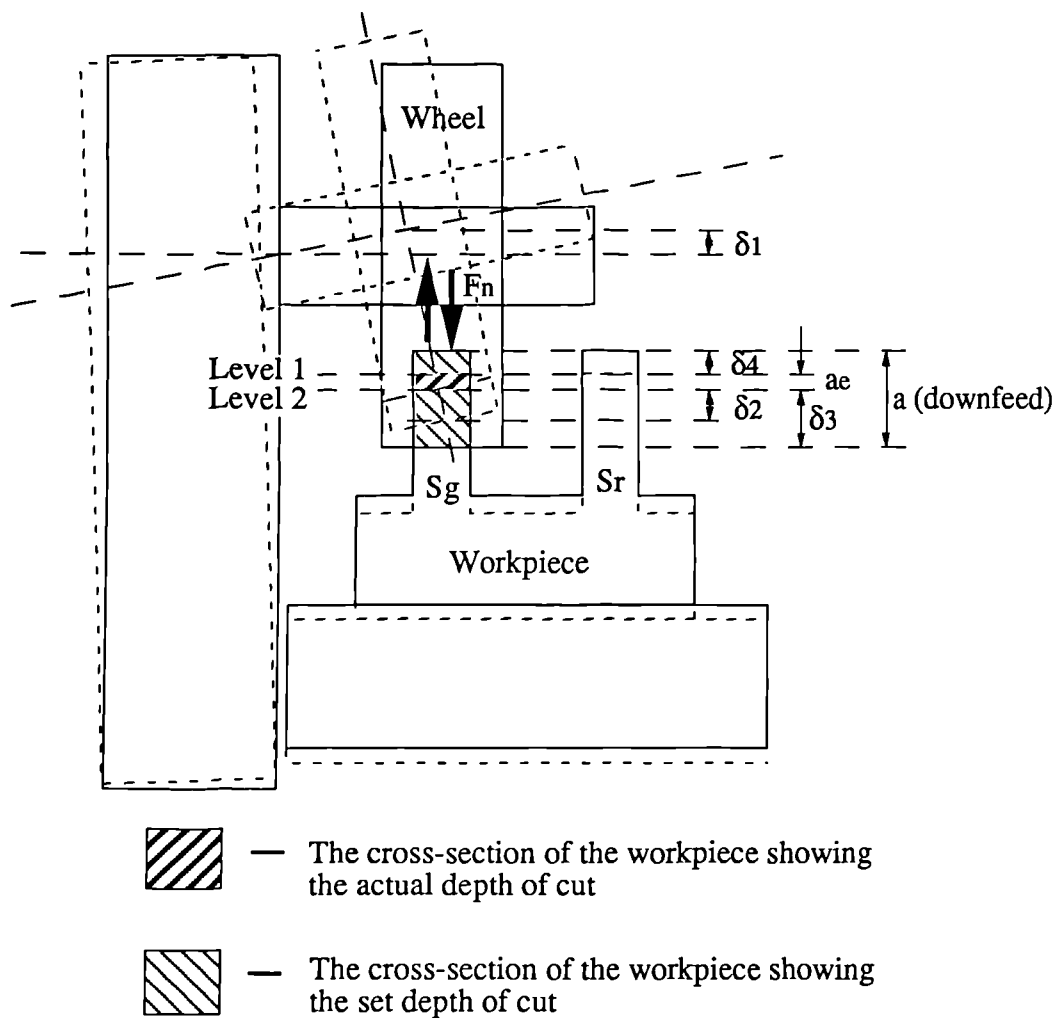


Figure 5.6 Measurement system for the real contact length and temperature



δ_1 is the deflection in the grinding wheel spindle

δ_2 is the radius deflection of grinding wheel

$$\delta_3 = \delta_1 + \delta_2$$

δ_4 is the deflection in the machine table, the load sensor and the workpiece

a_e is the true depth of cut

a is the downfeed

S_g is the grinding surface

S_r is the reference grinding surface

Figure 5.7 Scheme for measuring the actual depth of cut

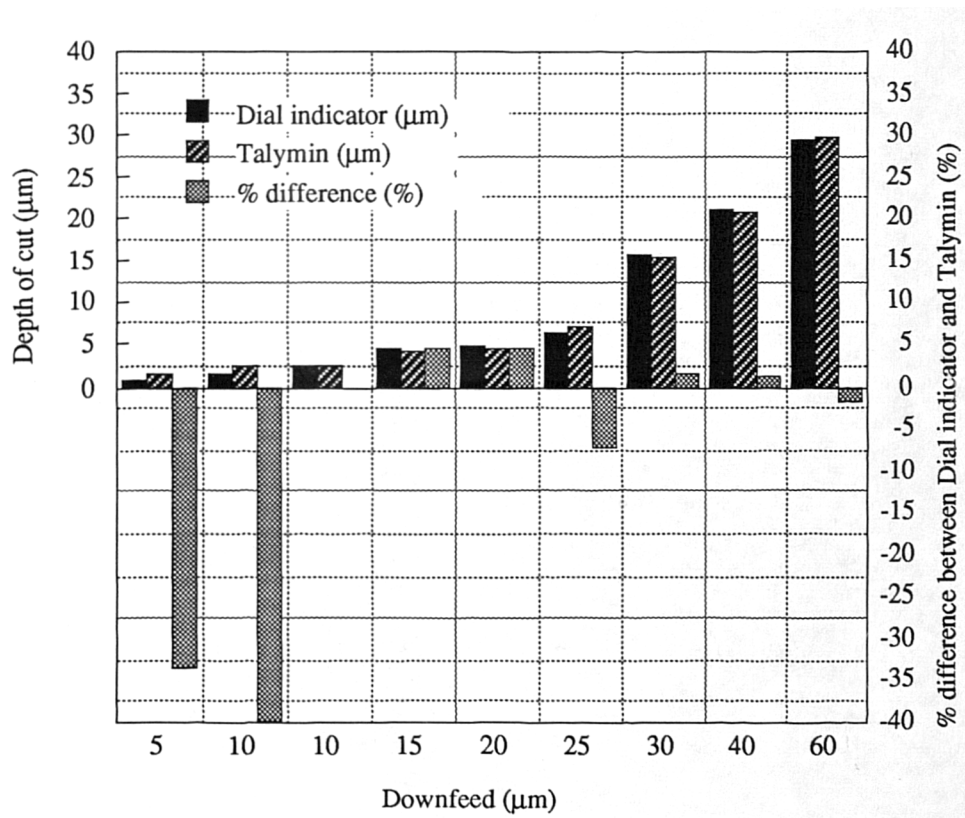
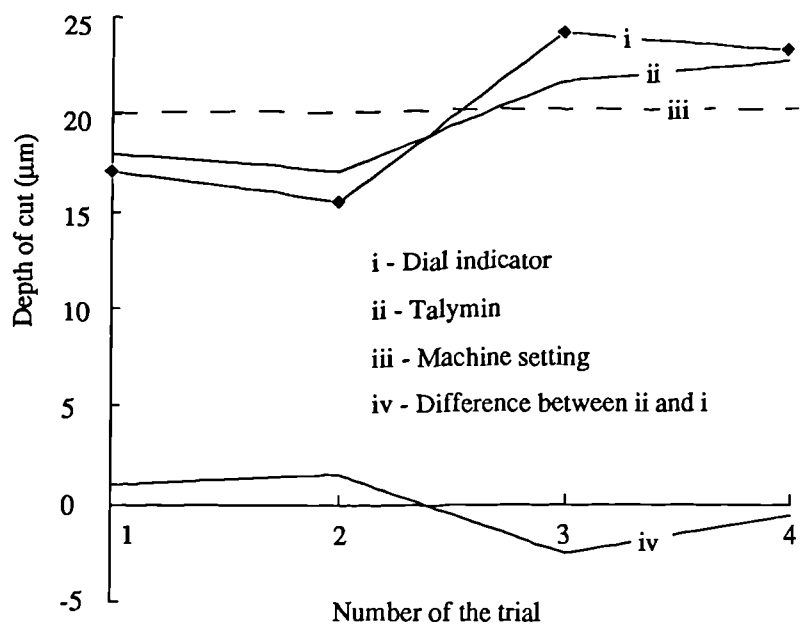


Figure 5.8 A comparison of the measured results by the dial indicator and by the Talymin

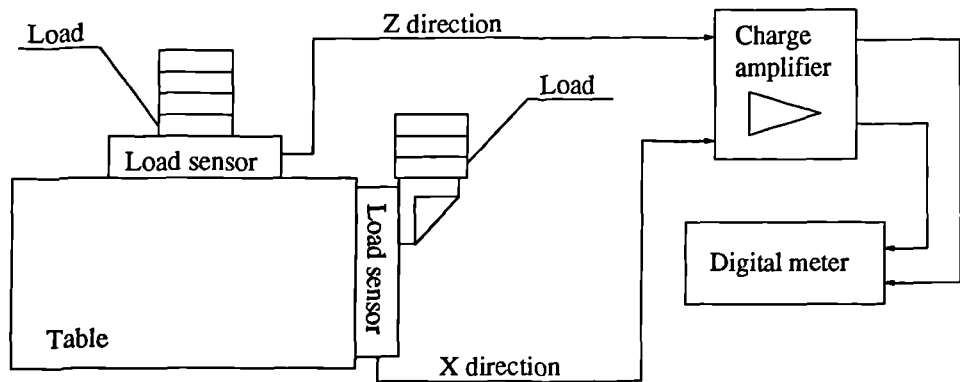


Figure 5.9(a) Calibration set-up for the piezoelectric force table

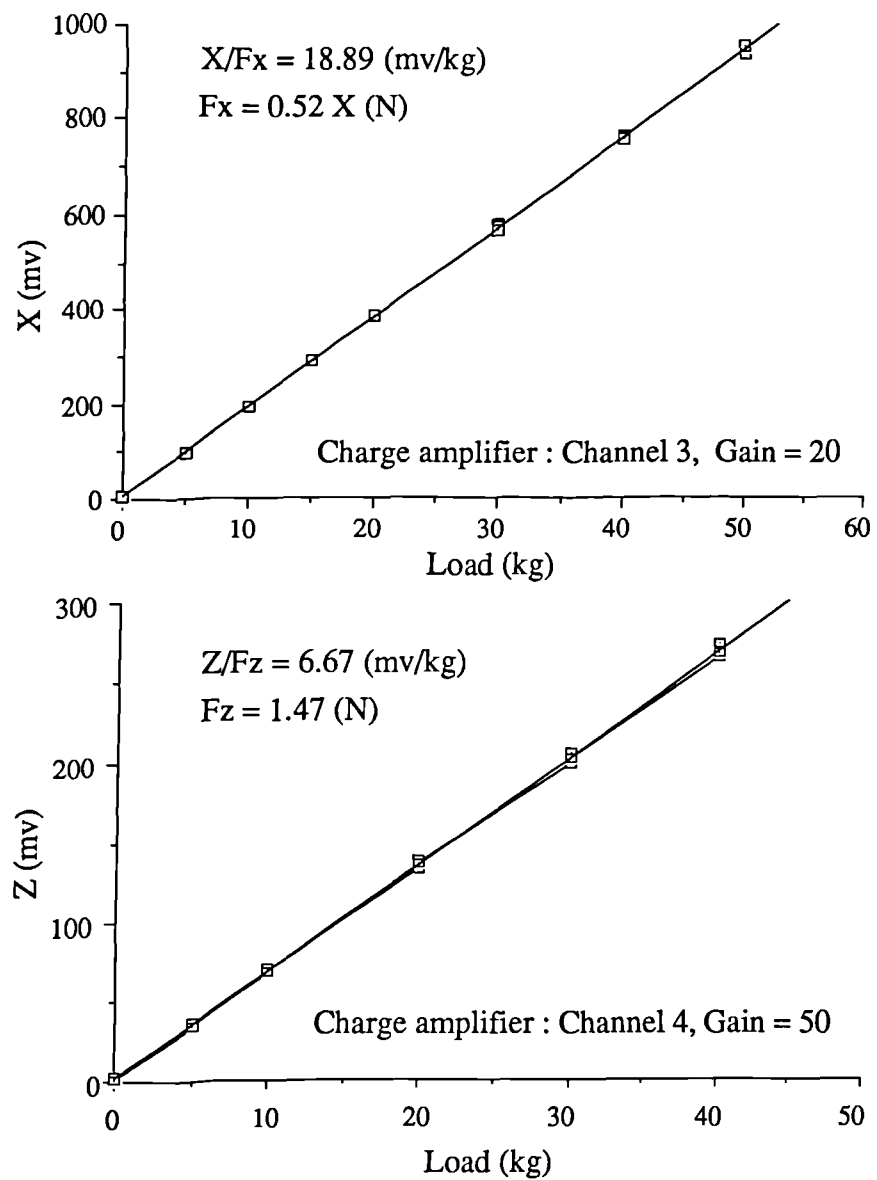


Figure 5.9(b) Calibration results of the piezoelectric force table

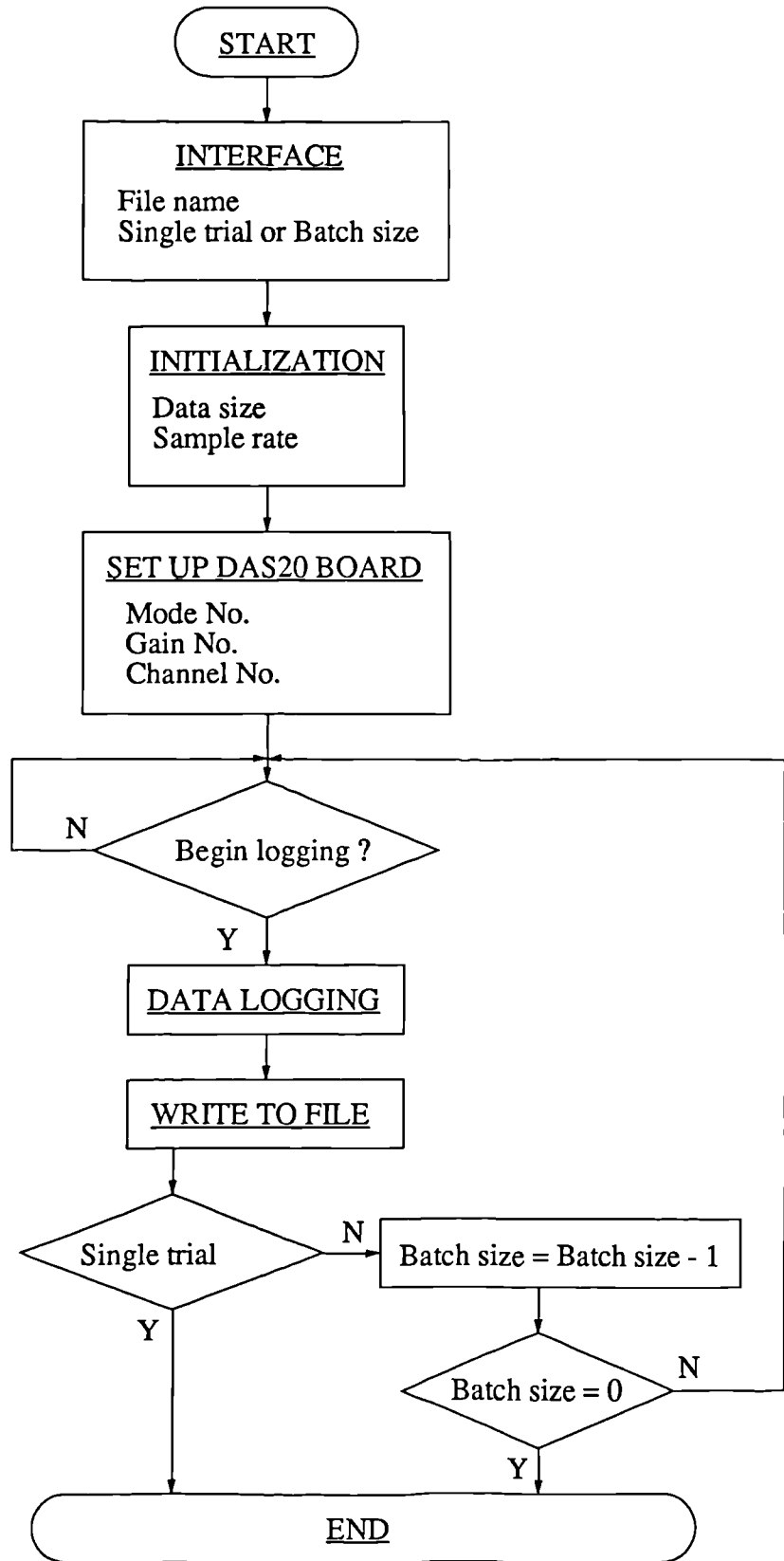


Figure 5.10 A flowchart of the data logging programme in C

Wheel : 19A60K7V, Workpiece : En9
 Dressing : $ad = 20 \mu\text{m}$, $fd = 0.2 \text{ mm/r}$, $nd = 10$ passes
 Size of workpiece : $L = 94 \text{ mm}$, $b = 13 \text{ mm}$

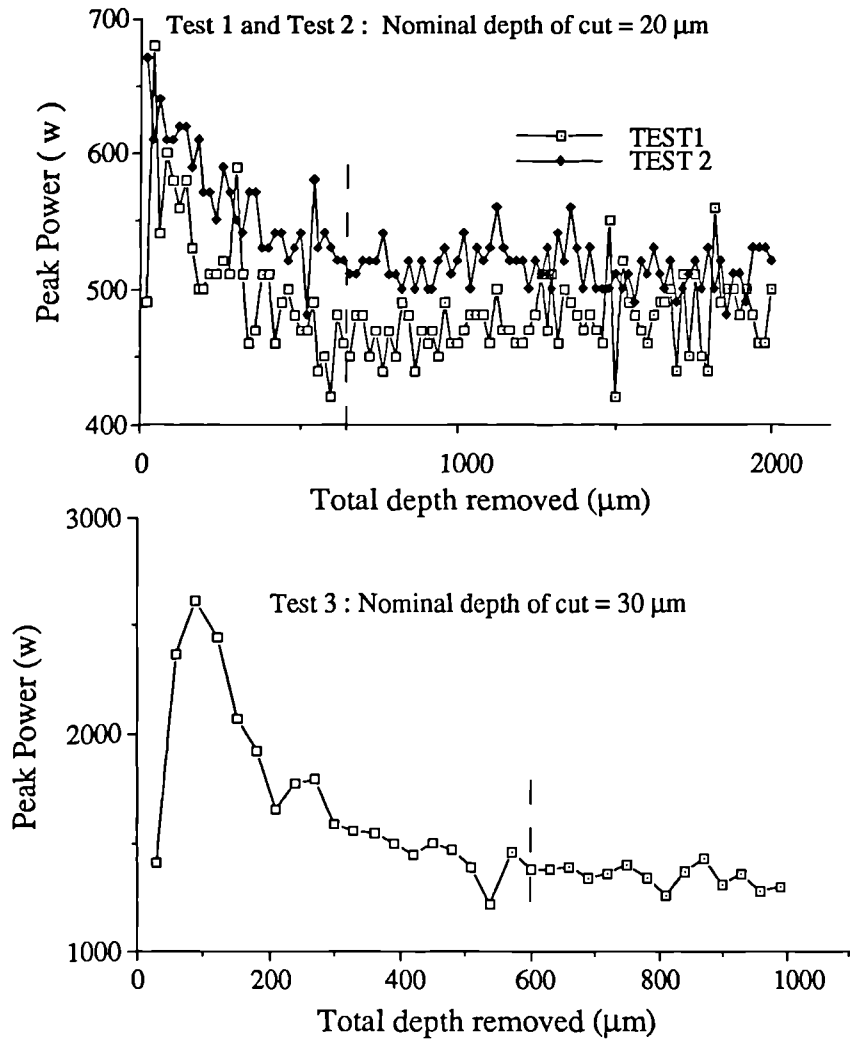


Figure 5.11 Wheel stabilising results

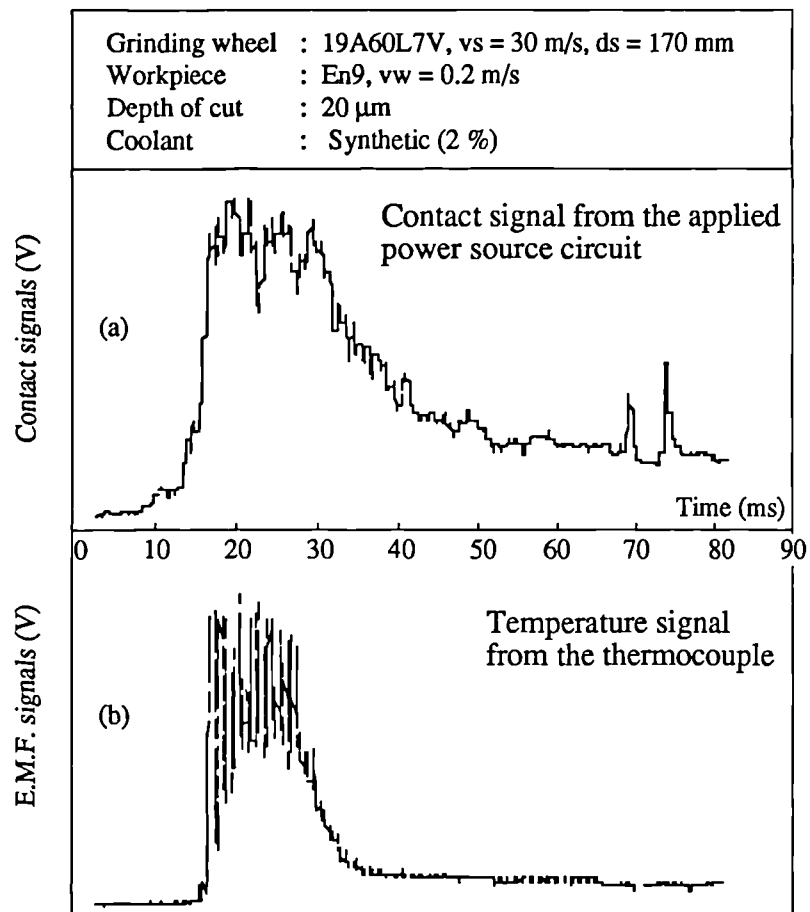


Figure 5.12 A typical plot of contact signals in wet grinding

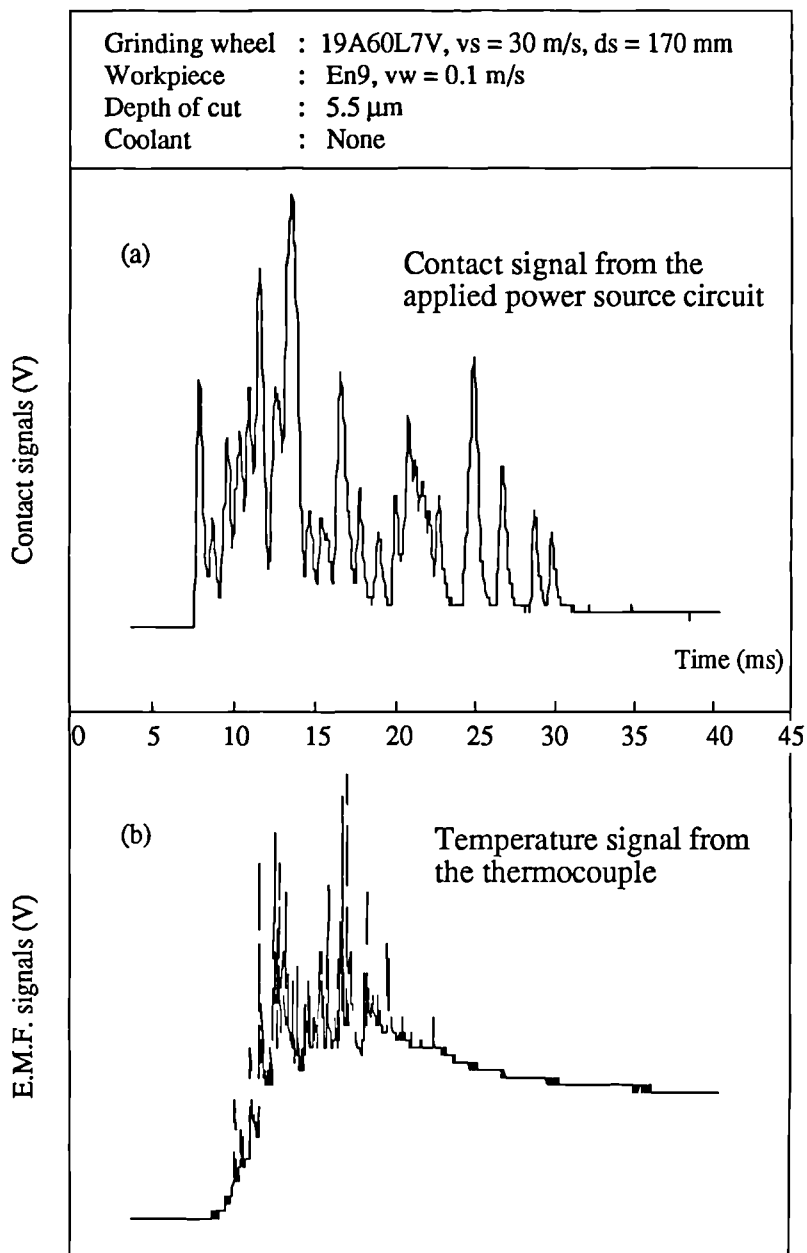


Figure 5.13 A typical plot of contact signals in dry grinding

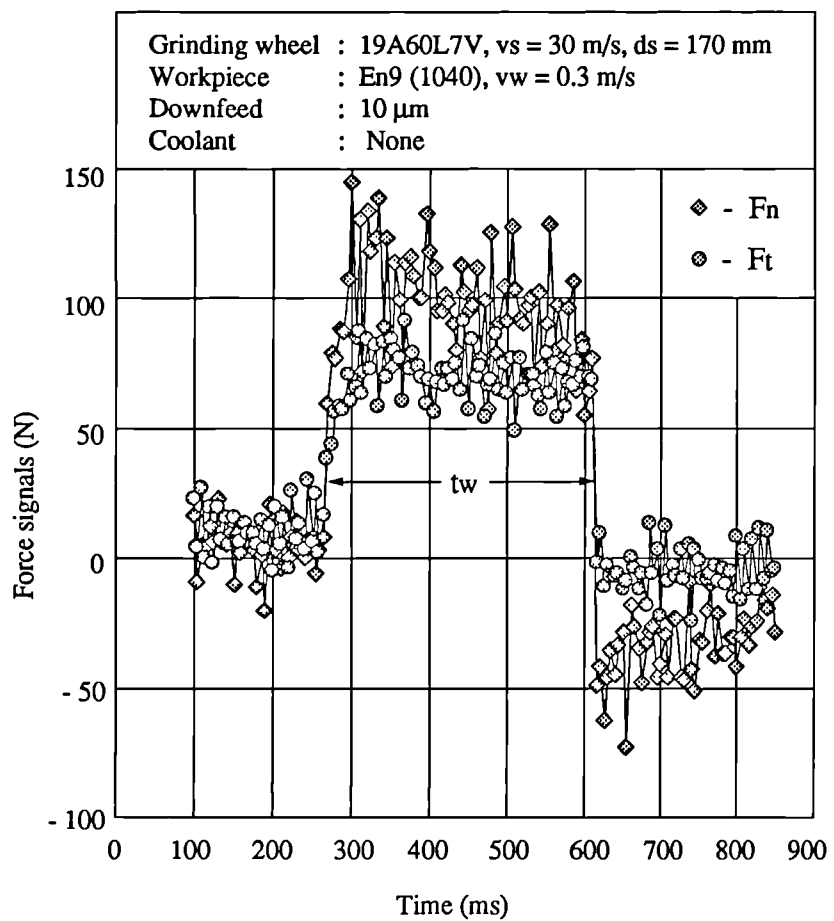


Figure 5.14 Typical grinding force signals

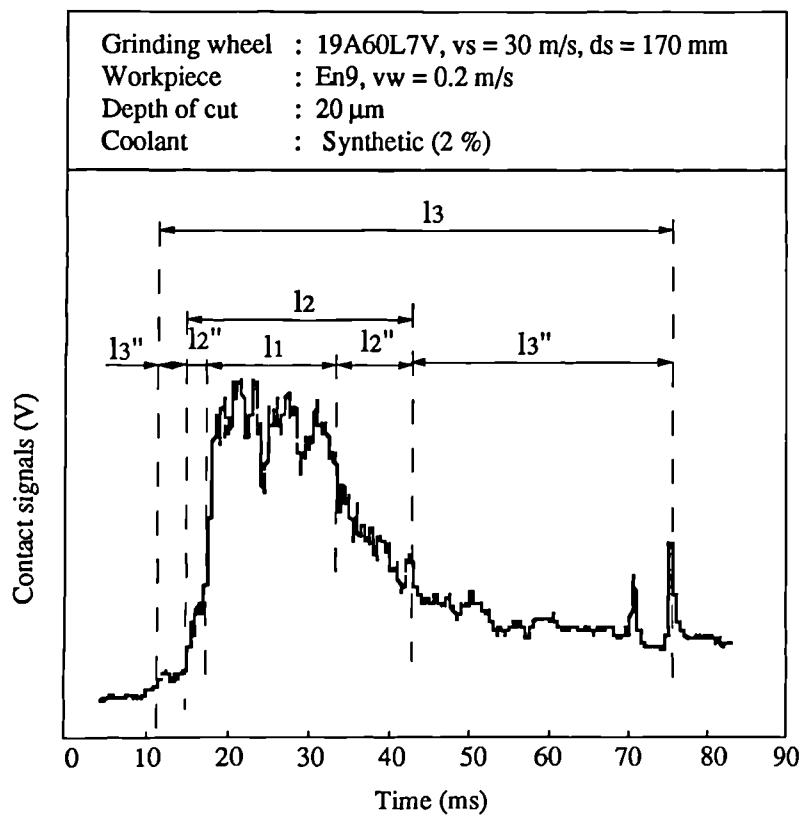


Figure 6.1 A typical contact signal

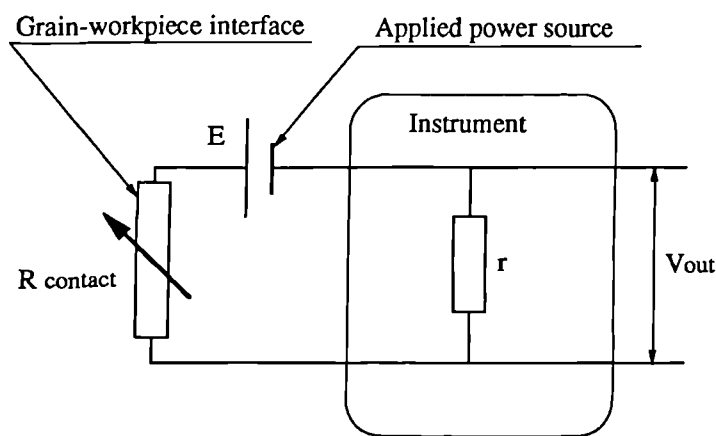


Figure 6.2 An equivalent circuit of the applied power source transducer

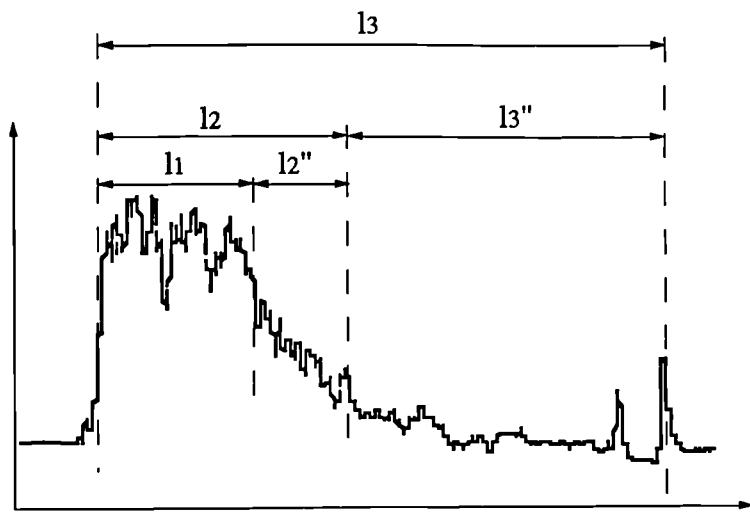


Figure 6.3 An illustration of the three stages of contact between the grains and the workpiece

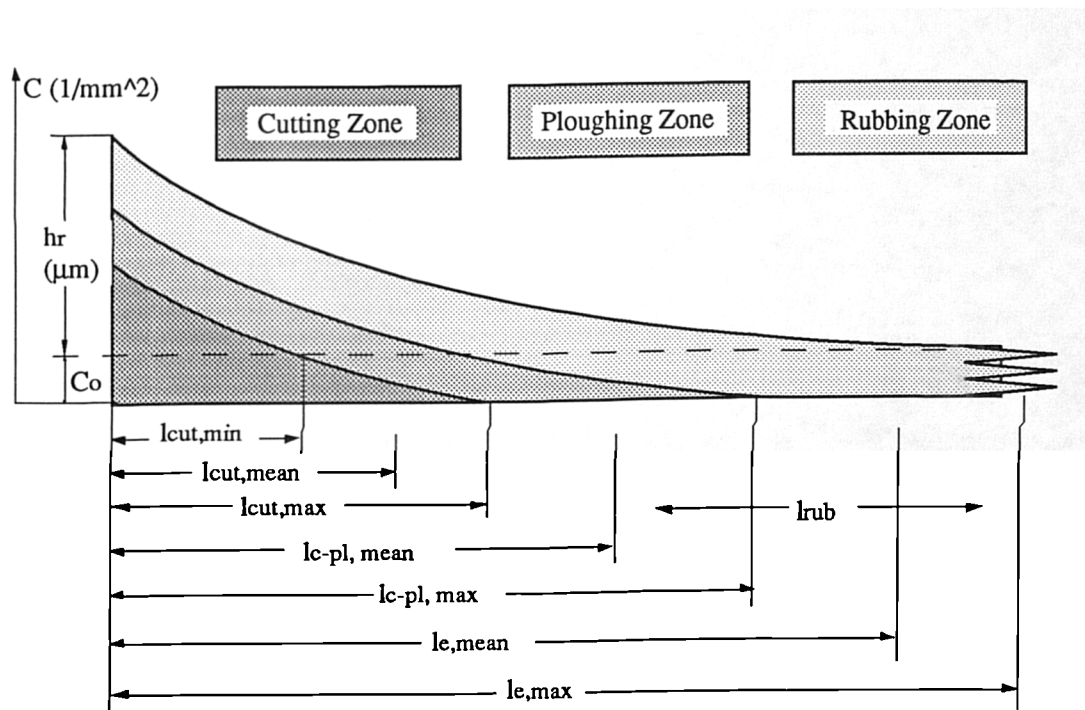


Figure 6.4 The distributions of the intensities of different grains acting along the contact length

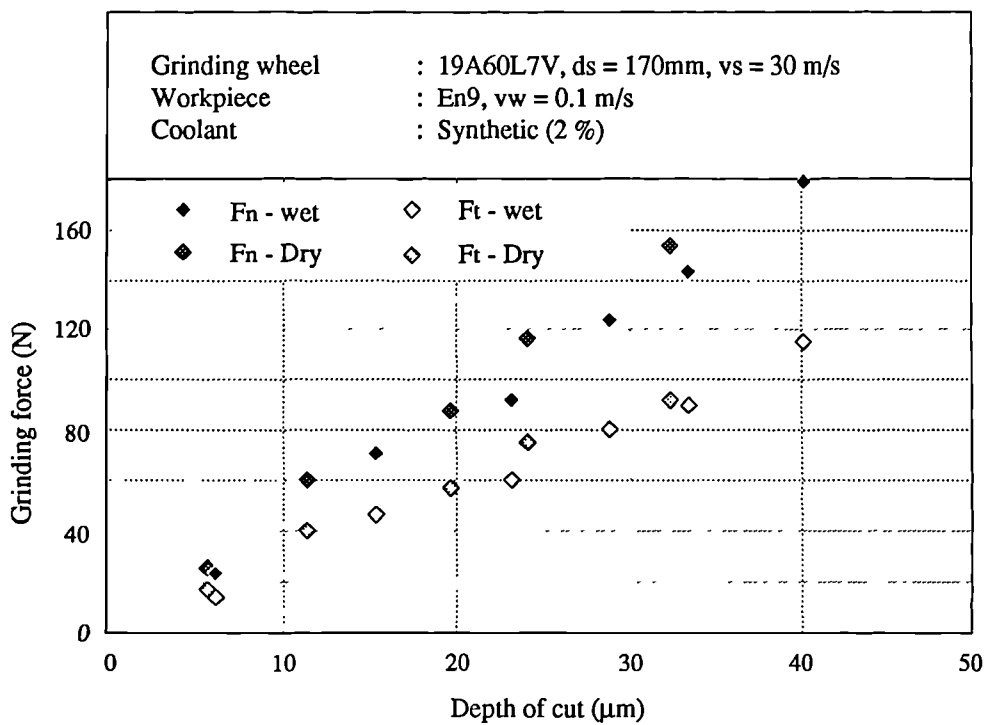


Figure 7.1 Grinding forces and depth of cut - Alumina/En9 steel, $q = 300$, $\mu = 0.65$

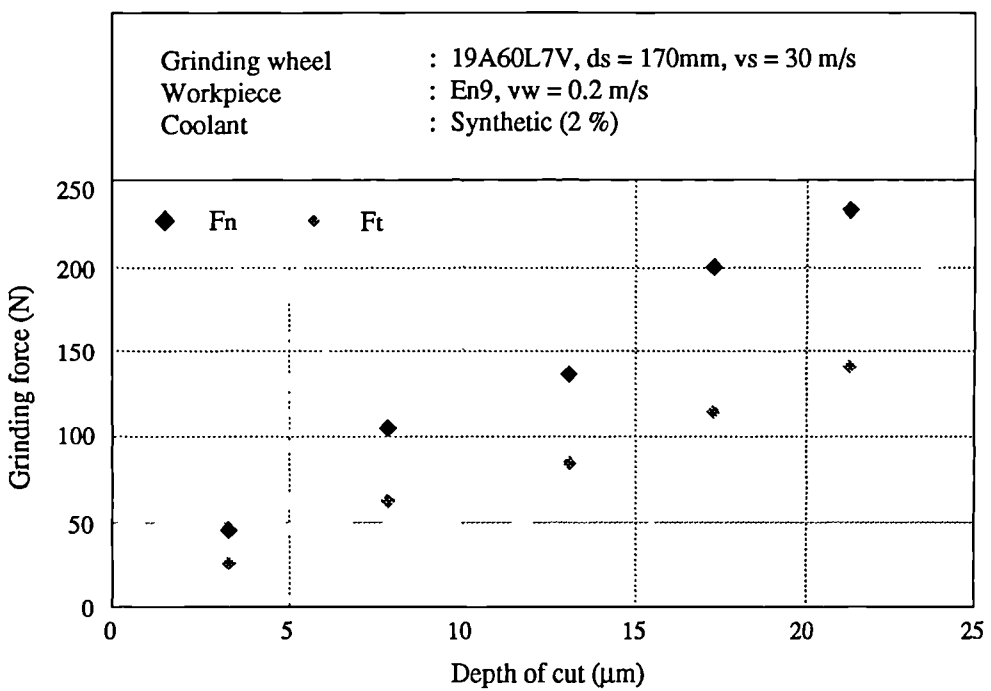


Figure 7.2 Grinding forces and depth of cut - Alumina/En9 steel, $q = 150$, $\mu = 0.59$

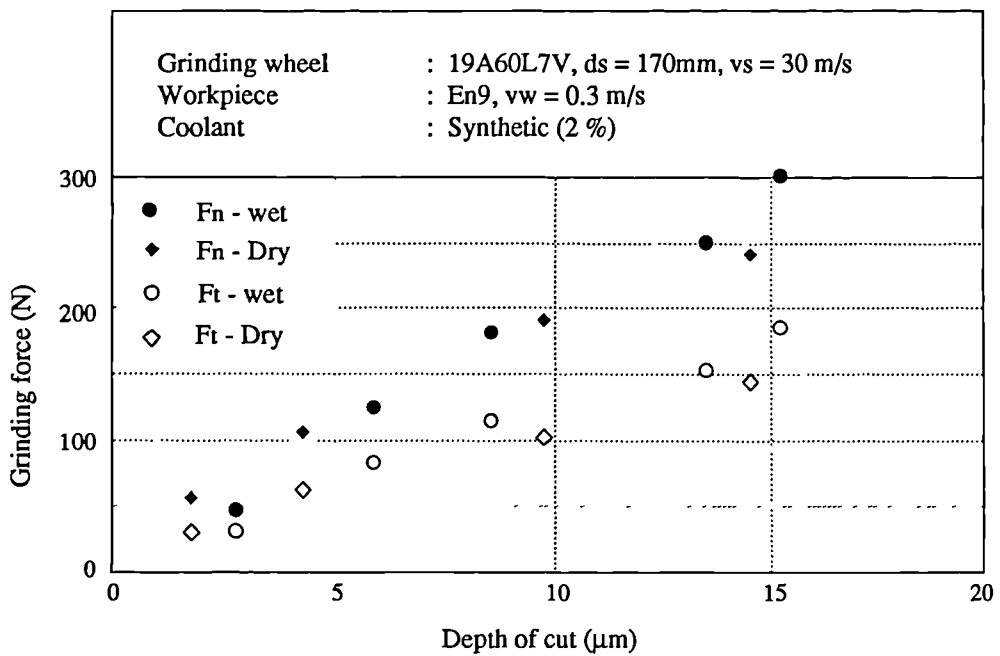


Figure 7.3 Grinding forces and depth of cut - Alumina/En9 steel,
 $q = 100$, $\mu_w = 0.63$, $\mu_d = 0.57$

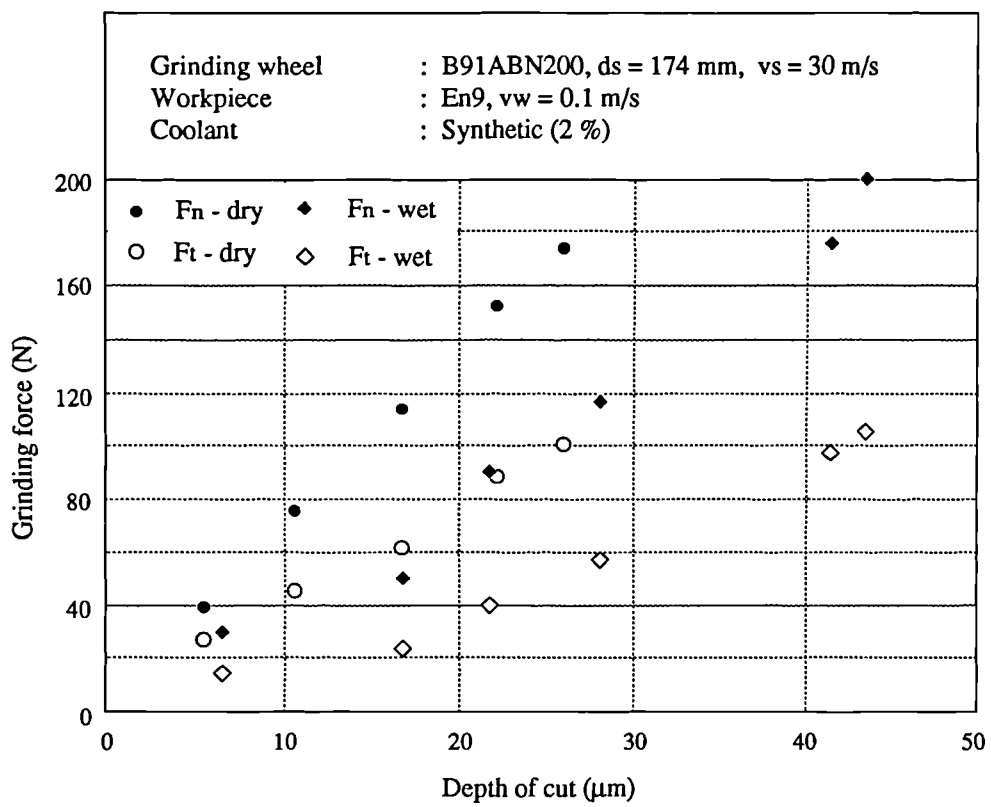


Figure 7.4 Grinding forces and depth of cut - CBN/En9 steel, $\mu_w = 0.5$, $\mu_d = 0.6$

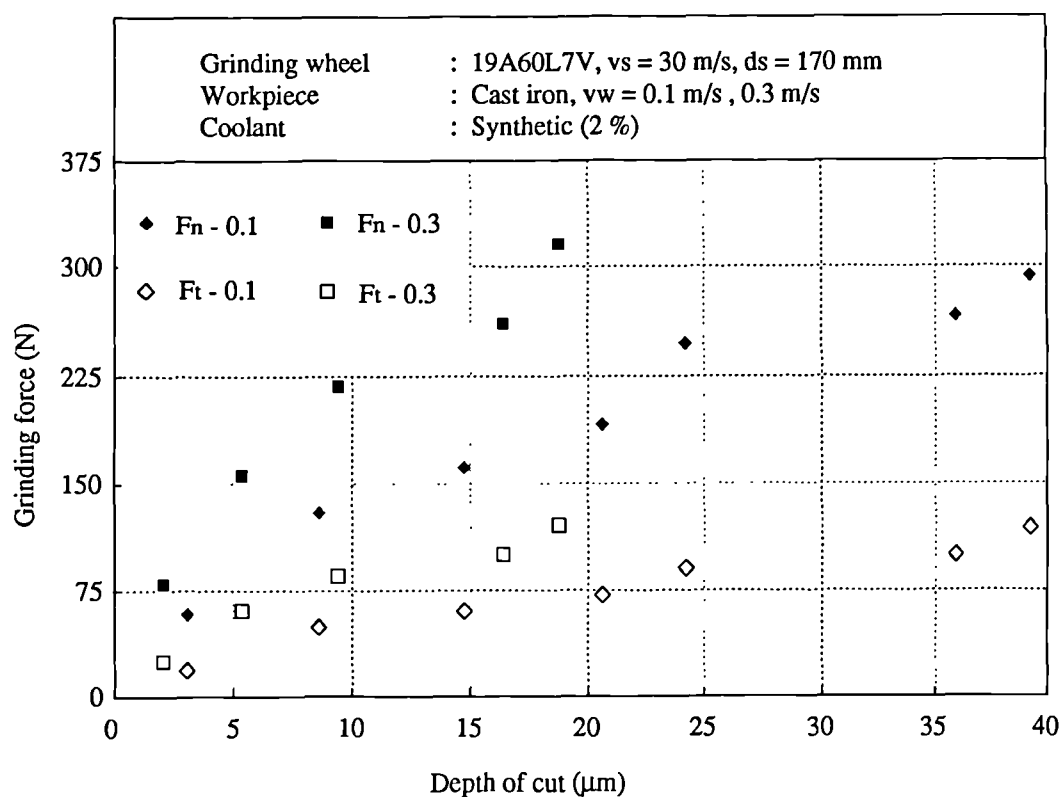


Figure 7.5 Grinding forces and depth of cut - Alumina/Cast iron, $\mu = 0.37$

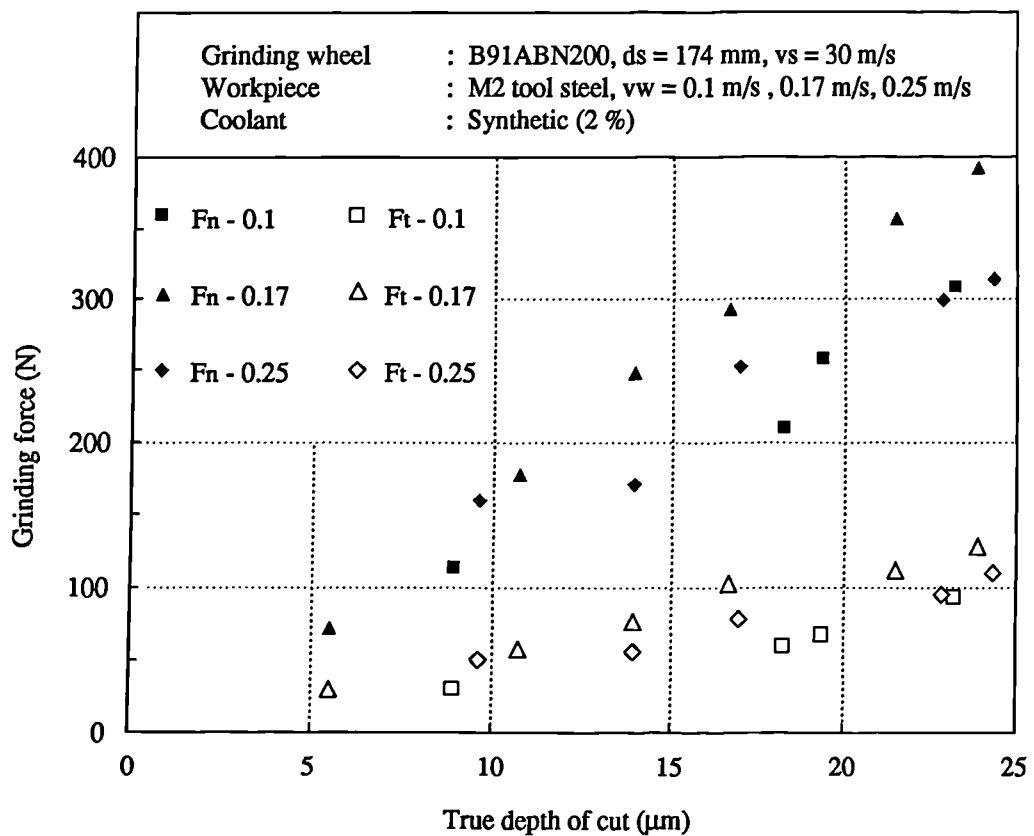


Figure 7.6 Grinding forces and depth of cut - CBN/M2,
 $\mu_{-0.1} = 0.28$, $\mu_{-0.17} = 0.37$, $\mu_{-0.25} = 0.33$

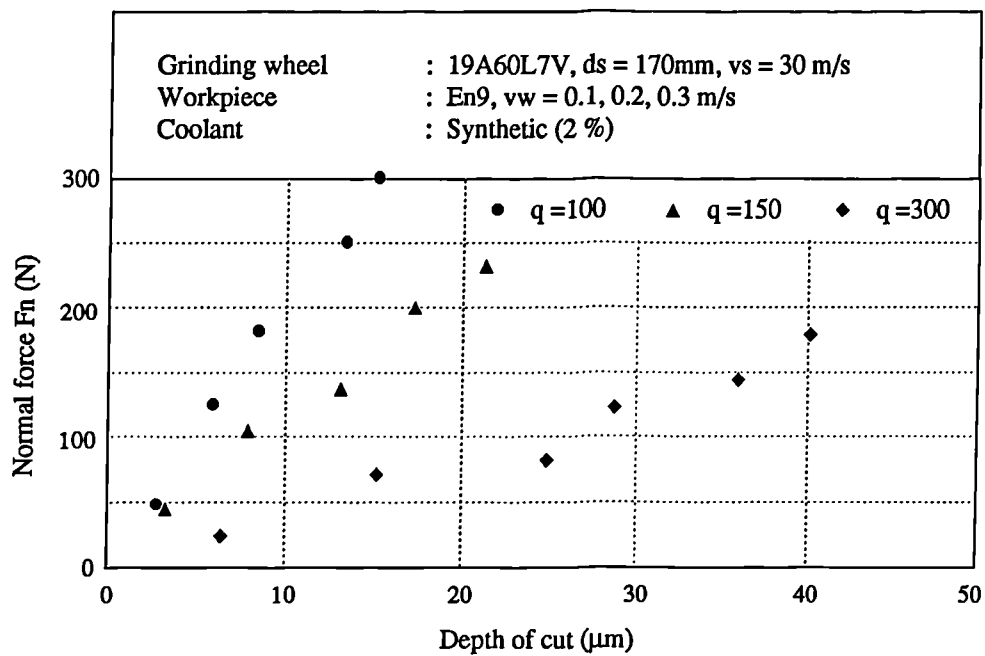


Figure 7.7 Normal forces and speed ratio - Alumina/En9 steel

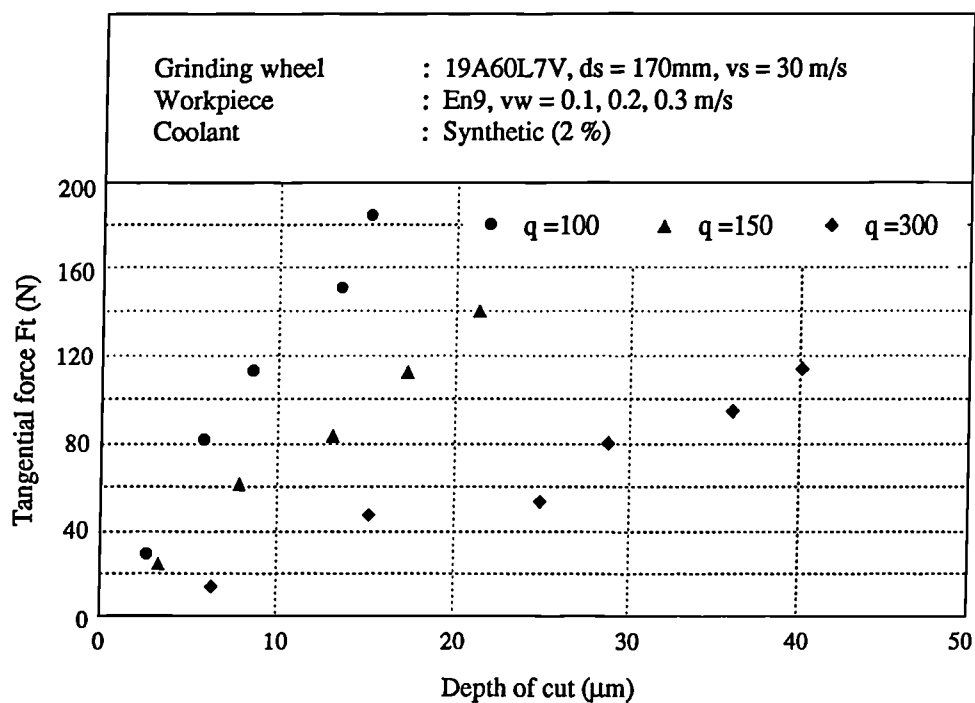


Figure 7.8 Tangential forces and speed ratio - Alumina/En9 steel

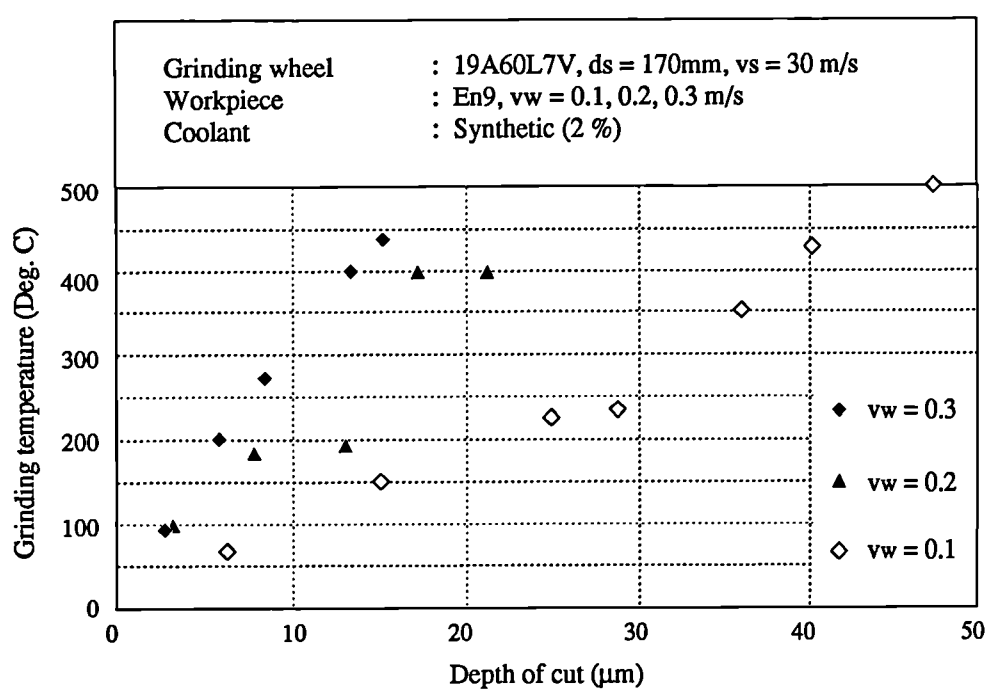


Figure 7.9 Grinding temperature and workpiece speed - Alumina/En9 steel

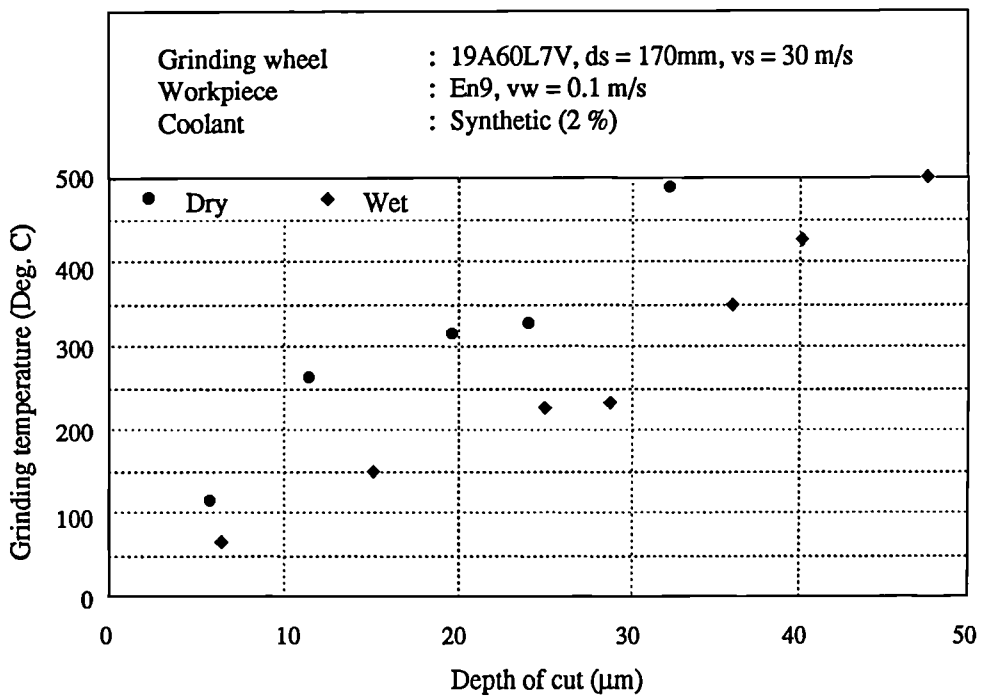


Figure 7.10 Grinding temperature in dry and wet grinding - Alumina/En9 steel

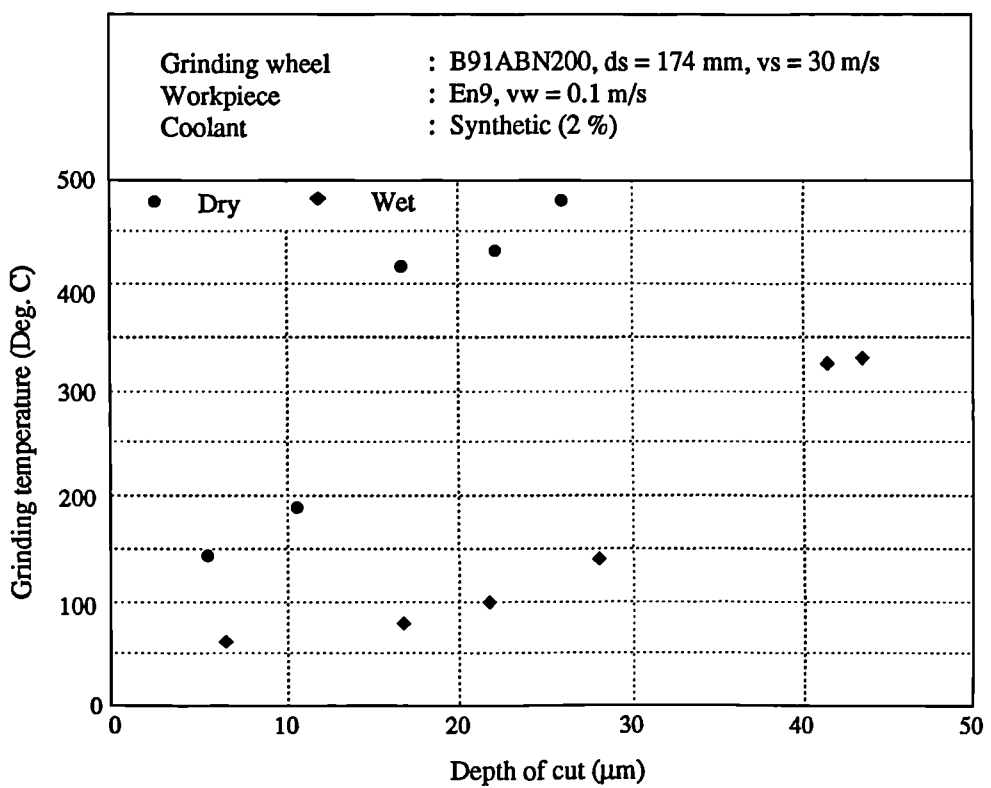


Figure 7.11 Grinding temperature in dry and wet grinding - CBN/En9 steel

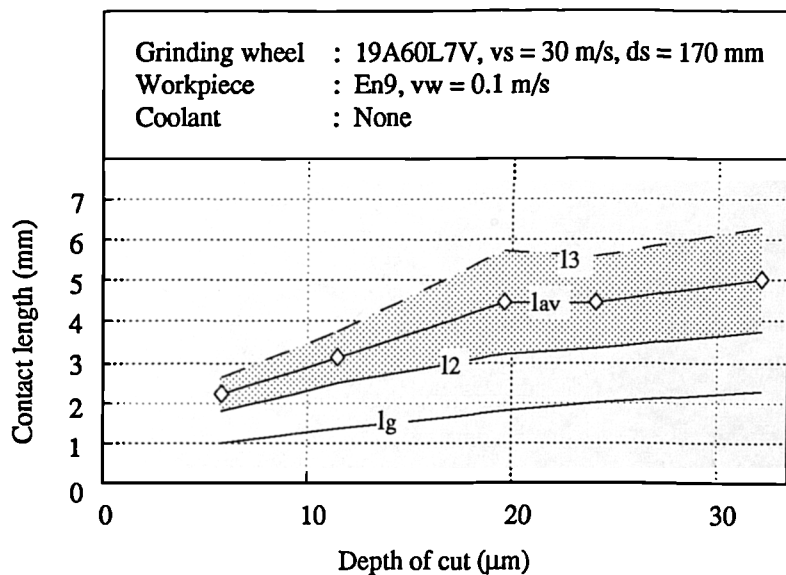


Figure 7.12 Grinding contact length and depth of cut - Alumina/En9 steel

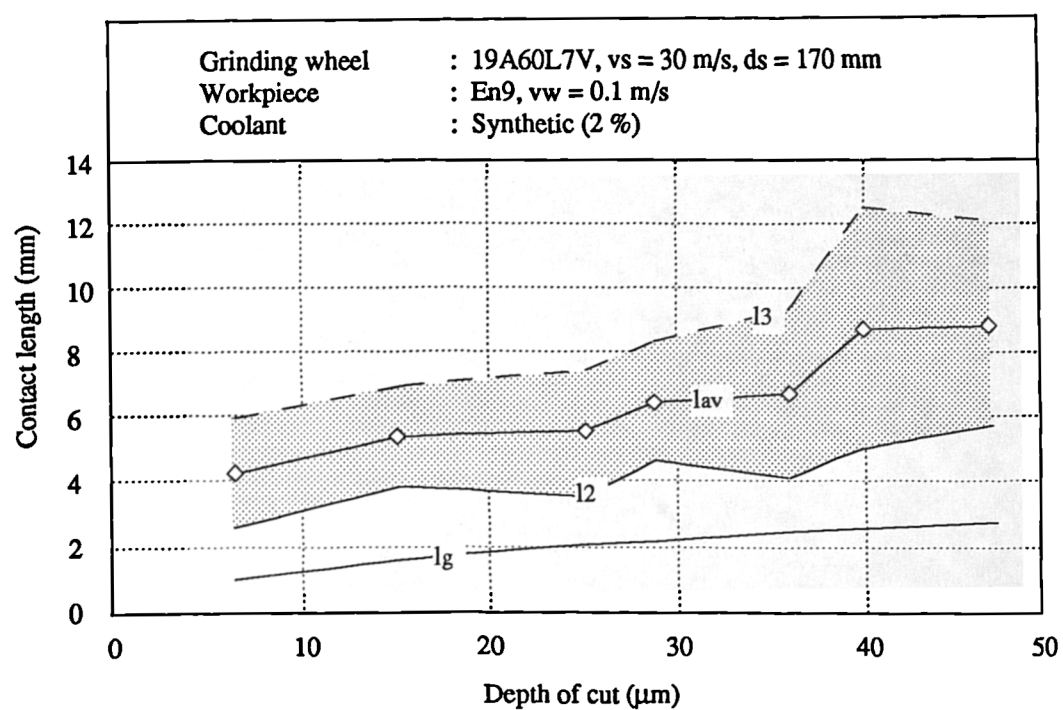


Figure 7.13 Grinding contact length and depth of cut - Alumina/En9 steel

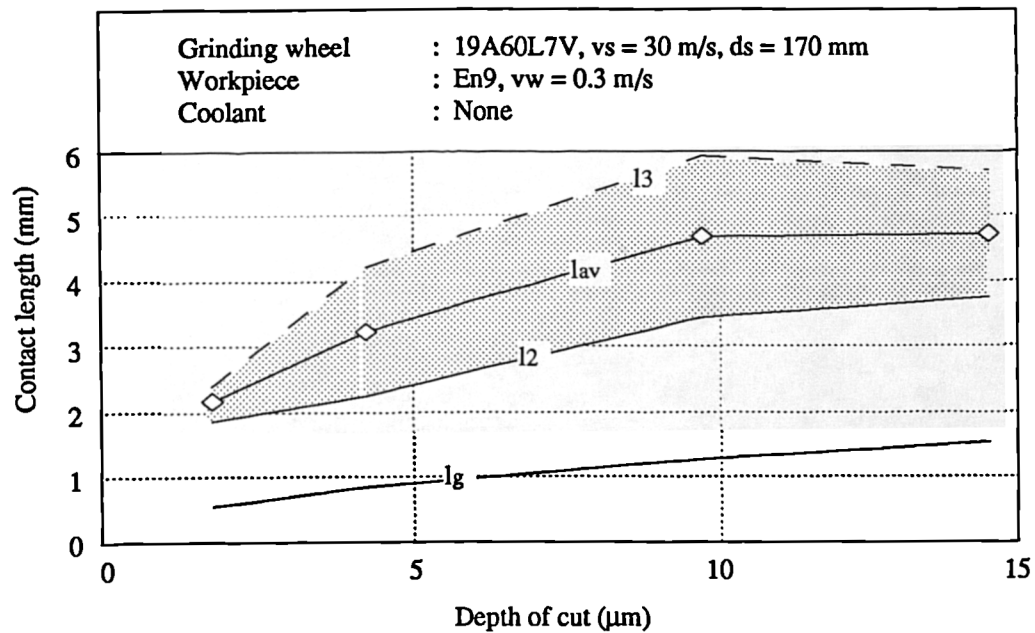


Figure 7.14 Grinding contact length and depth of cut - Alumina/En9 steel

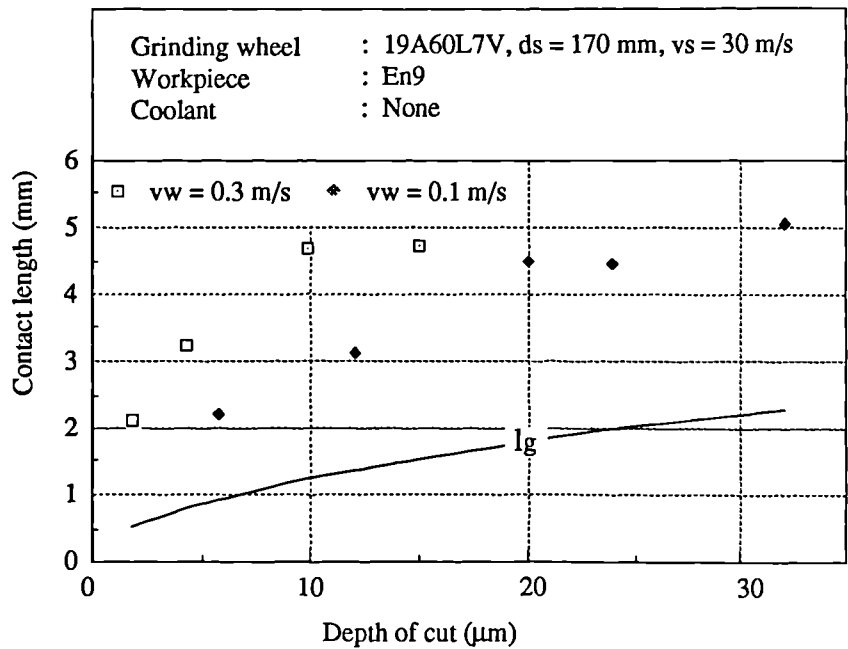


Figure 7.15 Grinding contact length and depth of cut - Alumina/En9 steel

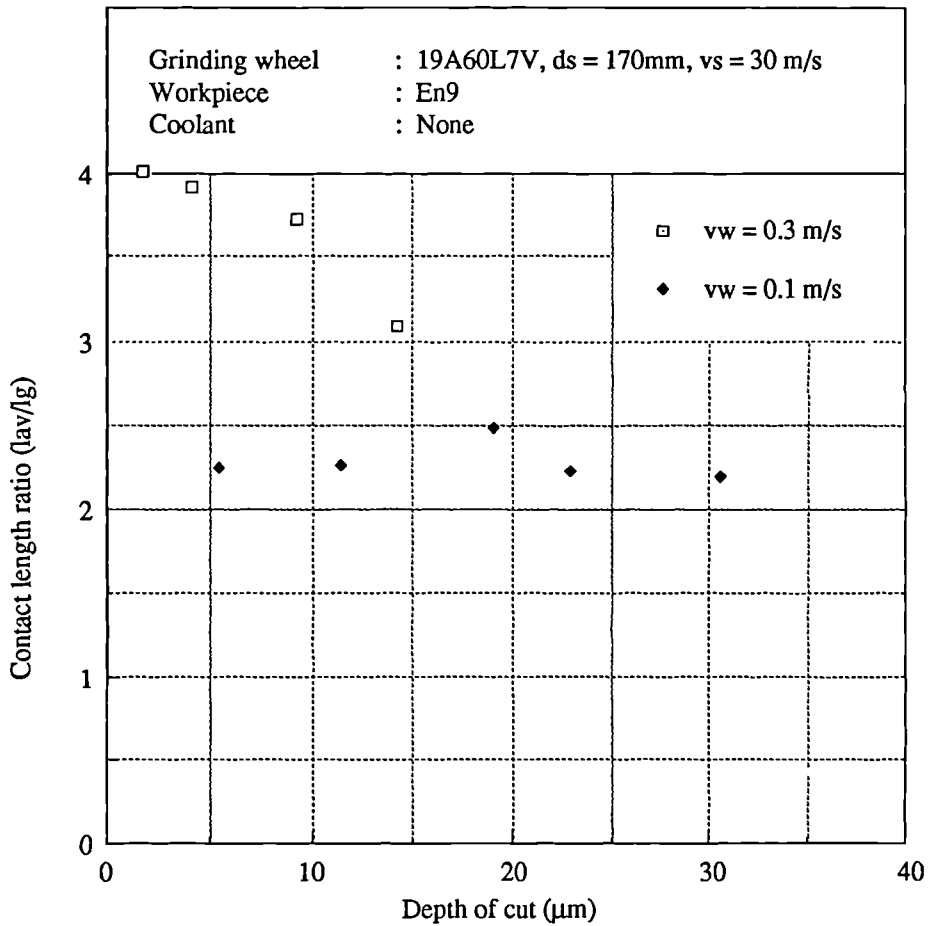


Figure 7.16 Contact length ratio and depth of cut - Alumina/En9 steel

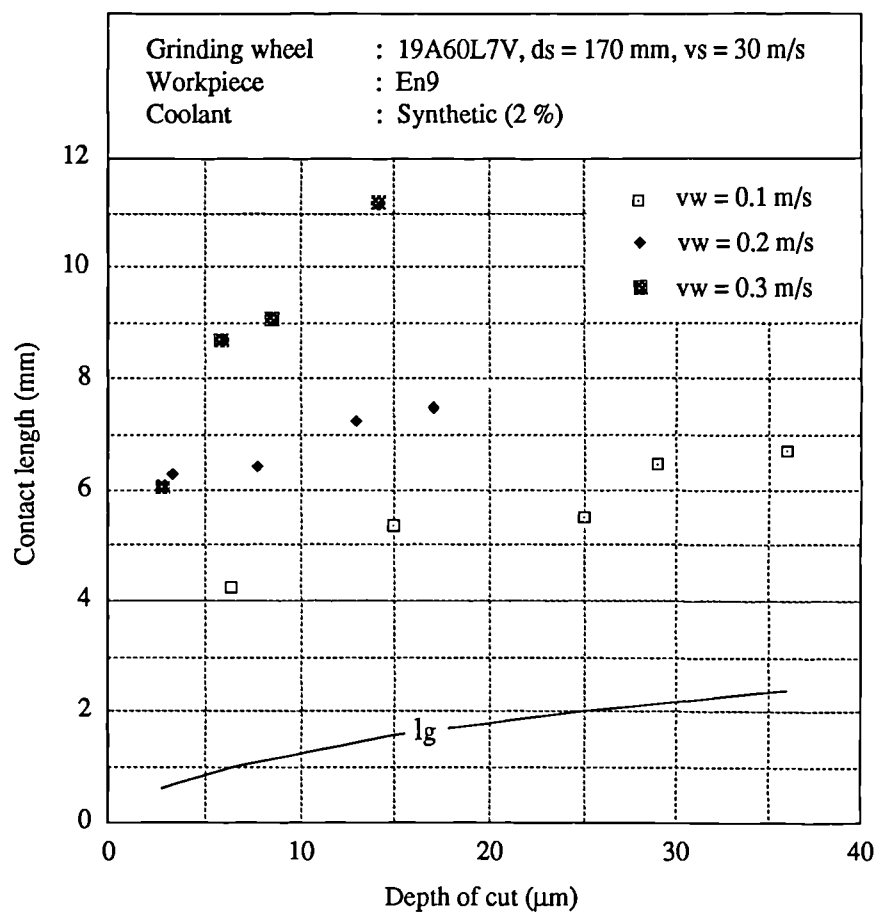


Figure 7.17 Grinding contact length and depth of cut - Alumina/En9 steel with coolant

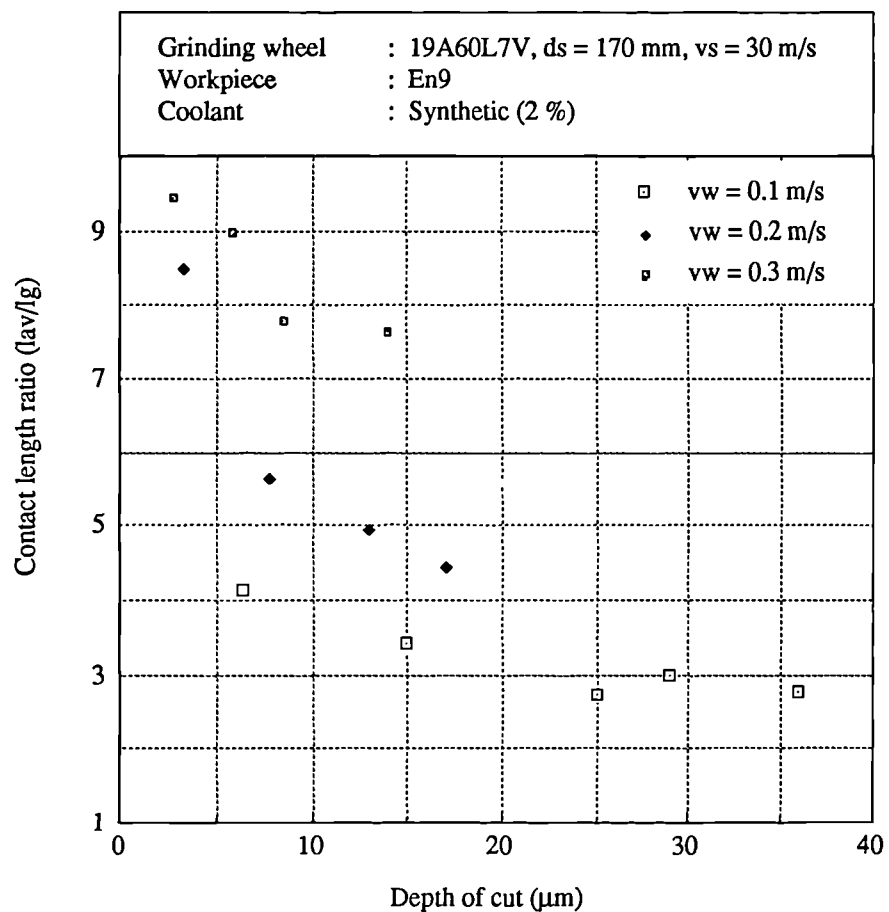


Figure 7.18 Contact length ratio and depth of cut - Alumina/En9 steel with coolant

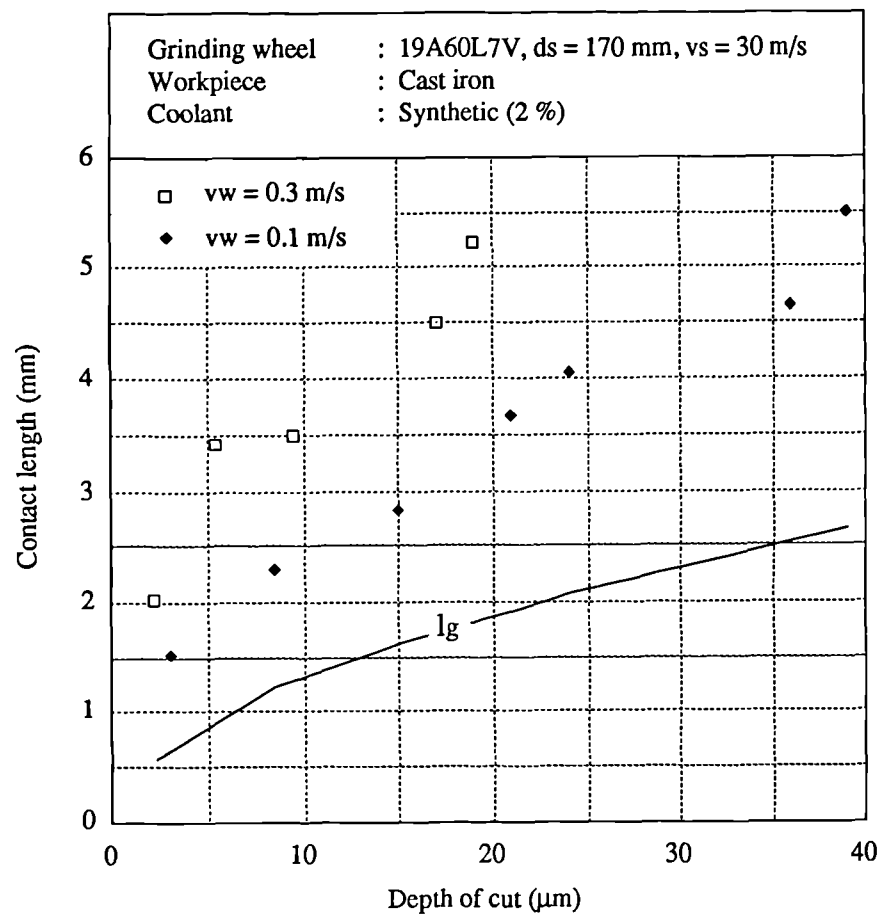


Figure 7.19 Grinding contact length and depth of cut - Alumina/cast iron with coolant

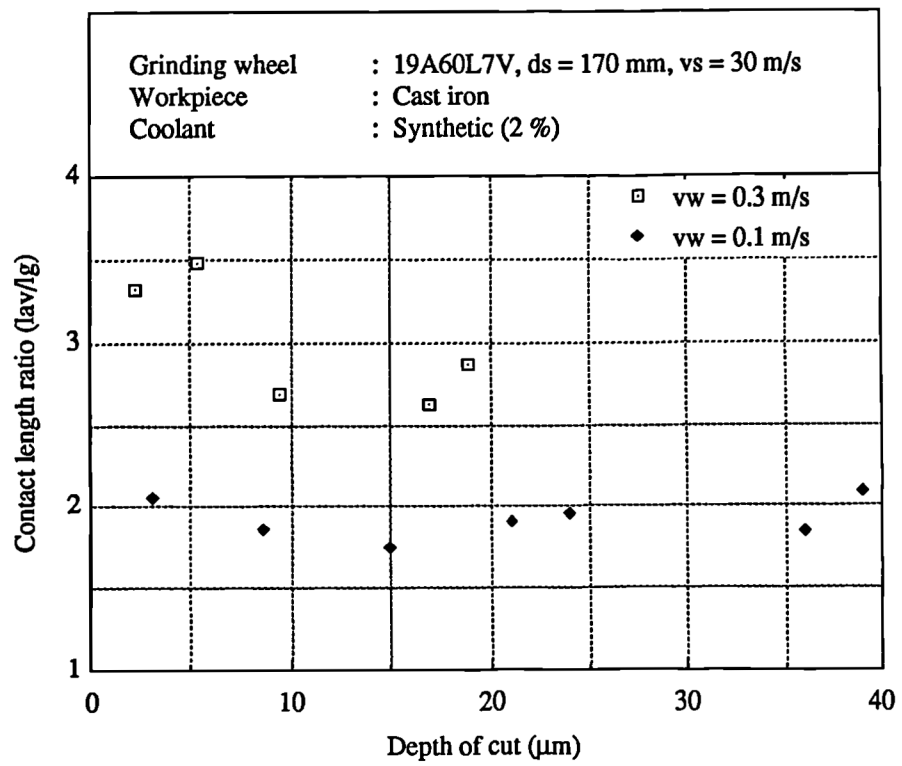


Figure 7.20 Contact length ratio and depth of cut - Alumina/cast iron

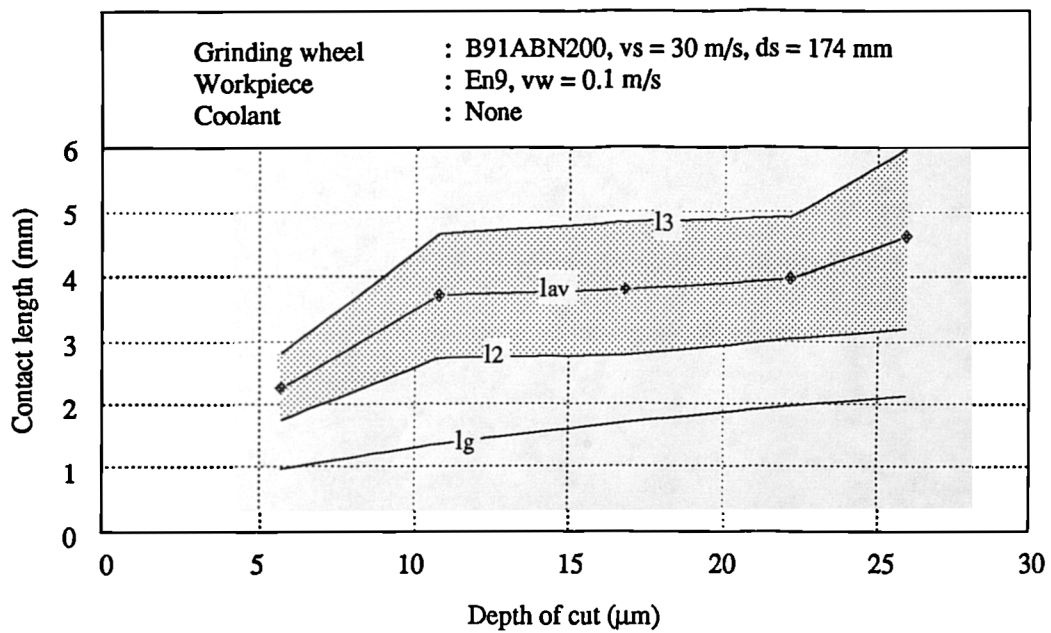


Figure 7.21 Grinding contact length and depth of cut - CBN/En9 steel without coolant

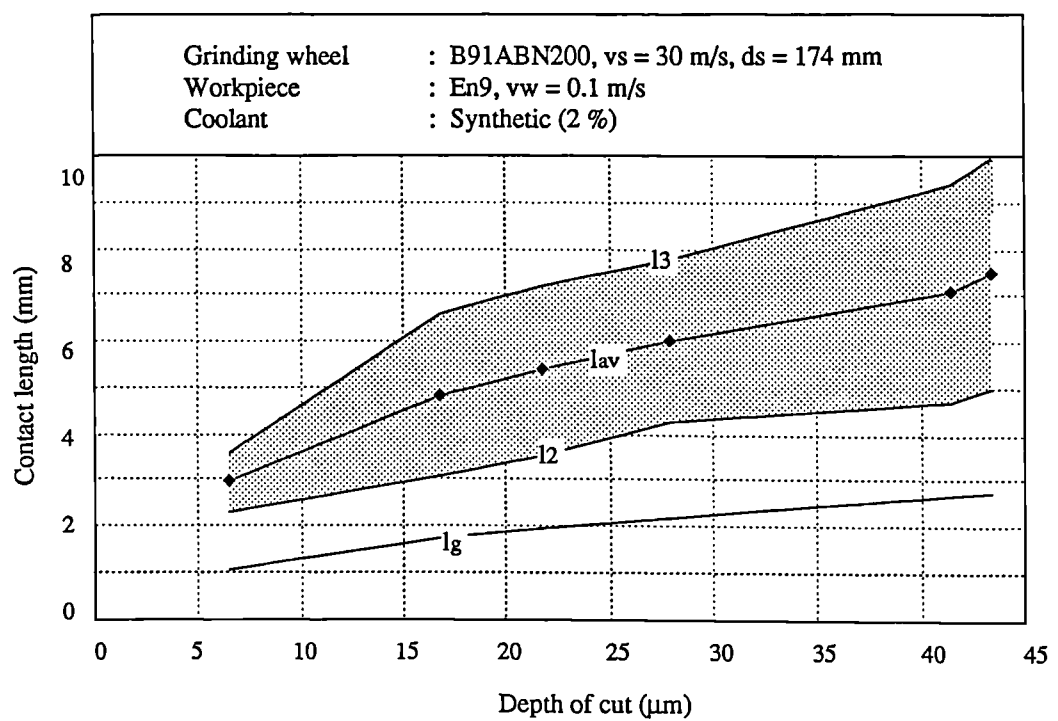


Figure 7.22 Grinding contact length and depth of cut - CBN/En9 steel with coolant

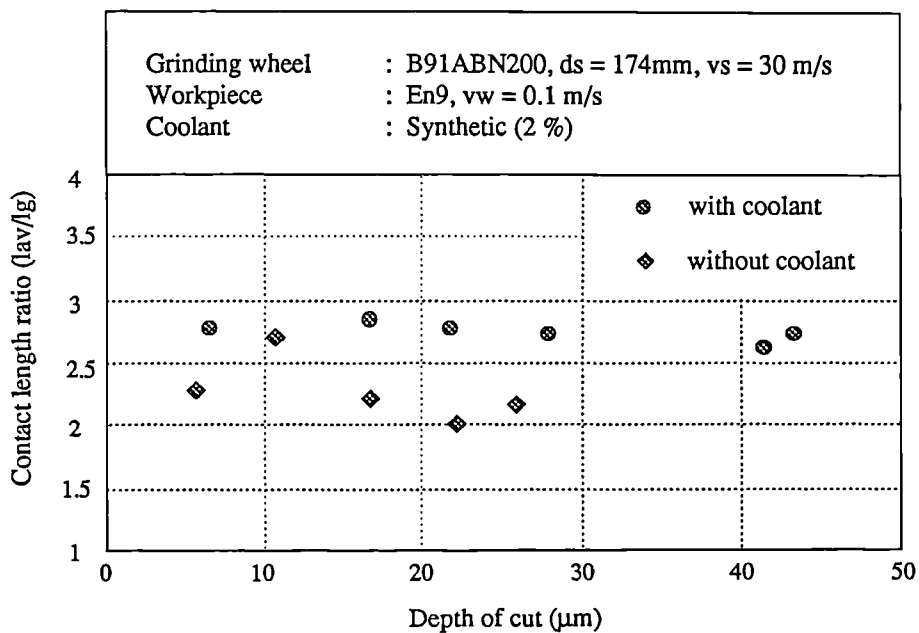


Figure 7.23 Contact length ratio and depth of cut - CBN/En9 steel

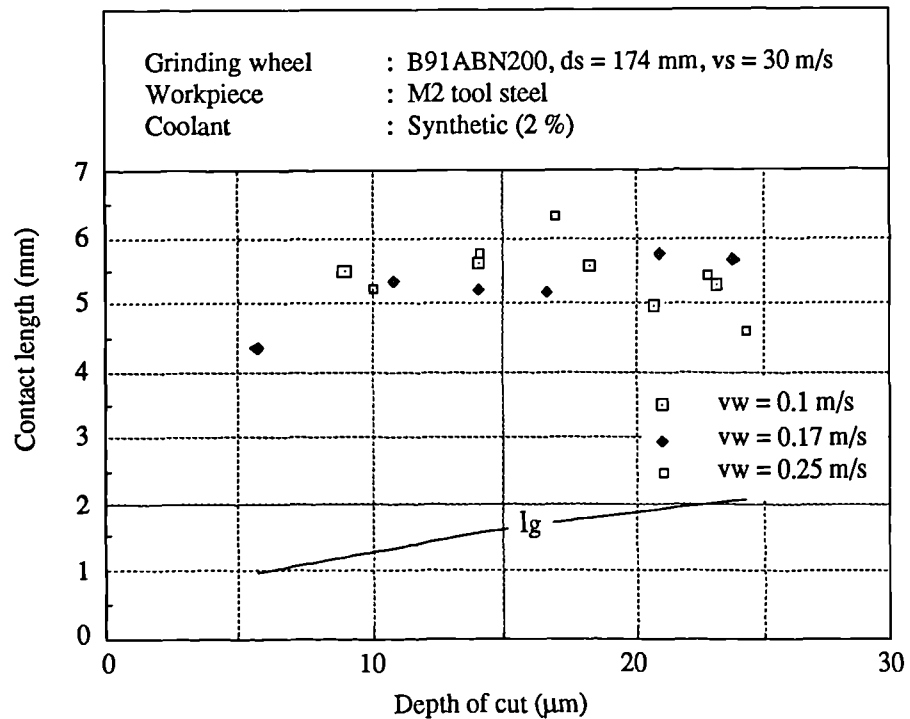


Figure 7.24 Grinding contact length and depth of cut - CBN/M2 tool steel

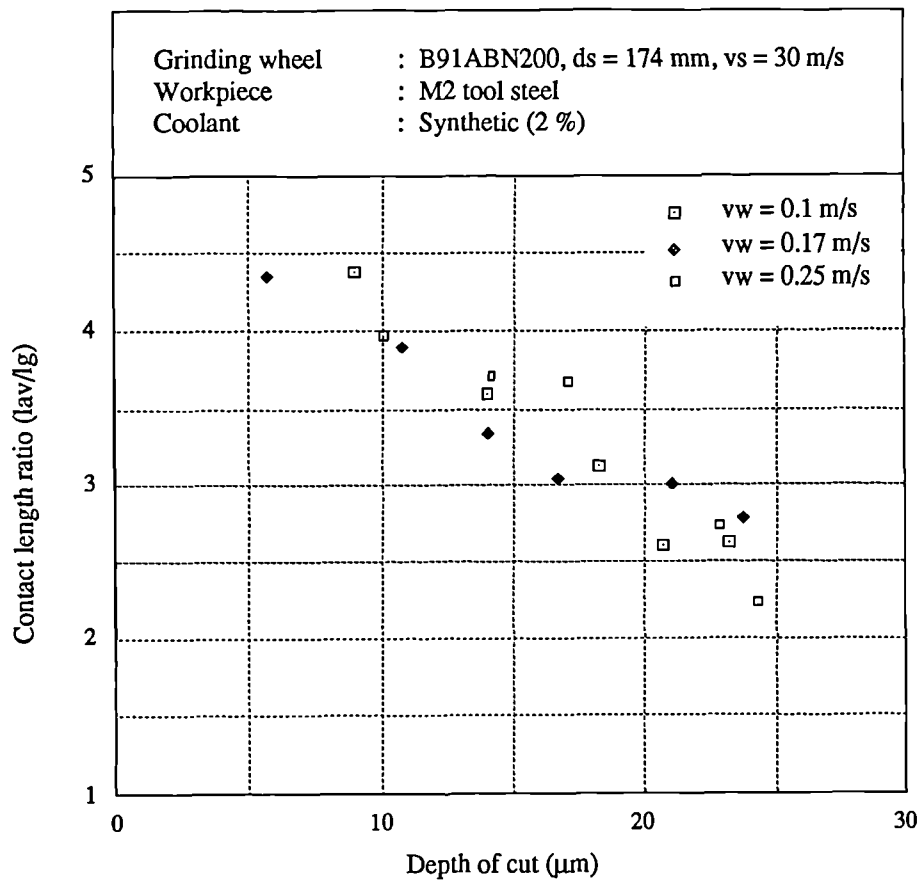


Figure 7.25 Contact length ratio and depth of cut - CBN/M2 tool steel

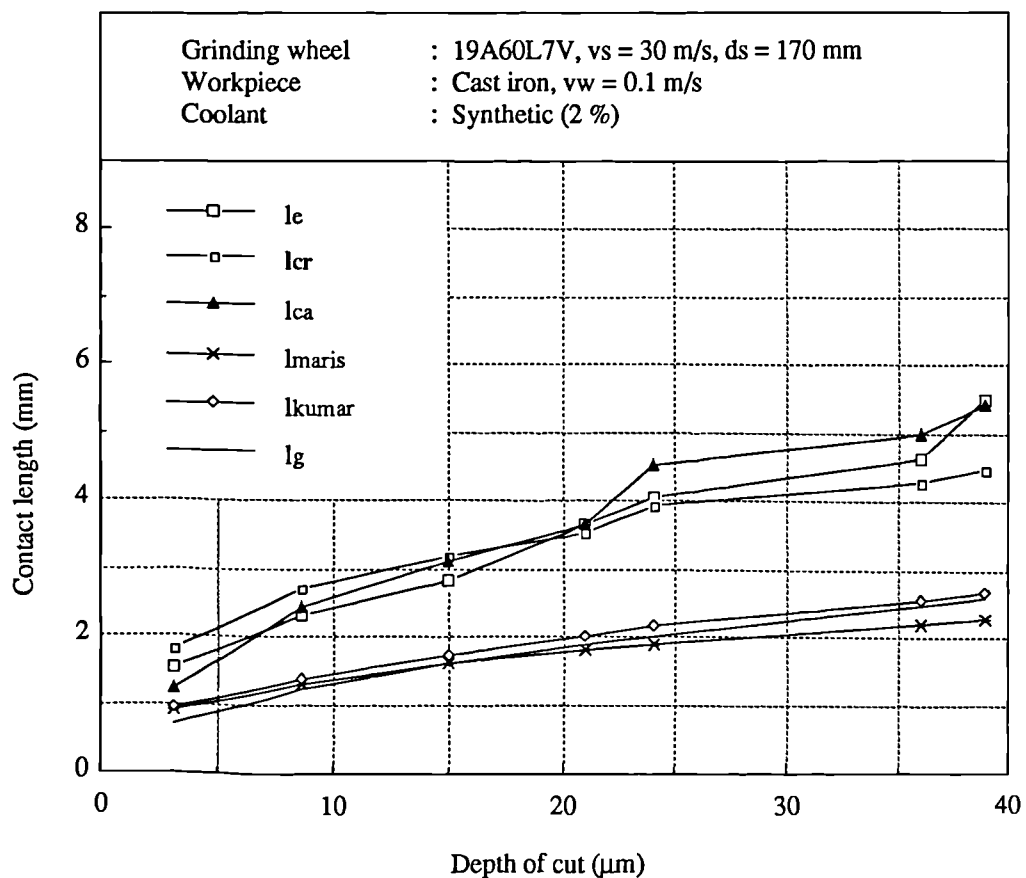


Figure 8.1 Evaluation of contact length models - Alumina/Cast iron $v_w = 0.1 \text{ m/s}$, wet

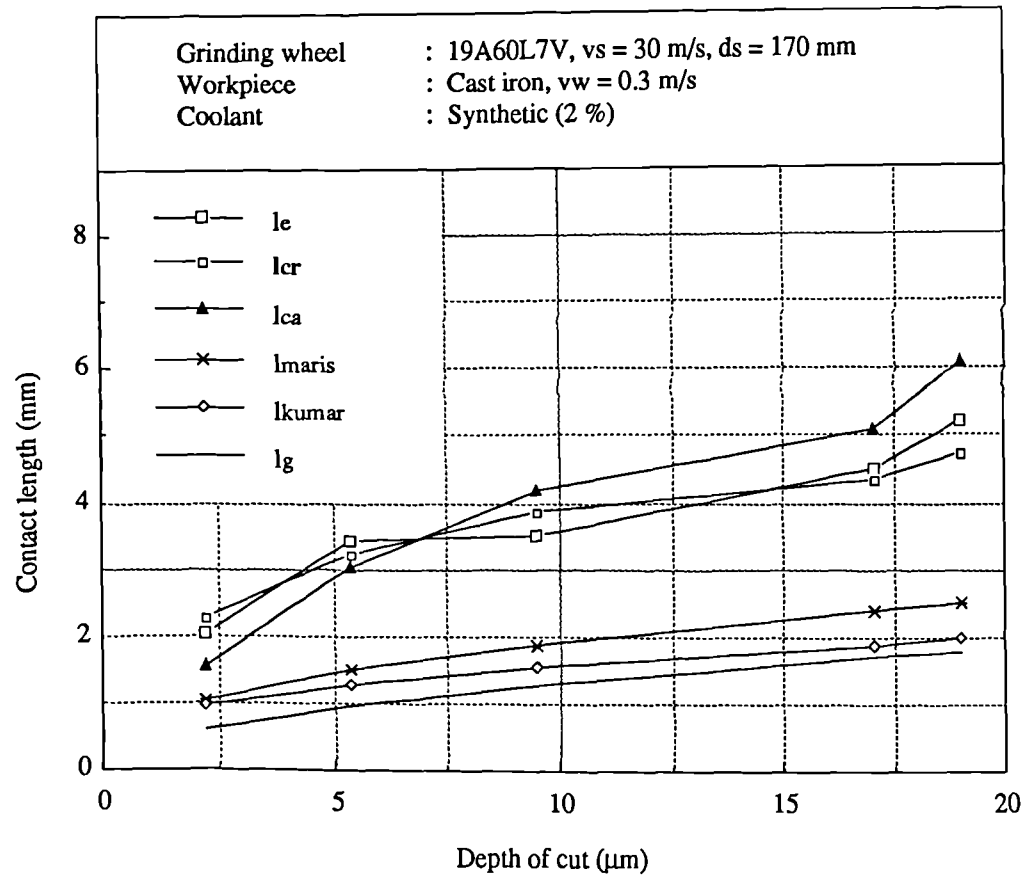


Figure 8.2 Evaluation of contact length models - Alumina/Cast iron $v_w = 0.3 \text{ m/s}$, wet

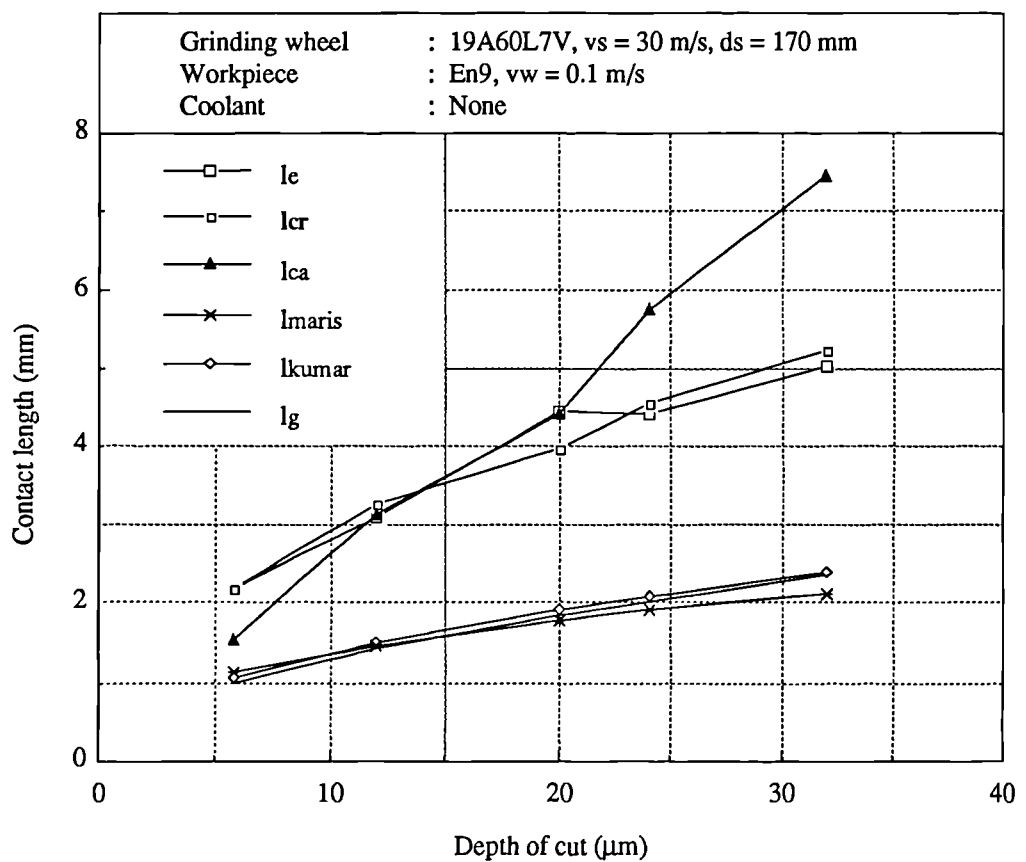


Figure 8.3 Evaluation of contact length models - Alumina/En9 steel $v_w = 0.1$, dry

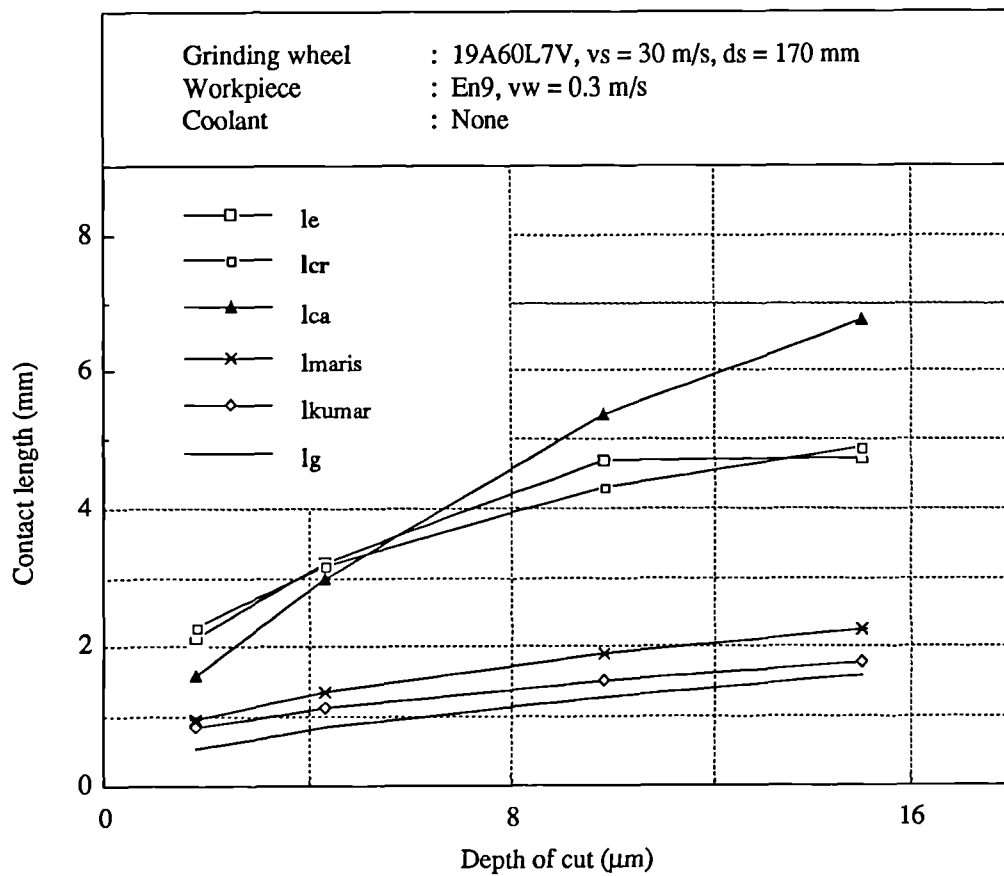


Figure 8.4 Evaluation of contact length models - Alumina/En9 steel, $v_w = 0.3$ m/s, dry

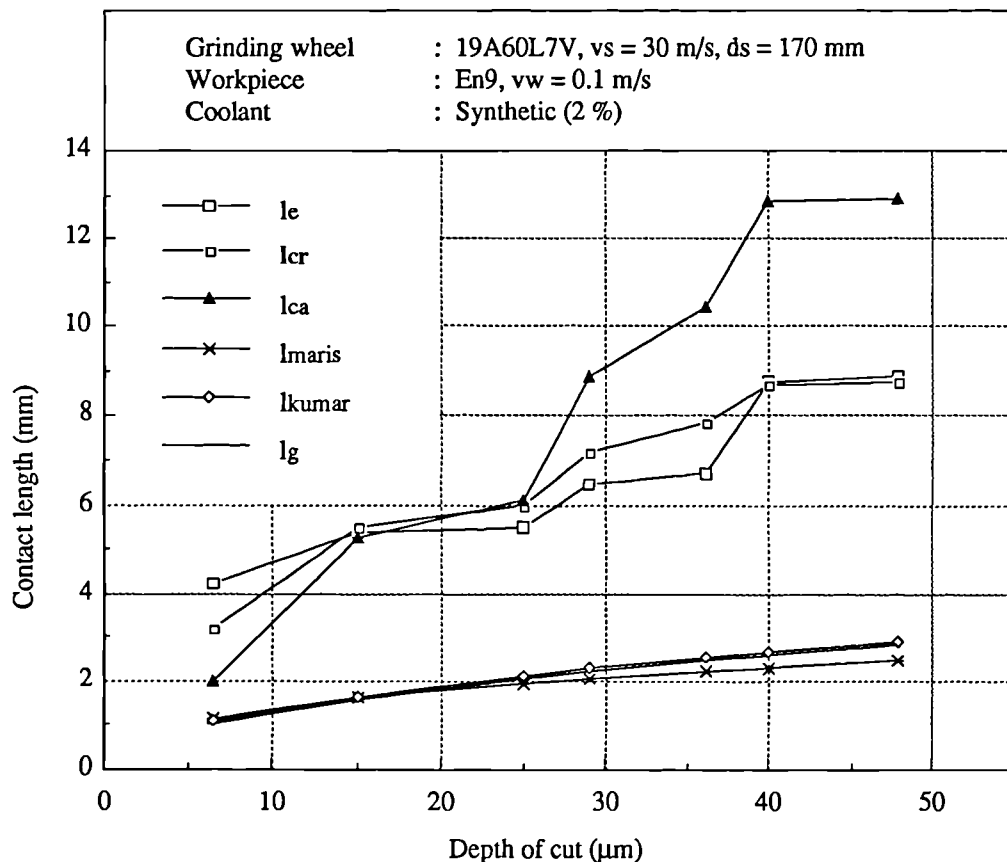


Figure 8.5 Evaluation of contact length models - Alumina/En9 steel $v_w = 0.1 \text{ m/s}$, wet

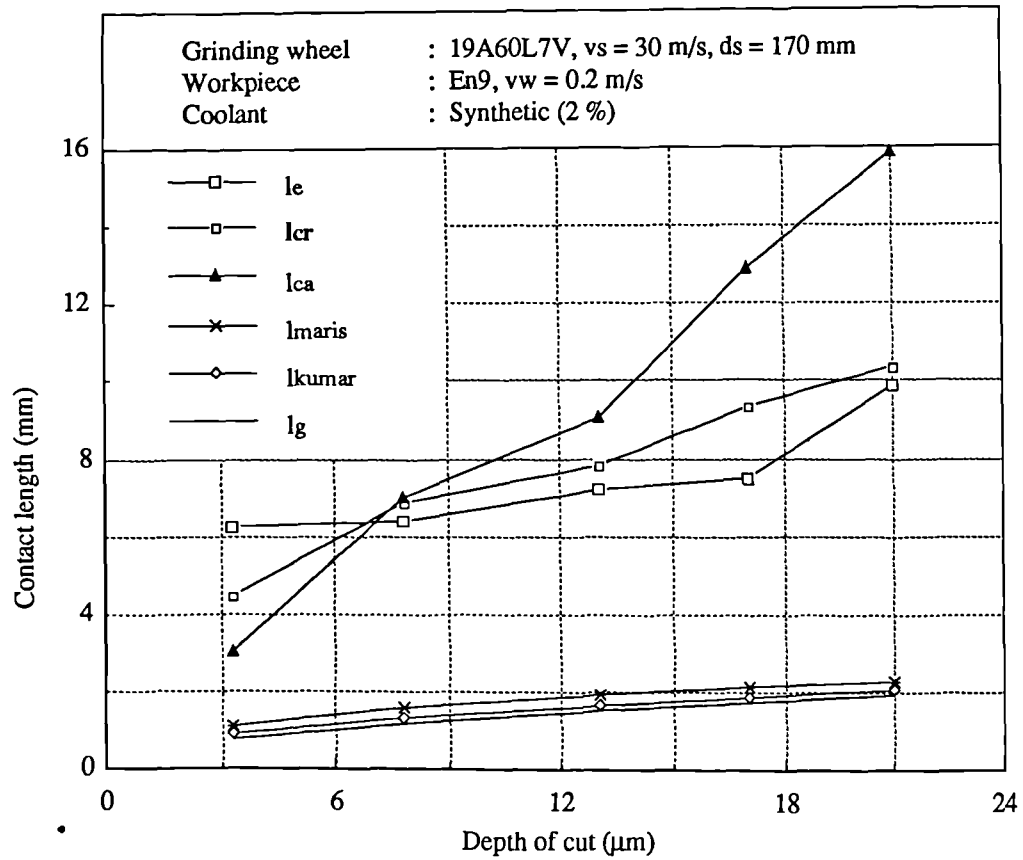


Figure 8.6 Evaluation of contact length models - Alumina/En9 steel $v_w = 0.2 \text{ m/s}$, wet

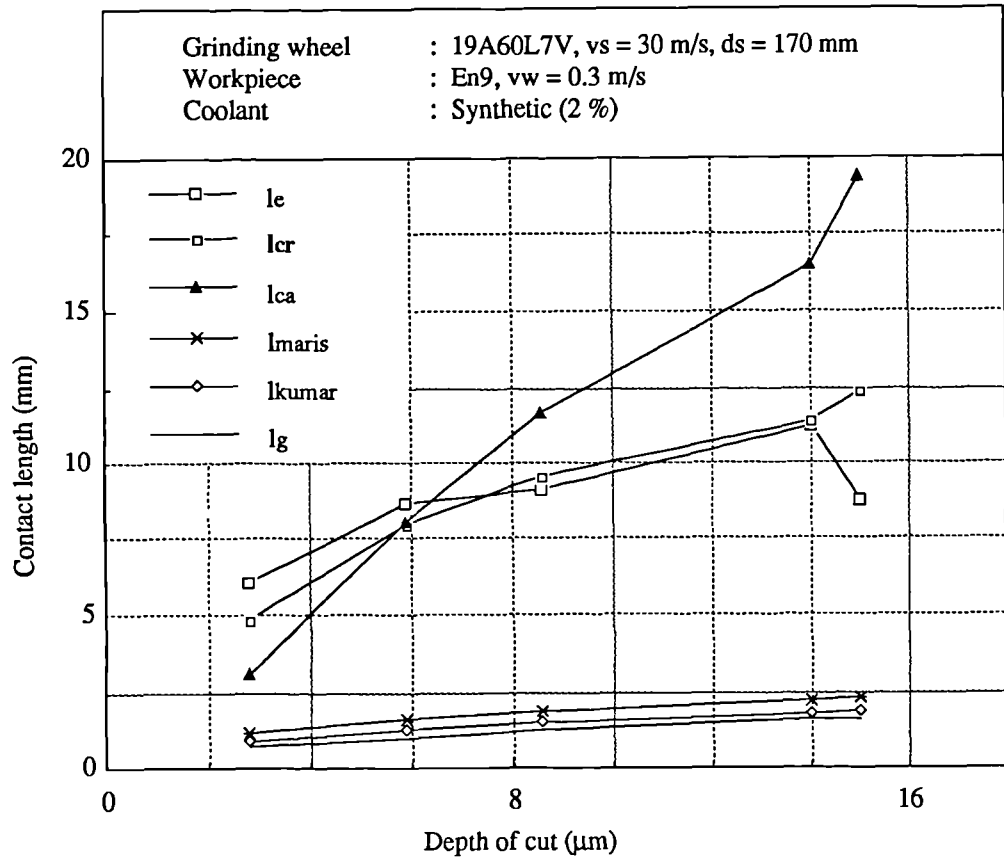


Figure 8.7 Evaluation of contact length models - Alumina/En9 steel $v_w = 0.3 \text{ m/s}$, wet

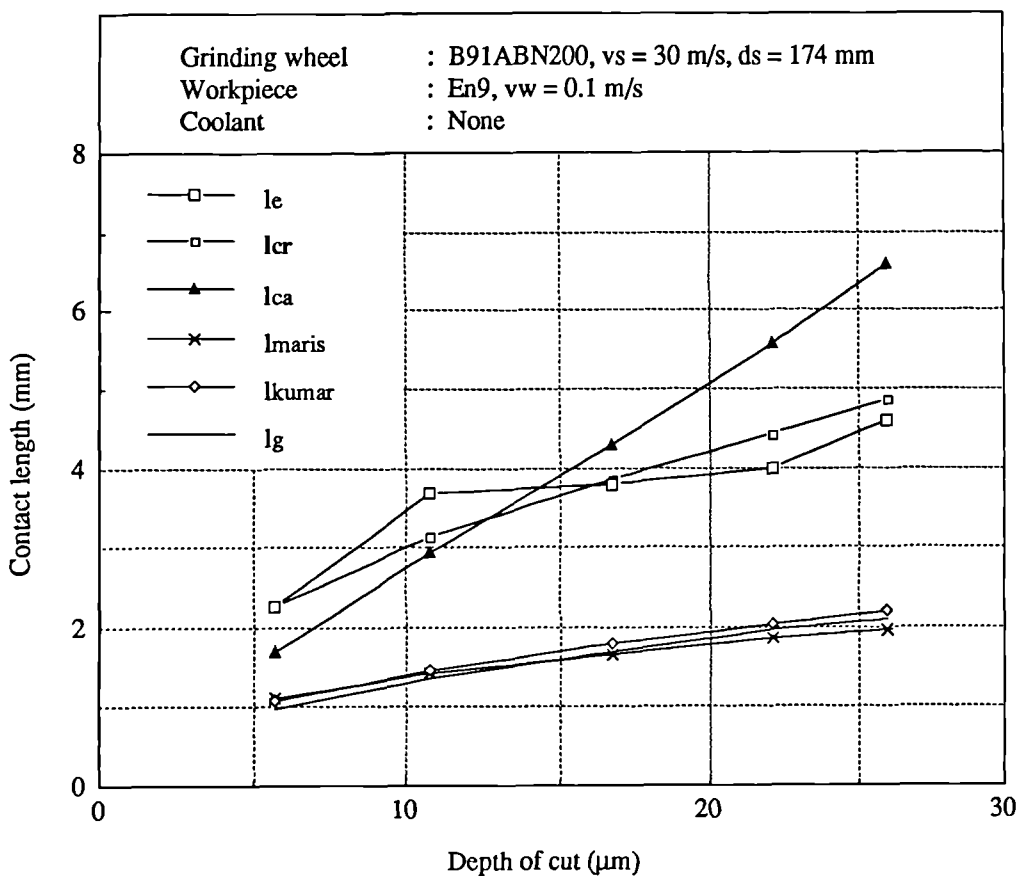


Figure 8.8 Evaluation of contact length models - CBN/En9 steel, $v_w = 0.1 \text{ m/s}$, dry

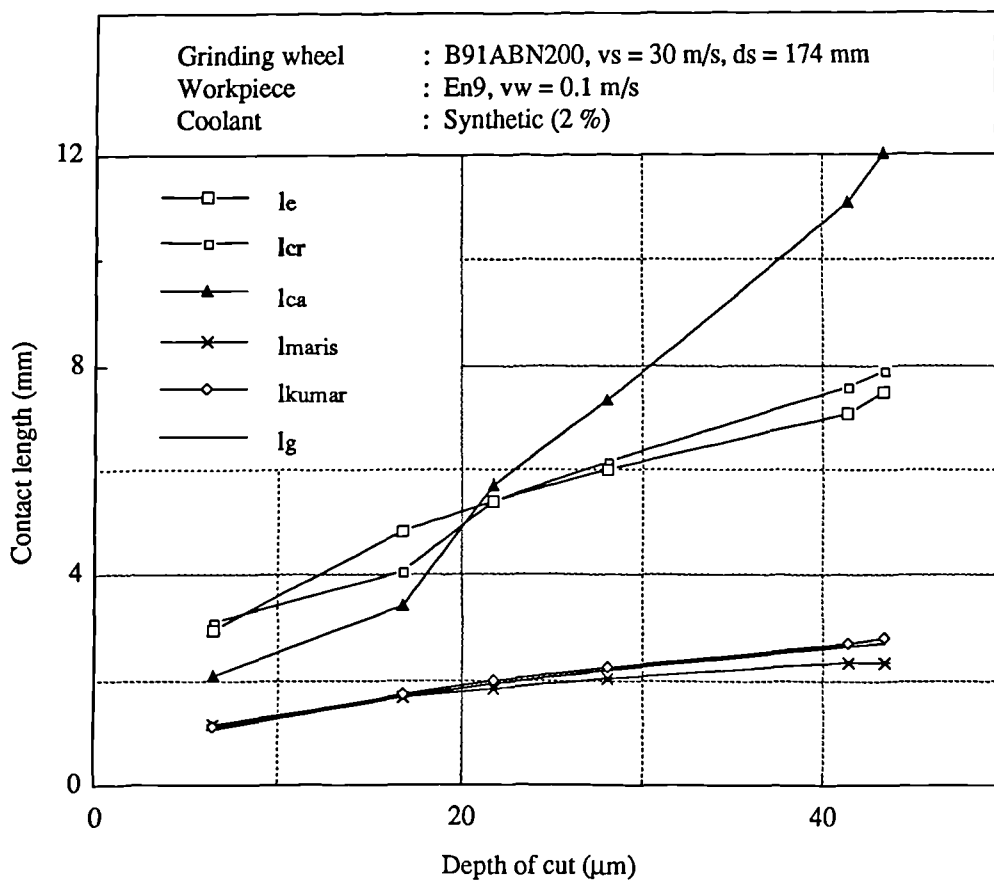


Figure 8.9 Evaluation of contact length models - CBN/En9 steel, $v_w = 0.1 \text{ m/s}$, wet

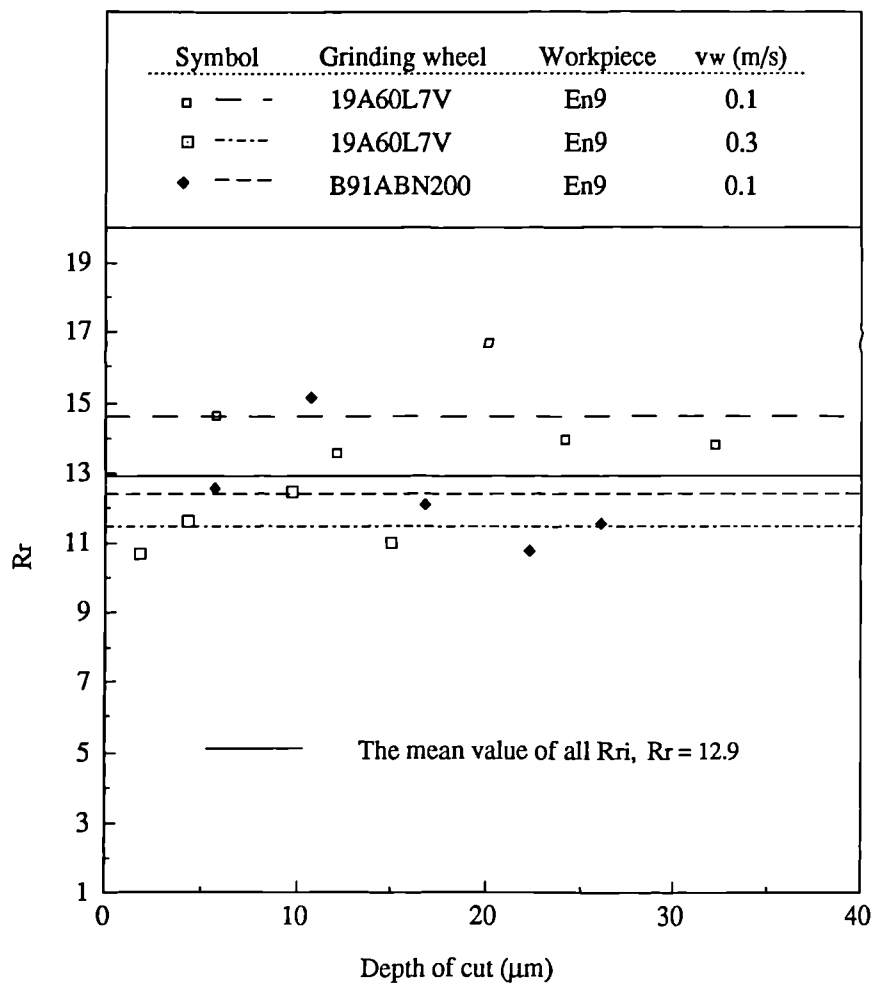


Figure 8.10 Evaluation of R_r for dry grinding, $v_s = 30$ m/s

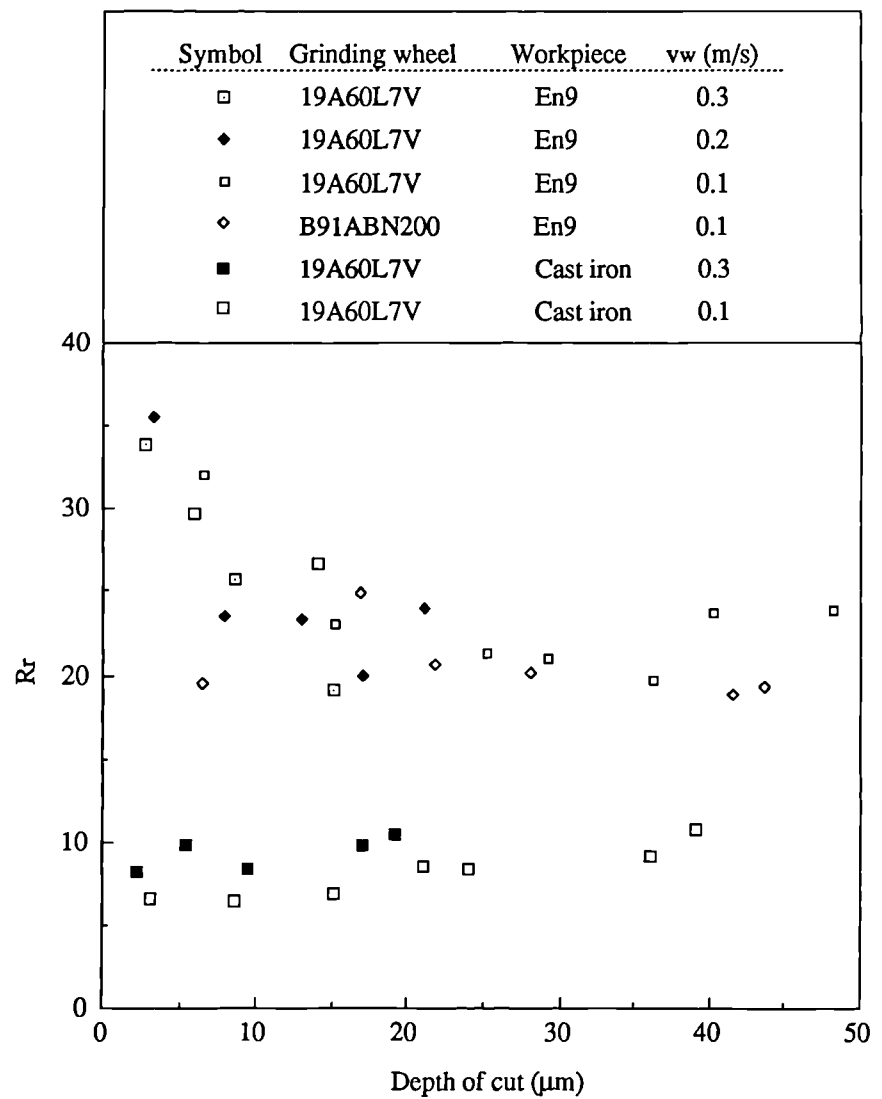


Figure 8.11 Evaluation of R_r for wet grinding, $v_s = 30$ m/s

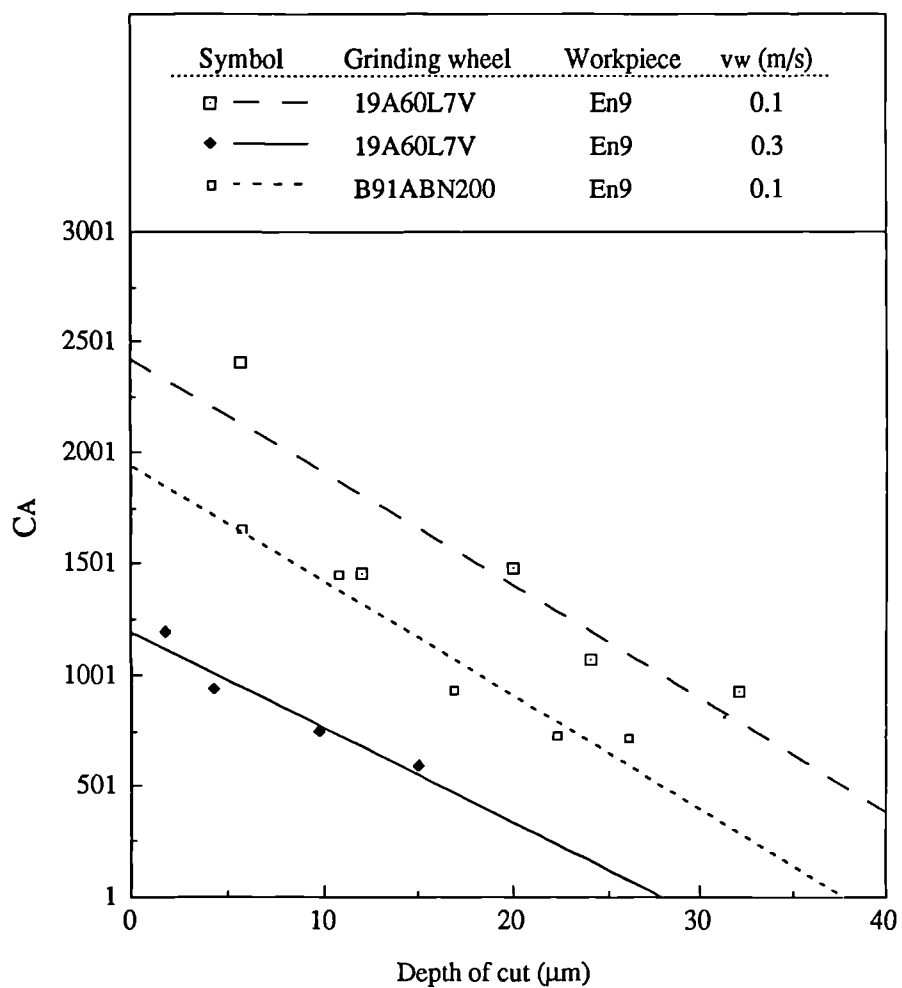


Figure 8.12 Evaluation of CA for dry grinding, $v_s = 30 \text{ m/s}$

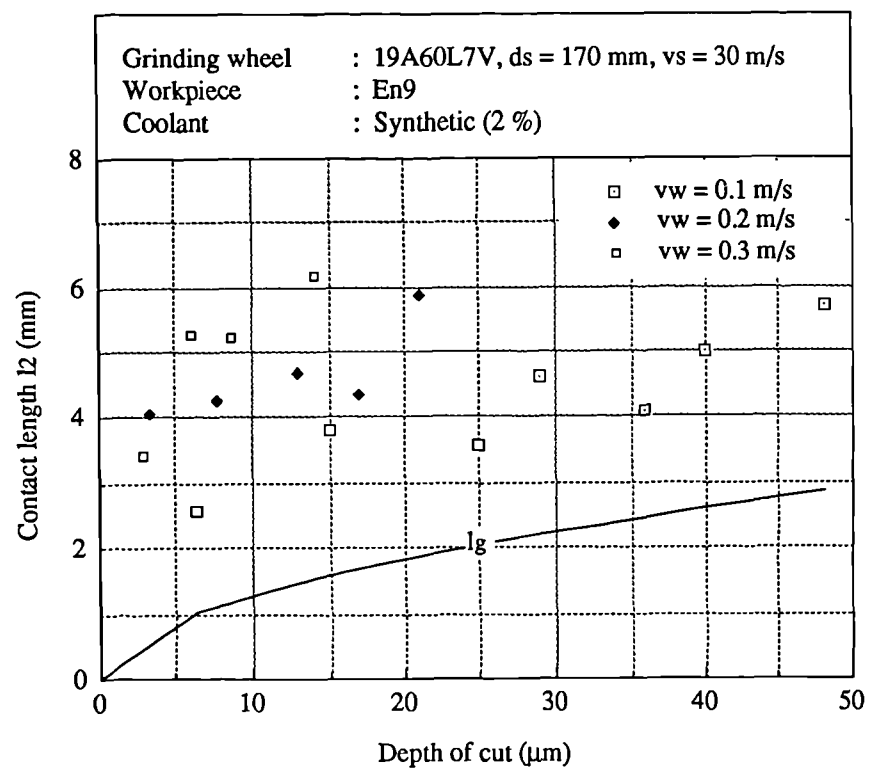


Figure 8.13 The contact length l_2 and depth of cut Alumina/En9 steel with coolant

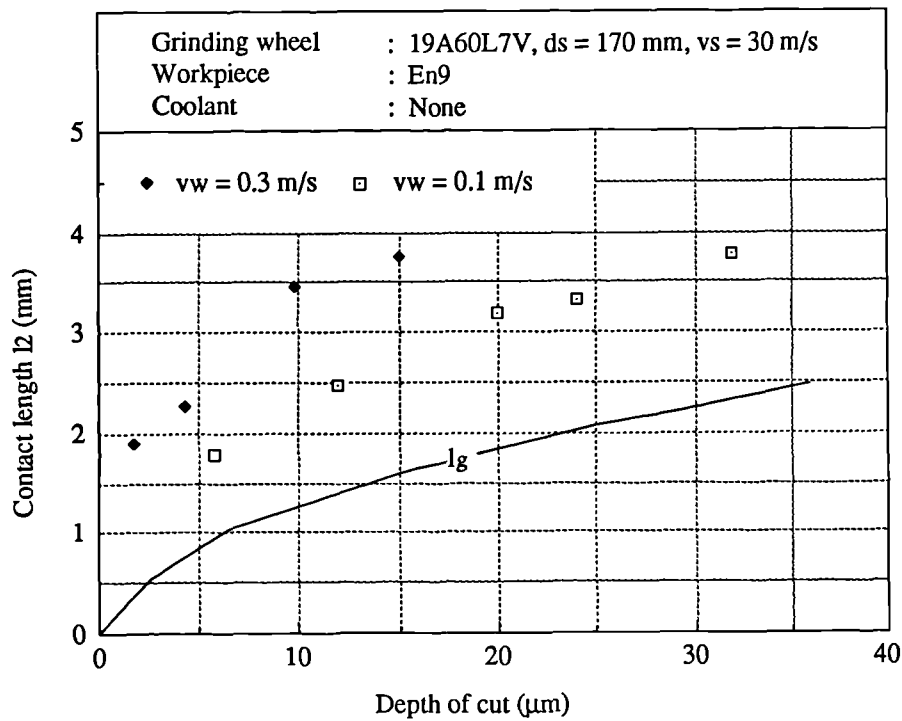


Figure 8.14 The contact length l_2 and depth of cut Alumina/En9 steel without coolant

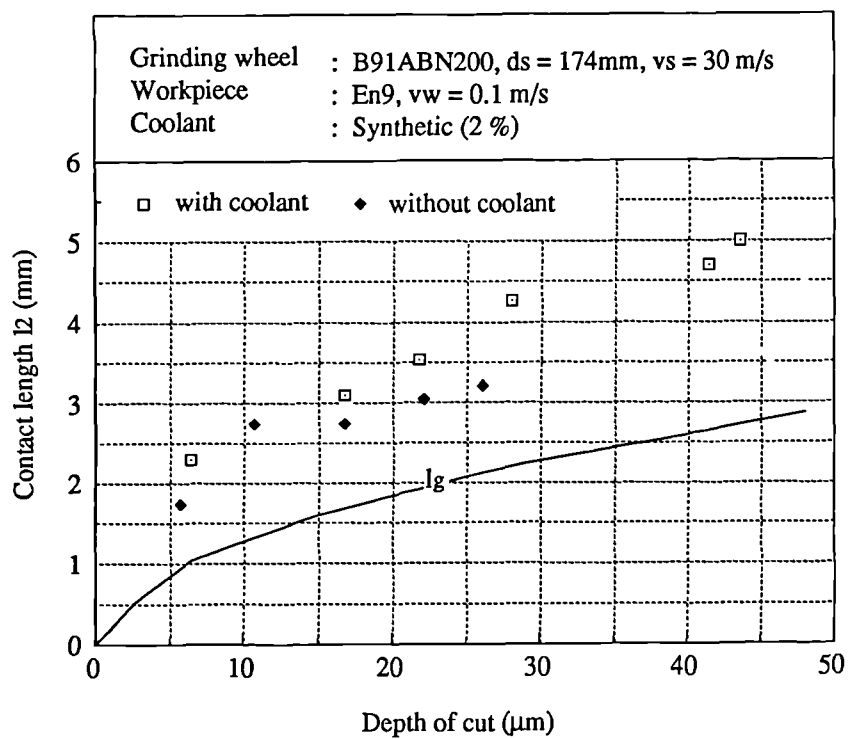


Figure 8.15 The contact length l_2 and depth of cut CBN/En9 steel

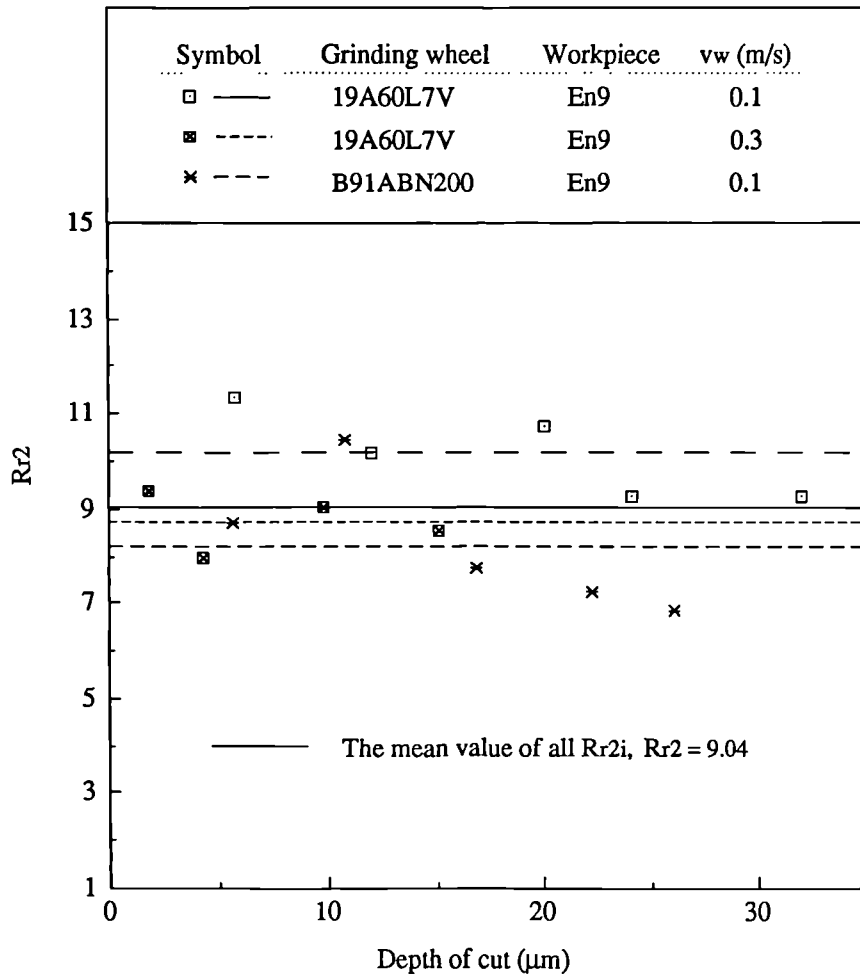


Figure 8.16 Evaluation of R_{r2} for dry grinding, $vs = 30$ m/s

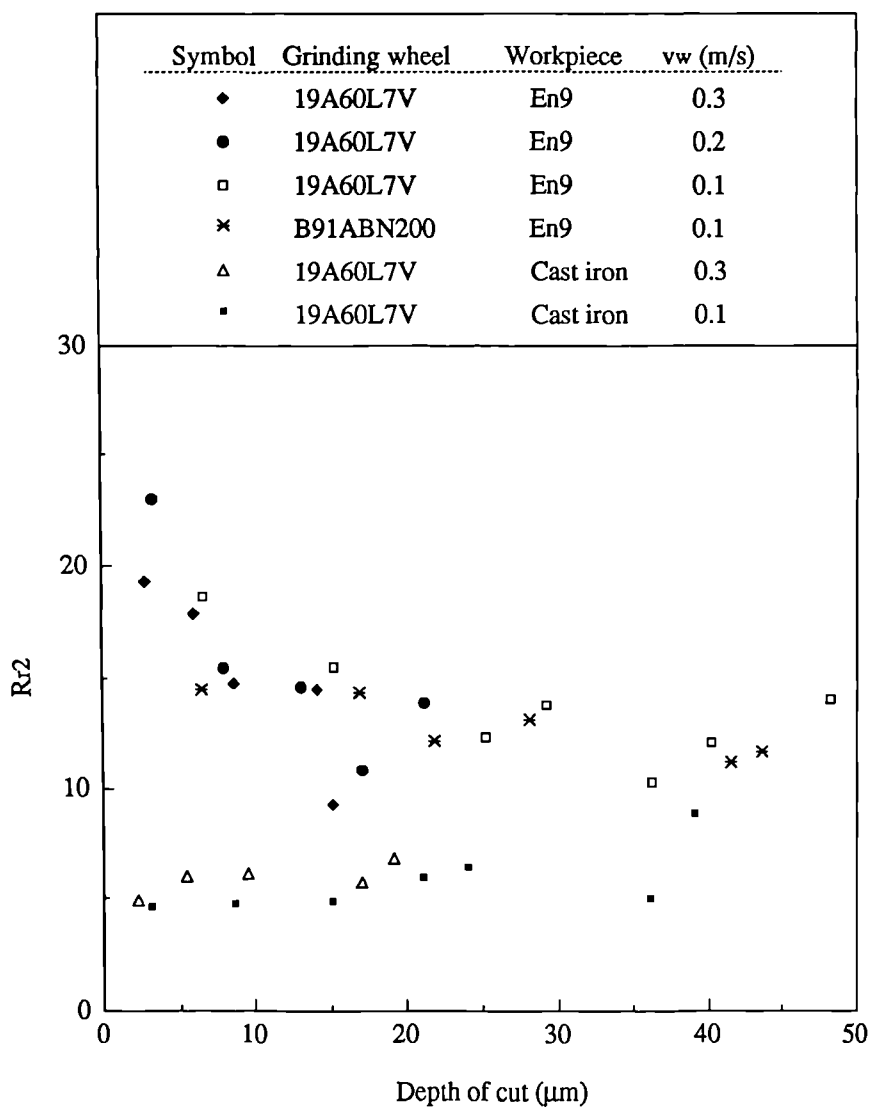


Figure 8.17 Evaluation of R_{r2} for wet grinding, $v_s = 30$ m/s

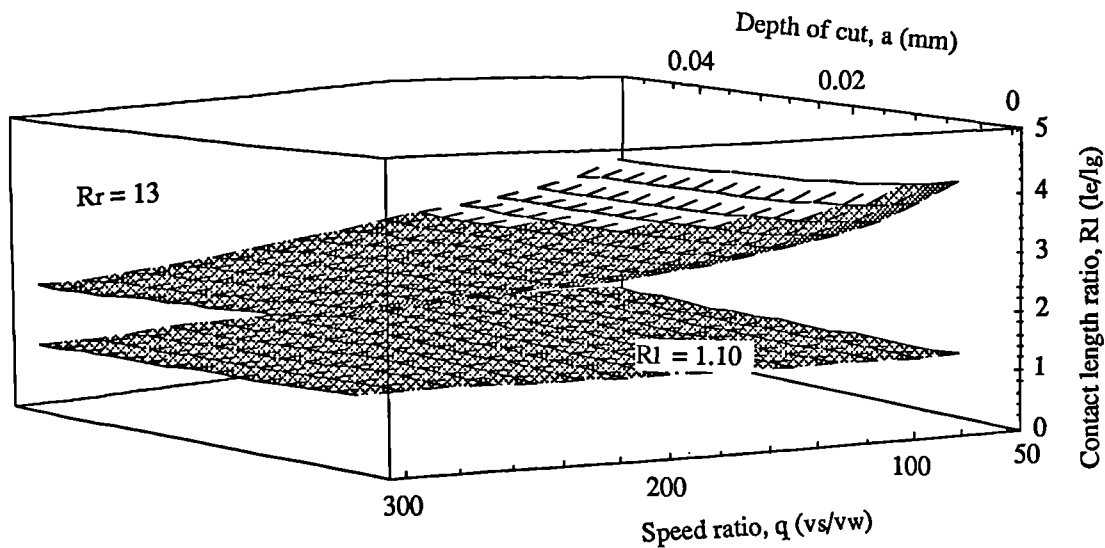


Figure 9.1 Prediction of contact length based on the contact length model

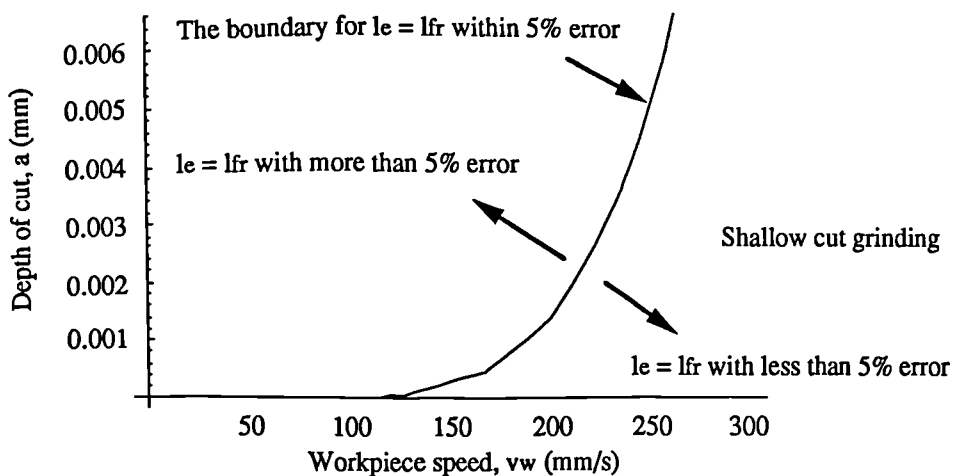


Figure 9.2 A boundary for the simplification, $le = lfr$

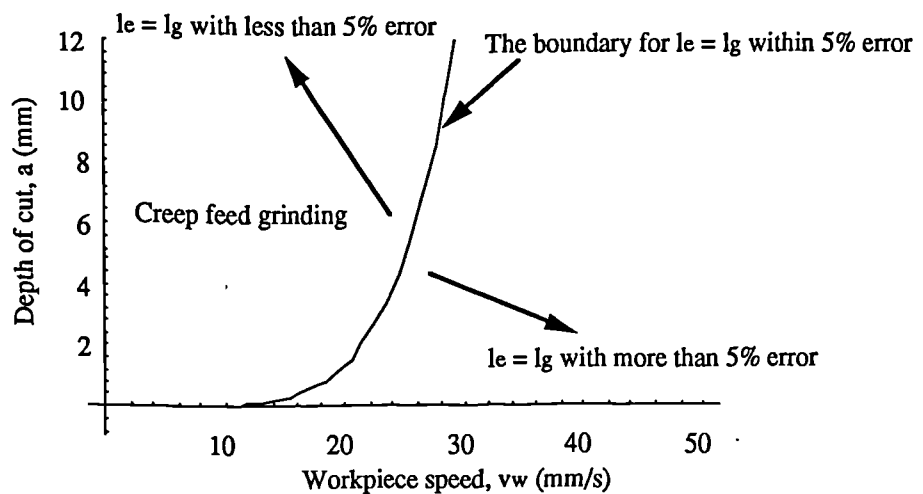


Figure 9.3 A boundary for the simplification, $le = lg$

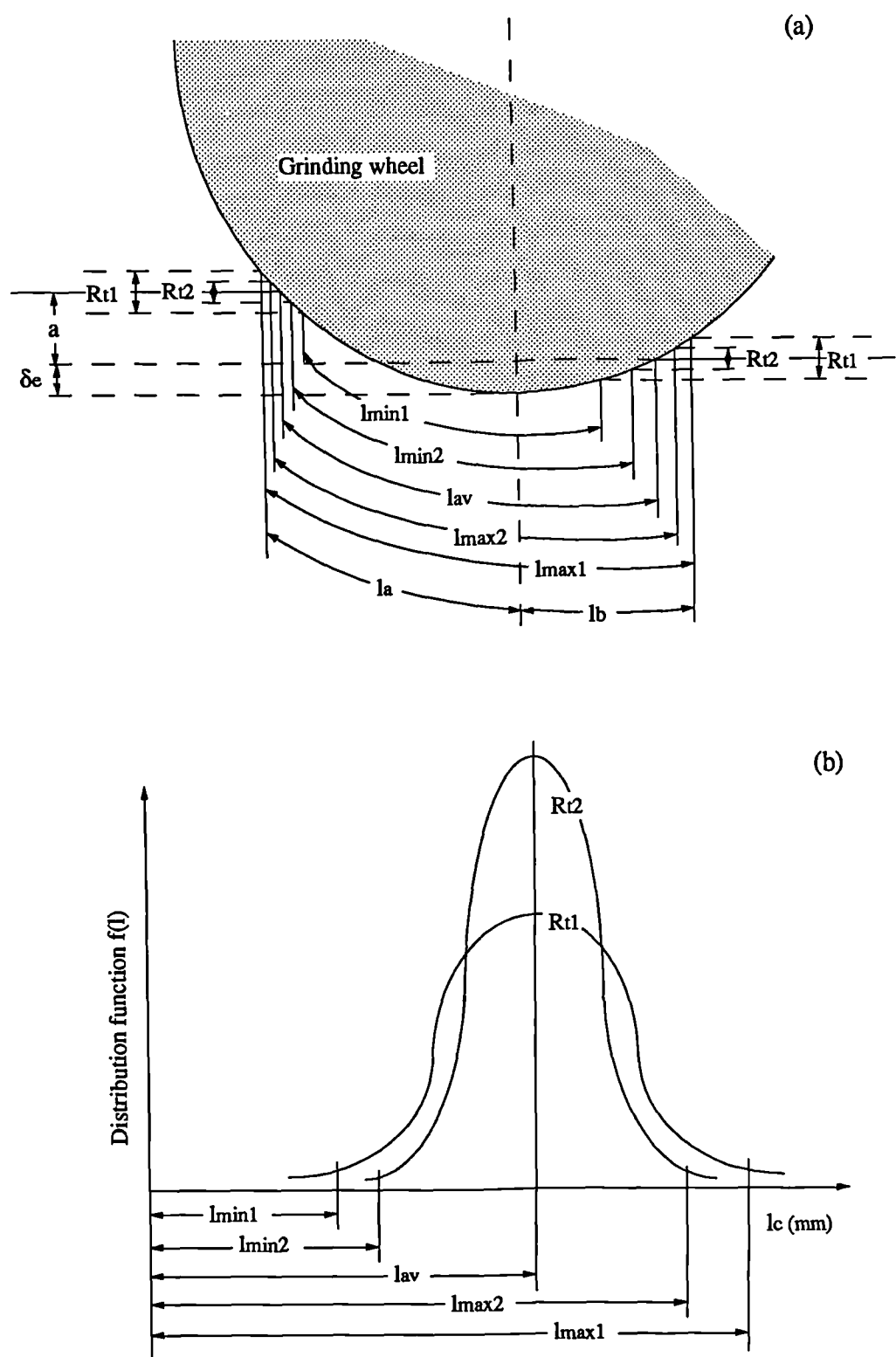


Figure 9.4 The effect of Rt on the grinding contact length